JUSTUS-LIEBIG-
UNIVERSITÄT
GIESSEN

KUMULATIVE INAUGURAL-DISSERTATION

Functional characterization of the membrane-depolarizing toxin TisB in *Escherichia coli*

Zur Erlangung des akademischen Grades

Doktor der Naturwissenschaften

– Dr. rer. nat. –

vorgelegt von

Florian Hartmut Leinberger

Justus-Liebig-Universität Gießen

Institut für Mikrobiologie und Molekularbiologie

Januar 2025

This project was initiated in January 2021 and terminated in August 2024 at the Institute of Microbiology and Molecular Biology, Department 08, Justus-Liebig University Giessen. It was supervised by Prof. Dr. Bork Berghoff.

1. Reviewer: Prof. Dr. Bork Berghoff
Justus-Liebig University Giessen
Institute of Microbiology and Molecular Biology
Heinrich-Buff-Ring 26-32, 35392 Giessen

2. Reviewer: Prof. Dr. Kai Thormann
Justus-Liebig University Gießen
Institute of Microbiology and Molecular Biology
Heinrich-Buff-Ring 26-32, 35392 Giessen

Table of Content

I. Zusammenfassung

Bakterien sind häufig Umweltstressoren ausgesetzt, welche ihr Überleben bedrohen. Dies führt zur Aktivierung von Stressreaktionssystemen, welche die Genexpression anpassen, um die zelluläre Integrität aufrechtzuerhalten. Sollten diese Systeme jedoch unzureichend sein, können Bakterien Persisterzellen bilden. Hierbei handelt es sich um eine ruhende Subpopulationen mit reduzierter Stoffwechselaktivität und erhöhter Antibiotikatoleranz. Im Gegensatz zu anderen Formen der bakteriellen Dormanz, wie beispielsweise Endosporen, weisen Persisterzellen morphologische Ähnlichkeiten mit aktiven Zellen auf, befinden sich jedoch in einem vorübergehenden Zustand reduzierter Aktivität. Diese Überlebensstrategie ermöglicht es Bakterien, widrigen Bedingungen standzuhalten, was zu Infektionsrückfällen und der Ausbreitung von Antibiotikaresistenzen führen kann.

Diese Arbeit befasst sich mit der Funktionalität von TisB, einem Toxin des Typ-I Toxin-Antitoxin-Systems *tisB/istR-1* in *Escherichia coli* (*E. coli*), sowie dessen Rolle bei der Aufrechterhaltung der Dormanz durch spezifische physiologische Mechanismen. Die Forschungsergebnisse legen nahe, dass die Insertion von TisB in die innere Membran zu einer Depolarisierung der Membran und einem ATP-Mangel führt, welche als wesentliche Auslöser für den mit der Antibiotikatoleranz verbundenen Ruhezustand betrachtet werden können. Die dargelegten Ergebnisse verdeutlichen den Einfluss von TisB auf die Physiologie von Persisterzellen und seine Rolle für das Überleben von Bakterien unter Antibiotikastress. Ein wesentlicher Aspekt dieser Arbeit ist die Anwendung eines moderaten Expressionssystems für TisB, welches eine kontrollierte Untersuchung seiner Auswirkungen ermöglicht, ohne dass dabei eine übermäßige Toxizität auftritt. Das System ermöglicht eine Untersuchung des Zusammenhangs zwischen der durch TisB induzierten Dormanz und der Proteinaggregation. Die Ergebnisse zeigen, dass die TisB-abhängige Proteinaggregation die Dauer des Ruhezustandes während der Antibiotikaexposition beeinflusst. Des Weiteren konnten Aminosäuren identifiziert werden, die für die Funktionalität von TisB von entscheidender Bedeutung sind. Dadurch konnten Erkenntnisse über die Strukturelemente gewonnen werden, die für dessen Aktivität unerlässlich sind. Diese Erkenntnisse tragen zu einem besseren Verständnis von TisB bei und unterstreichen die Bedeutung spezifischer Aminosäuren für die Aufrechterhaltung seiner Funktionalität innerhalb der Membran.

Zusammenfassend kann festgehalten werden, dass die erzielten Ergebnisse unser Verständnis des *tisB/istR-1* Systems sowie dessen Rolle bei der Persistenz von Bakterien vertieft. Durch die Aufklärung der Mechanismen, durch die TisB die Persistenz, die Proteinaggregation und den Energiegehalt beeinflusst, liefert diese Studie eine Wissensgrundlage, die als Ausgangspunkt für die Entwicklung von Strategien zur Eindämmung bakterieller Persistenz, sowie zur Verbesserung der Wirksamkeit von Antibiotika dienen kann.

II. Summary

Bacteria are frequently exposed to environmental stressors that threaten their survival. This leads to the activation of stress response systems that adjust gene expression to maintain cellular integrity. However, if these systems are inadequate, bacteria can form persister cells. These are a dormant subpopulation with reduced metabolic activity and increased antibiotic tolerance. Unlike other forms of bacterial dormancy, such as endospores, persister cells are morphologically similar to active cells but are in a transient state of reduced activity. This survival strategy allows bacteria to withstand adverse conditions that can lead to relapse of infection and the spread of antibiotic resistance.

This work examines the functionality of TisB, a toxin of the type I toxin-antitoxin system *tisB/istR-1* in *Escherichia coli* (*E. coli*), and its role in maintaining dormancy through specific physiological mechanisms. The research suggests that insertion of TisB into the inner membrane leads to membrane depolarization and ATP depletion, which can be considered as key triggers for the dormant state associated with antibiotic tolerance. The results presented illustrate the influence of TisB on persister cell physiology and its role in bacterial survival under antibiotic stress. An important aspect of this work is the use of a moderate expression system for TisB, which allows a controlled investigation of its effects without causing excessive toxicity. This allows for an examination of the relationship between TisB-induced dormancy and protein aggregation. The results show that TisB-dependent protein aggregation influences the duration of dormancy during antibiotic exposure. In addition, amino acids critical for TisB functionality were identified. This provided insight into the structural elements that are essential for its activity. These findings contribute to a deeper understanding of TisB and highlight the importance of specific amino acids in maintaining its functionality within the membrane.

In summary, the results presented here deepen our understanding of the *tisB/istR-1* system and its role in bacterial persistence. By elucidating the mechanisms by which TisB influences persistence, protein aggregation and energy content, this study provides a foundation of knowledge that can serve as a starting point for developing strategies to curb bacterial persistence and improve the efficacy of antibiotics.

III. List of Abbreviations

Abbreviation	Meaning
TA system	Toxin-antitoxin system
RBS	Ribosome binding site
RSS	Ribosome stand-by site
RM system	Restriction-modification system
VBNC	Viable but nonculturable
UTR	Untranslated region
min	Minutes
SD	Shine-Dalgarno

IV. List of Figures

V. List of publications

Type I toxin-antitoxin systems in bacteria: from regulation to biological functions

Selene F. H. Shore, Florian H. Leinberger, Elizabeth M. Fozo, Bork A. Berghoff

EcoSal Plus (2024)

Protein aggregation is a consequence of the dormancy-inducing membrane toxin TisB in *Escherichia coli*

Florian H. Leinberger, Liam Cassidy, Daniel Edelmann, Nicole E. Schmid, Markus Oberpaul, Patrick Blumenkamp, Sebastian Schmidt, Ana Natriashvili, Maximilian H. Ulbrich, Andreas Tholey, Hans-Georg Koch, Bork A. Berghoff

mSystems (2024)

In vivo relevance of charged and polar amino acids for functionality of membrane toxin TisB

Florian H. Leinberger & Bork A. Berghoff

Scientific Reports (2024)

Further contribution:

Elevated Expression of Toxin TisB Protects Persister Cells against Ciprofloxacin but Enhances Susceptibility to Mitomycin C

Daniel Edelmann, Florian H. Leinberger, Nicole E. Schmid, Markus Oberpaul, Till F. Schäberle and Bork A. Berghoff

Microorganisms (2021)

1. Toxin-antitoxin systems in bacteria: An introduction and summary of new insights into TisB functionality

Toxin-antitoxin (TA) systems are genetic modules widely distributed across bacterial species. They consist of two closely linked genes: one encoding a toxin that disrupts cellular processes and another encoding an antitoxin that neutralizes the toxin's harmful effects. These systems were first identified in the 1980s as part of research efforts to understand plasmid stability in bacteria. It was initially hypothesized that TA systems contribute to the post-segregational stability of plasmids by eliminating cells that lost the plasmid, thereby promoting the plasmid's retention within bacterial populations (Gerdes et al. 1986, Ogura & Hiraga 1983).

The discovery of TA systems constituted a substantial advancement in the comprehension of bacterial genetics and physiology. It was subsequently demonstrated that these systems not only maintain plasmid stability but are also encoded within chromosomal DNA, participating in a variety of cellular functions (Christensen et al. 2001, 2003). This realization has enhanced our understanding of the complex mechanisms by which bacteria respond to stress and ensure their survival. Despite their ubiquitous presence and recognized importance, the full scope of TA systems' roles in bacterial physiology remains elusive, making the study of these systems an active and evolving area of research.

1.1 Localization of toxin-antitoxin systems

TA systems in bacteria are encoded on plasmids and in the chromosome. The specific functional properties and regulatory mechanisms exhibited by these systems are contingent upon their localization. A comparative analysis of these two forms of TA systems reveals both differences and similarities that are crucial for understanding their biological roles (Wagner & Unoson 2012, Lee & Lee 2016).

Plasmid-encoded TA systems are widely recognized for their role in maintaining the stability of plasmids. These systems function as a "post-segregational killing" mechanism, whereby the less stable antitoxin is degraded at a faster rate when a bacterial cell loses the plasmid, while the more long-lived toxin kills the cell (Kawano et al. 2002, Weaver et al. 2003). These mechanisms guarantee that only cells that retain the plasmid survive, thereby contributing to the stability of the plasmid within the bacterial population (Gerdes & Rasmussen 1986, Ogura & Hiraga 1983).In terms of regulation, plasmid-encoded TA systems are often relatively straightforward to regulate, as their primary function is directly linked to the presence or absence of the plasmid. These systems frequently regulate themselves using the difference in stability of toxin and antitoxin (Wagner & Unoson 2012). Furthermore, certain systems, such as *ccdB/ccdA*, have been observed to function as transcriptional repressors when a protein complex is formed between the toxin and the antitoxin (Fraikin et al. 2020).

In contrast, chromosomally encoded TA systems are frequently associated with the regulation of a more diverse range of cellular processes. These systems can be triggered in response to a variety of environmental factors, including stressors such as nutrient deficiency or antibiotic stress (Dörr et al. 2010, Michaux et al. 2014). A notable difference between plasmid-encoded and chromosomally encoded TA systems is their role in the formation of persister cells. These cells exist in a dormant, non-dividing state, which makes them tolerant to many environmental influences, including antibiotics (Berghoff et al. 2017, Dörr et al. 2010, Edelmann et al. 2021, Lewis 2010). The regulation of chromosomal TA systems is frequently more complex and can be modulated by various global regulatory networks that respond to environmental signals. Therefore, these systems are not only involved in the stress response but may also play a role in the long-term adaptation and evolution of bacteria (Fozo et al. 2010, Jurėnas et al. 2022).

Nevertheless, there are notable similarities between the two systems. Both forms are composed of genes that are in close proximity to one another and encode a toxin and an antitoxin. They also share identical molecular mechanisms for neutralizing the toxin through the antitoxin. Moreover, both plasmid- and chromosomally encoded systems are capable of contributing to cellular homeostasis under specific conditions. They achieve this primarily through the controlled inhibition of cellular functions, such as translation or DNA replication, under stress conditions (Fozo et al. 2010, Hayes 2003, Jurėnas et al. 2022).

1.2 Biological functions of toxin-antitoxin systems

TA systems affect a variety of bacterial cellular processes and play crucial roles in various biological functions (Figure 1) that enhance bacterial survival and adaptability. TA systems are involved in the stabilization of mobile genetic elements, including plasmids and prophages (Peltier et al. 2020), defense against bacteriophages (LeRoux & Laub 2022), and the formation of persister cells, which contribute to bacterial survival in hostile environments (Lewis 2010).

1.2.1 Stabilization of mobile genetic elements

TA systems are of crucial importance in the maintenance of plasmids and prophages within bacterial cells. This is achieved through a mechanism known as "plasmid addiction" (Gerdes & Rasmussen 1986) and “prophage stabilization” (Lehnherr et al. 1993). In these systems, the toxin is relatively stable, whereas the antitoxin is more labile and degraded rapidly when the plasmid or prophage is lost. As long as the plasmid or prophage is retained, the antitoxin is continuously produced, thereby neutralizing the toxin. However, in the event of plasmid or prophage loss, antitoxin production is no longer possible, resulting in its rapid degradation. The more stable toxin than exerts its lethal effect, resulting in growth inhibition or cell death (Figure 1). This selective pressure ensures that only cells that retain the plasmid or prophage can proliferate, thereby stabilizing these genetic elements within the bacterial population (Gerdes et al. 1990). The process designated as "anti-addiction" represents the only method by which the bacteria can overcome this system. This is achieved by incorporating the antitoxin gene into their own genome, enabling bacteria to survive

even in the absence of the plasmid or prophage (Gerdes et al. 1986, Ramisetty & Santhosh 2015, Van Melderen & De Bast 2009).

1.2.2 Phage defense

TA systems represent a crucial line of defense against phage infections in bacterial populations (LeRoux & Laub 2022). Each of these systems serves to protect individual cells by degrading phage genomes and transcripts through a variety of mechanisms (Figure 1). Some of the earliest systems to be recognized as phage defense were restriction-modification (R-M) systems, which are to some extent analogous to TA systems (Mruk & Kobayashi 2014). In these systems, a restriction enzyme (analogous to the toxin) recognizes and cleaves specific sequences in DNA, such as those from a phage. To prevent self-damage, the bacterial DNA is protected by a modification enzyme (analogous to an antitoxin) that methylates the host DNA at the same recognition sites, thereby ensuring that the restriction enzyme does not attack it (Guo et al. 2014). Other systems for individual protection are the CRISPR-Cas systems, which are also capable of discriminating between the host genome and the invading genome, and only attack the phage genome (Barrangou et al. 2007, Hampton et al. 2020). In addition to providing individual protection, TA systems contribute to population-wide defense through a process known as abortive infection (Figure 1). In this scenario, an infected cell undergoes self-poisoning by activating the toxin, which results in cell death or growth inhibition. This sacrificial action prevents the replication and spread of the phage to neighboring cells, thereby protecting the bacterial community as a whole (Gerdes 2024, LeRoux & Laub 2022).

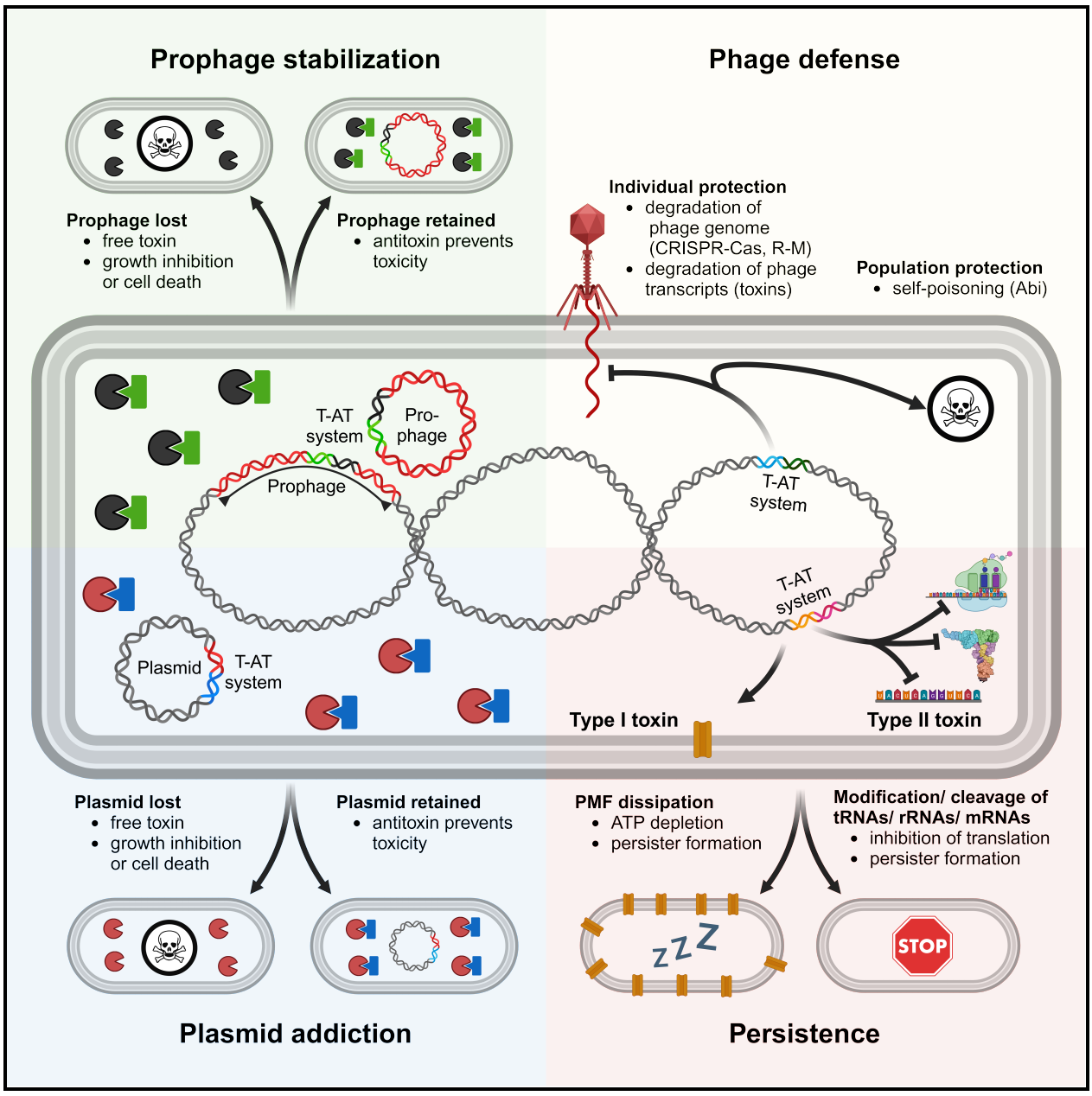

Figure 1: Biological functions of toxin-antitoxin systems
Top left: Prophage stabilization. Prophages (red) are either integrated or episomal. If the prophage and its TA system are not inherited by a progeny cell, the unstable antitoxin (green) is degraded, and the stable toxin (black) leads to growth inhibition or cell death. If the prophage is retained, the antitoxin prevents toxicity. **Bottom left:** Plasmid addiction. Same principle as for prophage stabilization. Unstable antitoxin (blue) and stable toxin (red). **Top right:** Phage defense. Like CRISPR-Cas and restriction-modification (R-M) systems, TA systems provide individual protection. While CRISPR-Cas and R-M systems degrade the phage genome, toxins from TA systems degrade phage transcripts. Alternatively, TA systems provide population protection by self-poisoning of infected cells (abortive infection, Abi). **Bottom right:** Persistence. Type I toxins form pores in the inner membrane. The proton motive force (PMF) is dissipated, which leads to ATP depletion and persister formation. Type II toxins modify or cleave tRNAs, rRNAs and mRNAs. The translation inhibition may lead to persister formation.

1.2.3 Persistence

TA systems are of significant importance in the process of bacterial persistence, a survival strategy whereby a subpopulation of bacteria enters a dormant state, thereby becoming highly tolerant to antibiotics. Persistence is a phenomenon distinct from genetic resistance (Lewis 2010).

Bacteria that have developed resistance to a particular antibiotic possess genetic alterations that allow them to continue to grow and reproduce even in the presence of the antibiotic. In contrast, susceptible bacteria lack the relevant mutations and are effectively killed by antibiotics (Figure 2) (Alekshun & Levy 2007). It is important to distinguish between the reversible physiological state of a subpopulation that persister cells represent and the concept of a permanent genetic change. Persister cells are not genetically resistant; rather, they survive antibiotic exposure by entering a dormant state in which their metabolic activity is reduced, thereby limiting the efficacy of the antibiotics (Figure 2) (Balaban et al. 2019).

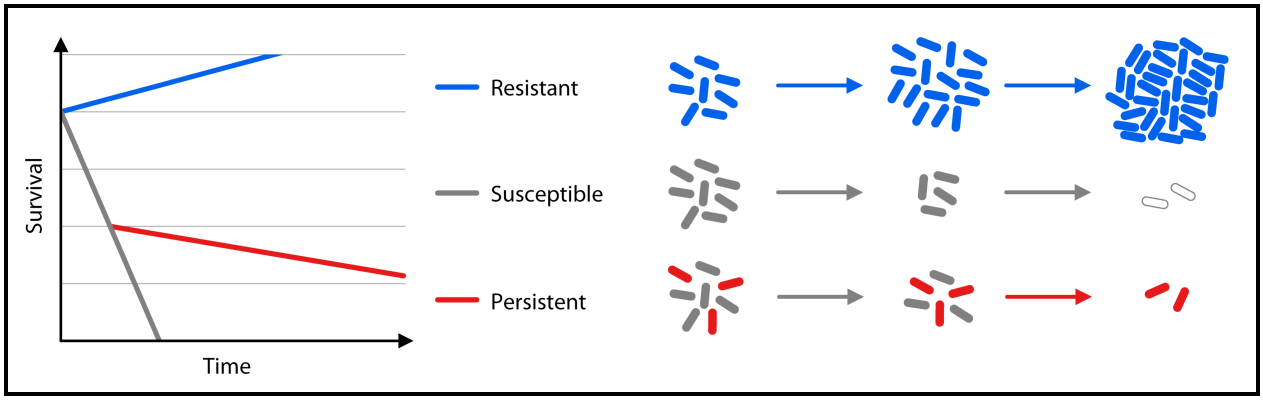

Figure 2: Antibiotic resistance, persistence, and bacterial survival
Illustration of antibiotic killing kinetics (left) and corresponding bacterial populations (right). Susceptible cells are rapidly killed (grey), while resistant cells continue growing (blue) in the presence of drugs (e.g. bactericidal antibiotics). If persister cells are present, a biphasic killing curve emerges due to long-term antibiotic tolerance of the persister subpopulation (red).
(Shore et al. 2024)

In contrast to type II TA systems, which typically induce persistence by inhibiting translation through the modification or cleavage of tRNAs, rRNAs, or mRNAs (Jurėnas & Van Melderen 2020), type I TA systems achieve persistence by interfering with the bacterial inner membrane and depleting cellular ATP levels (Wilmaerts et al. 2018, Gurnev et al. 2012, Verstraeten et al. 2015, Cheng et al. 2014, Dörr et al. 2010). For example, the type I TA system *tisB/istR-1* of *E. coli* involves the integration of the TisB toxin into the bacterial inner membrane, which results in disruption of the proton motive force. This disruption impairs ATP synthesis, resulting in depletion of cellular energy. The subsequent reduction in metabolic activity induces a dormant-like state that provides protection from the lethal effects of antibiotics (Wagner & Unoson 2012, Unoson & Wagner 2008).

In contrast to other biological functions of TA systems, such as plasmid addiction or phage defense, which can result in cell death, the induction of persistence by these systems is not intended to cause cell death. This mechanism enables the bacteria to survive extended periods of environ-

mental stress, such as antibiotic exposure, without fatal consequences. The capacity to induce persistence is crucial for the long-term survival of bacterial populations, particularly during antibiotic exposure. Consequently, TA systems represent a significant research focus, with the objective of developing strategies to disrupt these pathways and thereby enhance the efficacy of antibiotic treatments against persistent bacterial infections (Lewis 2010).

1.2.3.1 The spiderweb hypothesis as multifactorial model of bacterial persistence

Persistence in bacterial cells is a complex phenomenon that can be influenced not only by TA systems but also by a range of other factors, including starvation, oxidative stress, protein aggregation, low energy and inhibition of core processes (Ayrapetyan et al. 2015, 2018, Pu et al. 2019).

In this work, we would like to suggest a hypothesis regarding the induction of persistence by TA systems and other factors, denoted the "spiderweb hypothesis". The hypothesis suggests that the number and strength of several factors influence the process of persistence. In the absence of these factors, the bacterial cell displays normal growth and metabolic activity (Figure 3). The presence of a single factor is sufficient to induce persistence, given that the strength of the factor is high enough (Balaban et al. 2004, Lewis 2010). However, persistence can also be triggered when multiple factors are only partially present, collectively leading to a reduction in metabolic activity sufficient to induce dormancy (Figure 3). An extreme scenario occurs when all factors are present at full strength, resulting in a state known as "viable but non-culturable" (VBNC). In this state, the bacterial cells are still alive but unable to grow or reproduce in standard laboratory culture conditions, representing an even deeper level of dormancy (Figure 3) (Ayrapetyan et al. 2018).

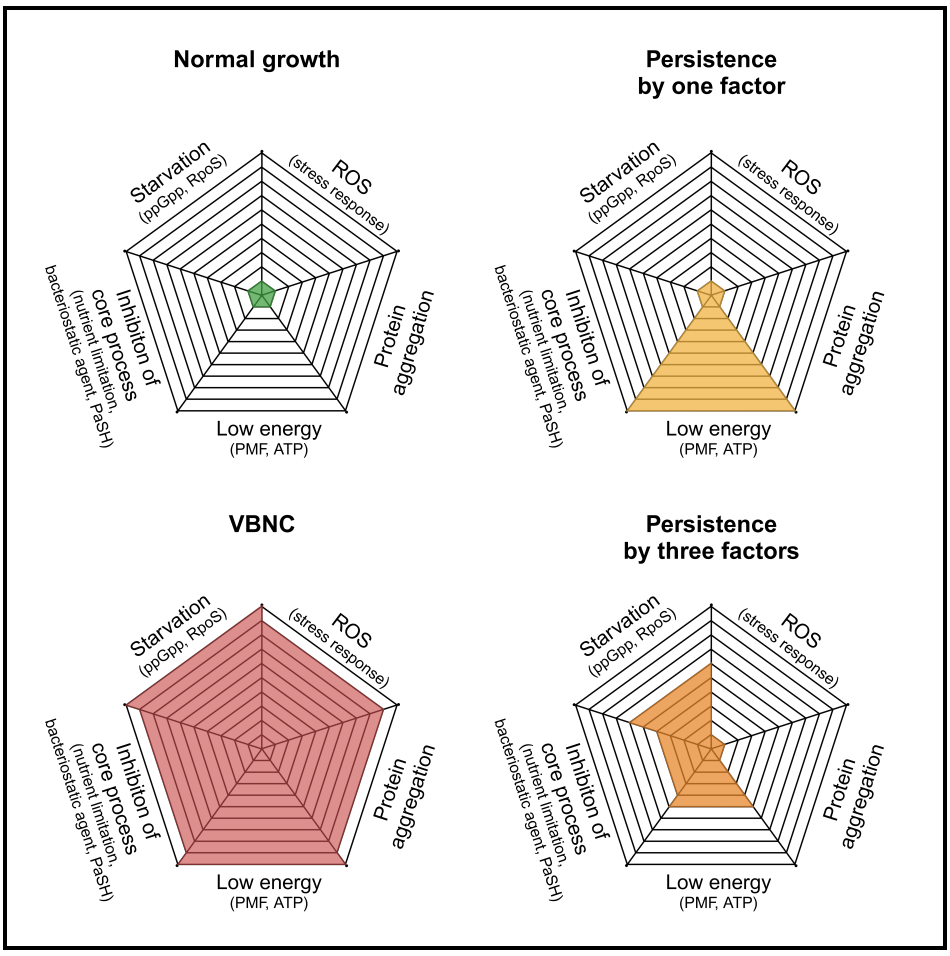

Figure 3: Spiderweb hypothesis of persistence
Top left: Normal growth; no active factor for persister induction. **Top right:** Persistence by one factor; only one factor is fully active and sufficient to induce persistence. **Bottom right:** Persistence by three factors; multiple factors are partially active and sufficient to induce persistence. **Bottom left:** Viable but non-culturable (VBNC); all factors are fully active and induce an even deeper dormancy.

1.3 Categorization of toxin-antitoxin systems

TA systems in bacteria are categorized based on the type of antitoxin and its mechanism of action. Currently, eight different types of TA systems have been identified, each with unique structural and functional characteristics. These systems play critical roles in bacterial physiology, including stress response, plasmid maintenance, and regulation of cellular processes (Harms et al. 2018, Jurėnas et al. 2022).

1.3.1 Overview of the eight types of toxin-antitoxin systems

The eight types of TA systems are classified primarily by the nature of the antitoxin and the mechanism through which it neutralizes the corresponding toxin (Figure 4).

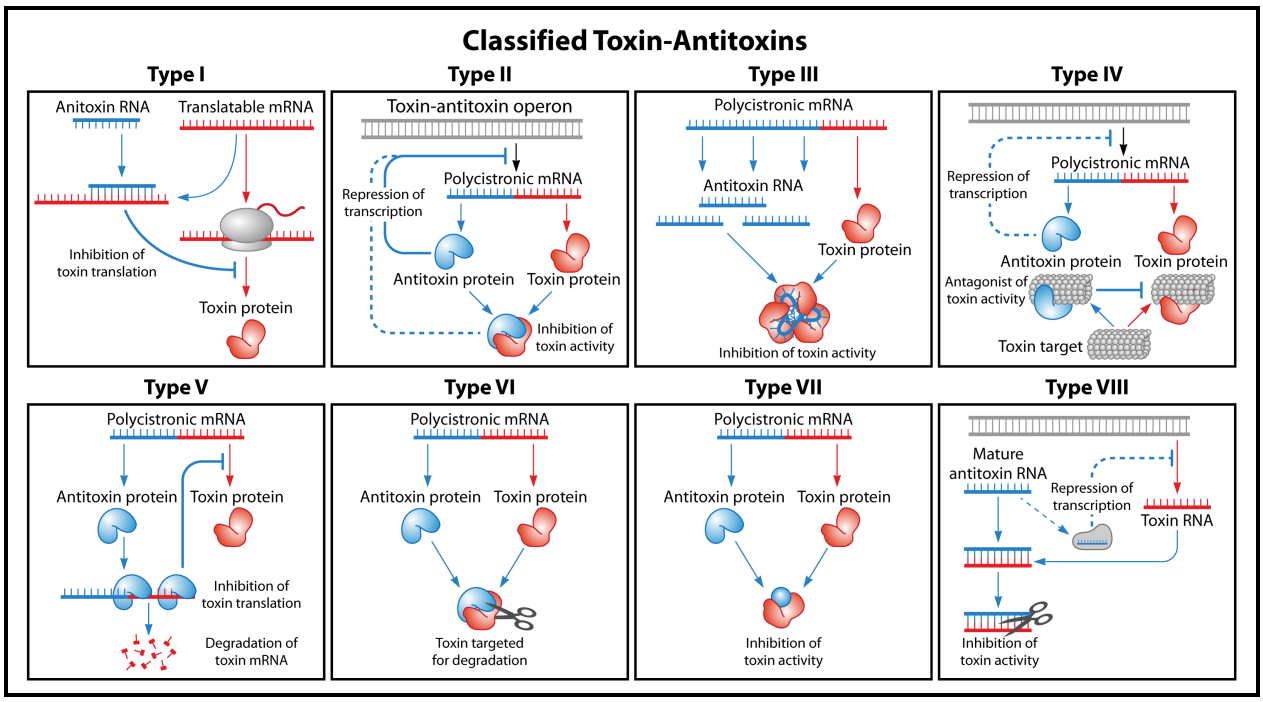

Figure 4: Toxin-antitoxin systems overview
Overview of the different types of toxin-antitoxin systems and classification based on toxin-antitoxin interaction. The toxin is represented in red and the antitoxin in blue.
(Shore et al. 2024)

Type I TA systems: involve an RNA antitoxin that is complementary to the toxin mRNA. By binding to the toxin mRNA, the translation of the toxin protein is inhibited, thereby preventing its effect (Gerdes et al. 1986).

In **Type II TA systems**, both the toxin and antitoxin are proteins, which are translated from a polycistronic mRNA. Antitoxins neutralize toxins by binding to them. Under stress, antitoxins may be degraded, releasing the toxin, which disrupts cellular processes like replication or translation (Singh et al. 2021). The *ccdB/ccdA* system was the first discovered and has a role in stabilizing plasmids (Ogura & Hiraga 1983).

Type III TA systems feature RNA antitoxins that bind directly to protein toxins, preventing toxicity. The first discovered type III system, *toxN/toxI*, functions as a phage abortive infection system (Fineran et al. 2009). Toxins are usually sequence-specific endoribonucleases that can cleave the antitoxin precursor RNA into individual repeats, which it then binds to form a stable, catalytically inactive complex (Manikandan et al. 2022).

In **Type IV TA systems**, antitoxins do not bind directly to toxins but to their targets, preventing toxin-induced damage. The *cbtA/cbeA* system was the first described, where CbeA counteracts CbtA's inhibition of cytoskeletal polymerization (Masuda et al. 2012).

In **Type V TA systems**, the antitoxin is an enzyme that cleaves the toxin mRNA, thereby preventing the translation of the toxin. One example is the *ghoT/ghoS* pair, wherein the GhoT toxin forms pores in the cell membrane, ultimately leading to cell death. The GhoS antitoxin is an RNase that degrades *ghoT* mRNA, thereby preventing toxin production (Wang et al. 2012).

Type VI TA systems involve an antitoxin protein that binds to the toxin protein, thereby forming a complex that is targeted for degradation. The *socB/socA* system is such a type VI system. SocB inhibits DNA replication by interacting with the β sliding clamp, and SocA serves as a proteolytic adaptor that triggers degradation of the SocB toxin (Aakre et al. 2013).

Type VII TA systems are characterized by antitoxins neutralizing toxins via post-translational modifications, such as phosphorylation or oxidation. The *hha/tomB* system exemplifies this, with TomB promoting the oxidation of the Hha toxin, reducing its toxicity (Marimon et al. 2016).

In **Type VIII TA systems**, the toxin and the antitoxin are both RNAs. But instead of regulating the toxin directly, these systems may involve complex regulatory networks where the antitoxin modulates toxin activity indirectly. As example, the *creT/creA* system in *Haloarcula hispanica* is linked with CRISPR-Cas, where CreT toxin halts growth by sequestering tRNA, while CreA suppresses *creT* transcription through CRISPR-Cas (Li et al. 2021).

1.3.2 Type I toxin-antitoxin systems

Type I TA systems were first discovered through the study of plasmid stability in *E. coli*, where the *hok/sok* module was found to mediate post-segregational killing of plasmid-free cells (Gerdes & Rasmussen 1986). This system was crucial in maintaining plasmids in bacterial populations by ensuring that cells without the plasmid would undergo cell death. Since the discovery of *hok/sok*, numerous other type I TA systems have been identified, such as *symE/symR* (Kawano et al. 2007), *tisB/istR-1* (Vogel et al. 2004), *bsrE/SR5* (Meißner et al. 2016) *sprA2/sprA2AS* (Germain-Amiot et al. 2019), and *zorO/orzO* (Wen et al. 2014).

Type I TA systems are based on the interaction between the toxin mRNA and an antisense RNA antitoxin. The toxin gene is typically transcribed in one direction, while the antitoxin RNA is transcribed in the opposite direction, forming a divergent gene pair (Brantl 2009, 2012). These antisense RNAs regulate toxin production by creating a double-stranded RNA duplex with the toxin mRNA, which either prevents its translation or promotes its degradation. Antitoxins prevent the translation of toxins by various mechanisms. For example, in the SymE/SymR system of *E. coli*, the antitoxin binds to the ribosome binding site (RBS) of the toxin mRNA, directly blocking ribosome access (Kawano et al. 2007). In other systems, such as Hok/Sok and LdrD/RdlD, the antitoxin binds to the Shine-Dalgarno (SD) sequence of the toxin leader peptide, indirectly inhibiting translation (Gerdes & Wagner 2007, Thisted & Gerdes 1992). In some cases, such as the TxpA/RatA system of *Bacillus subtilis*, the antitoxin forms a duplex with the toxin mRNA, which is then cleaved by RNase III, resulting in degradation of both RNAs (Durand et al. 2012).

The small hydrophobic toxin proteins from type I TA systems typically affect normal membrane function, eventually even by disrupting the bacterial membrane. Overexpression of toxin genes, such as *hok, srnB, pndA, fst, ibsC, shoB, tisB* and *dinQ* results in membrane depolarization or permeabilization, leading to the collapse of membrane potential, loss of ATP, and ultimately growth inhibition or cell death (Fozo et al. 2008, Gerdes et al. 1986, Weel-Sneve et al. 2013, Weaver & Tritle 1994, Unoson & Wagner 2008, Nielsen et al. 1991). Membrane disintegration often leads to the formation of "ghost" cells, which are cells with damaged membranes (Ono et al. 1986).

However, type I toxins can also be cytosolic toxins that act by cleaving DNA or RNA, as seen with SymE and RalR, which are RNA and DNA endonucleases, respectively (Guo et al. 2014, Kawano et al. 2007).

1.3.3 Mechanisms of action and cellular impact of type I toxins

TA systems affect essential cellular processes, with type I toxins exerting their effects primarily on the bacterial membrane (Unoson & Wagner 2008) and others targeting nucleic acids (Guo et al. 2014, Thompson et al. 2022). This results in substantial alterations of cellular processes, including the stabilization of mobile genetic elements such as plasmids (Gerdes & Rasmussen 1986) and prophages (Peltier et al. 2020), as well as morphological changes such as the transformation from spiral to coccoid form in *Helicobacter pylori* (El Mortaji et al. 2020). Additionally, there are instances where cell death may occur for the benefit of the surrounding cells, a phenomenon known as altruistic cell death (Germain-Amiot et al. 2019, Sayed et al. 2012) (Figure 5).

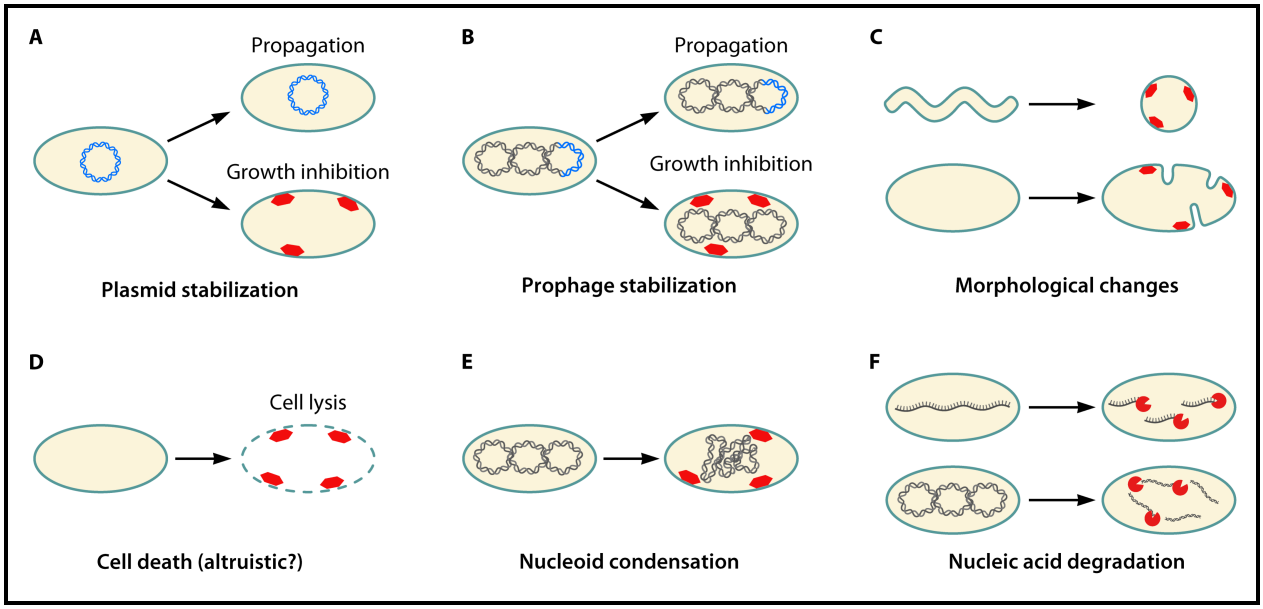

Figure 5: Cellular effects and biological functions of type I toxins
(A) Plasmid stabilization. If the plasmid (blue) and its type I TA system is not inherited by a progeny cell, the unstable antitoxin RNA is degraded and the toxin (red) is produced. Most type I toxins are small membrane proteins that cause growth inhibition (and probably cell death). If the plasmid is retained, the antitoxin prevents toxin production and the cell is able to propagate. **(B** Prophage stabilization follows the same principle as described for plasmid stabilization. The type I toxin (red) inhibits growth upon loss of the prophage (blue). **(C)** Morphological changes. If the type I toxin (red) is produced, it causes morphological changes, such as the transition from spiral-shaped to coccoid cells or cell division defects that are concomitant with membrane invaginations. **(D)** Cell death. If the type I toxin (red) is produced in sufficiently high amounts, it may induce cell lysis via membrane permeabilization. Cell death by lysis presumably represent an altruistic behavior of individual cells that benefits the remaining population. **(E)** Nucleoid condensation. Expression of the type I toxin (red) leads to compaction of chromosomal DNA. **(F)** Nucleic acid degradation. Some type I toxins (red) are cytosolic proteins that function as endonucleases and degrade either DNA or RNA. (Shore et al. 2024)

1.3.4 Membrane-targeting toxins and persistence

Membrane-targeting toxins represent one of the most well-characterized components of type I TA systems. These toxins integrate into the bacterial membrane, resulting in depolarization and disruption of the membrane's integrity (Unoson & Wagner 2008). In a healthy bacterial cell, the membrane remains polarized, which is essential for maintaining cellular homeostasis, including nutrient uptake and ATP production via the proton motive force (Panta & Doerrler 2021).

One of the earliest consequences of membrane depolarization is a reduced capability of the cell to take up drugs and other molecules that rely on active transport mechanisms. This reduction in drug uptake is of significant importance in the context of antibiotic persistence, as it can result in an overall decline in antibiotic efficacy (Su et al. 2022). Furthermore, membrane depolarization may result in ATP efflux, whereby the loss of membrane integrity causes the uncontrolled release of ATP from the cell. The massive loss of ATP from the cell results in a dormant state, which eventually promotes a persister state. As an example, in *E. coli*, the HokB toxin creates pores in the bacterial membrane, resulting in ATP efflux and triggering a persistent state without immediate cell death (Wilmaerts et al. 2018). Membrane-targeting toxins can also induce persistence through ATP depletion, as observed with the TisB toxin. By disrupting the proton motive force, TisB impairs ATP synthesis, further reducing the cell's metabolic activity. This state of low energy and reduced metabolic function allows the cell to survive in the presence of antibiotics, which typically target actively growing cells (Berghoff & Wagner 2019) (Figure 6).

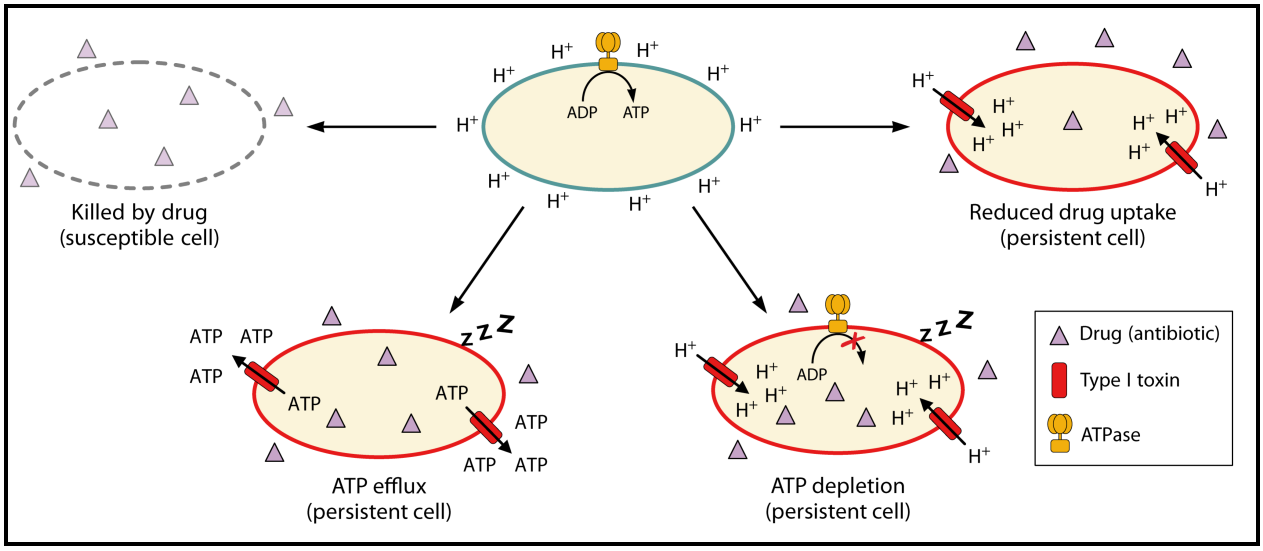

Figure 6: Mechanisms of membrane-targeting toxins
Induction of persistence by type I toxins. An active cell has a polarized membrane (as indicated by protons at the outside of its cytoplasmic membrane). The proton gradient is used by ATPases to produce ATP (top middle). Active cells are susceptible and rapidly killed when exposed to drugs (top-left). Some type I toxins are pore-forming membrane toxins (red) with the potential to promote a drug-tolerant persister state. Type I toxins may impede drug uptake due to depolarization of the cytoplasmic membrane (upper-right). In addition, depolarization inhibits ATP production and leads to ATP depletion (bottom-right). Alternatively, type I toxins form pores that are capable of promoting ATP efflux (bottom-left). Decreasing ATP levels cause cellular inactivity, which prevents killing by drugs. (Shore et al. 2024)

1.3.5 Nucleic acid-targeting type I toxins

In addition to membrane-targeting toxins (Unoson & Wagner 2008), some type I TA systems produce toxins that target nucleic acids, leading to nucleoid condensation (Thompson et al. 2022) and degradation of RNA (Kawano et al. 2007) or DNA (Guo et al. 2014). Such nucleic acid-targeting toxins have the potential to cause significant disruption of essential cellular processes, including replication, transcription, and translation. Nucleoid condensation is the process by which chromosomal DNA becomes highly compacted, thereby limiting access to the transcriptional machinery and effectively halting gene expression. This is frequently a stress response that can result from the indirect effects of toxin activity, such as when the cell's translational machinery is disrupted, leading to a secondary response that includes nucleoid condensation (Thompson et al. 2022). Moreover, nucleic acid-targeting toxins can directly degrade RNA or DNA, leading to a disruption of cellular functions and, in many cases, cell death (Unoson & Wagner 2008).

1.3.6 Regulation of the *tisB/istR-1* toxin-antitoxin system

The *tisB/istR-1* system represents a well-studied example of a type I TA system in *E. coli*. While the antitoxin gene *istR-1* is constitutively transcribed by the housekeeping sigma factor σ^{70} (Huerta & Collado-Vides 2003, Vogel et al. 2004), transcription of tisB is repressed by LexA, a DNA-binding transcriptional repressor that plays a role in the cellular response to DNA damage (D'Ari 1985, McKenzie et al. 2022, Henestrosa et al. 2000).

The *tisB* gene is only be transcribed when its repressor, LexA, undergoes self-cleavage. This self-cleavage is triggered when the RecA co-protease binds to single-stranded DNA at sites of DNA damage to form a filament (Chen et al. 2008, Cox 2007). The interaction between RecA, the damaged DNA, and LexA initiates the self-cleavage process, leading to the dissociation of LexA from its DNA targets and allowing the transcription of *tisB*. This regulation upon DNA damage is known as the SOS response and is mainly responsible for the induction of genes with a function in DNA repair (Giese et al. 2008, Little 1991).

However, the *tisB* primary transcript (+1 mRNA) is not translationally active, as it forms a secondary structure that obstructs ribosome binding. It is only after undergoing processing, whereby the first 41 nucleotides of the 5'UTR are removed, that the active +42 mRNA becomes available for translation or inhibition through the antitoxin IstR-1 (Figure 7). The processing event results in the exposure of a single-stranded region upstream of the RBS. This region may serve as a ribosome standby site (RSS) for translation or alternatively, as a translation inhibition site for the IstR-1 antitoxin (Darfeuille et al. 2007). The regulatory outcome likely depends on the ratio of +42 mRNA to IstR-1 in individual cells. In the event of a greater quantity of antitoxin relative to +42 mRNA, the translation process is impeded. IstR-1 effectively prevents the 30S subunit from binding by forming extensive and perfect base pairing with the single-stranded RSS. This inhibition is further reinforced by RNase III-mediated cleavage of the RNA duplex, which results in the generation of the translationally inactive +106 mRNA (Darfeuille et al. 2007, Unoson & Wagner 2008, Vogel et al. 2004).

In the event of a smaller quantity of antitoxin relative to +42 mRNA, the translation process is

initiated. The 30S ribosomal subunit is capable of binding to the single-stranded RSS and interacts with a structure at the 5' end in a sequence-unspecific manner, independent of the initiator tRNA ($tRNA^{fMet}$). This binding event is crucial for the translation process and is mediated by the ribosomal protein S1, which anchors the 30S subunit to the designated RSS. S1 is essential for directional unfolding of the mRNA, allowing the ribosome to access the sequestered RBS and initiate translation (De Smit & Van Duin 2003, Duval et al. 2013, Marzi et al. 2007, Sterk et al. 2018, Studer & Joseph 2006).

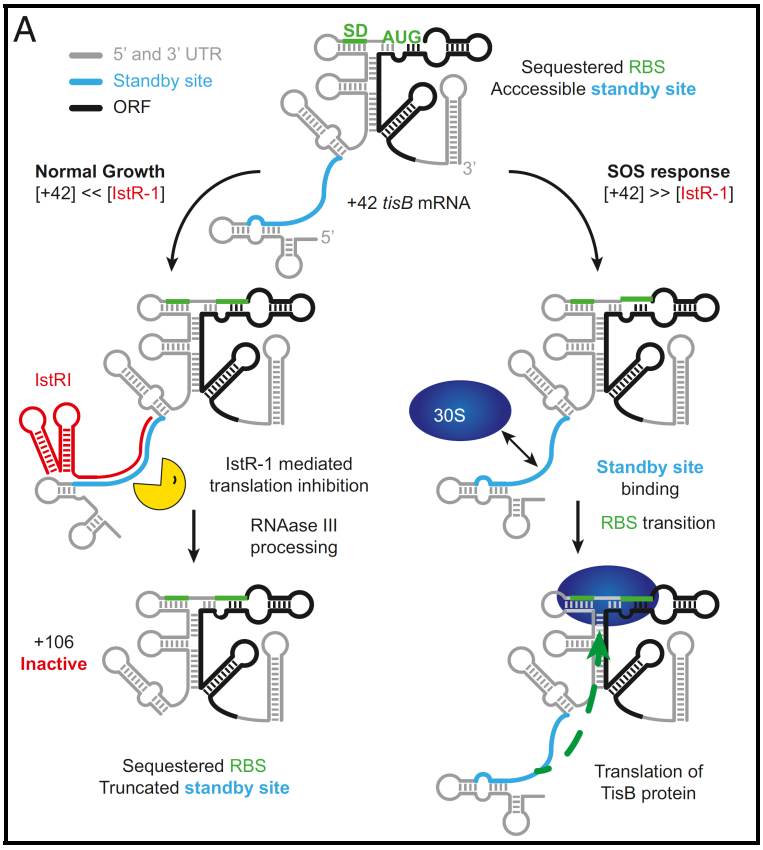

Figure 7: Regulation of *tisB/istR-1* toxin-antitoxin system in *E. coli*
Schematic secondary structure of the +42 mRNA: 5' and 3' UTR (gray), ORF (black), standby site (blue), SD and AUG (green).
(Romilly et al. 2019)

1.4 Protein aggregation in bacteria

The aggregation of proteins in bacteria is a well-documented response to a variety of environmental stresses, including temperature (Kitagawa et al. 2000, Kuczyn et al. 2002), oxidative stress (Dahl et al. 2015), energy deprivation (Pu et al. 2019), and exposure to antibiotics (Bollen et al. 2021, Ling et al. 2012). In the absence of stress, proteins are correctly folded and functional, with the assistance of molecular chaperones such as DnaK/DnaJ and GroEL/GroES (Markossian & Kurganov 2004). In the event that this process is unsuccessful, the proteins are degraded by proteases such as ClpP. These quality control systems are responsible for maintaining protein homeostasis by either refolding misfolded proteins or degrading those that are beyond repair (Kress et al. 2009). However, during periods of cellular stress, these protective mechanisms may become insufficient, resulting in the accumulation of misfolded proteins. In such instances, the misfolded proteins, due to their exposed hydrophobic regions, tend to aggregate into larger, insoluble complexes (Dougan et al. 2002). While protein aggregation can disrupt normal cellular functions, it also serves as a passive survival mechanism, particularly under extreme stress conditions (Ventura & Villaverde 2006).

When bacteria are exposed to environmental stressors, depletion of ATP is often observed, which subsequently restricts the energy available to maintain protein quality control. As the capacity of molecular chaperones and proteases to manage misfolded proteins is reduced, these proteins undergo aggregation (Pu et al. 2019). The formation of aggregates has the potential to disrupt a number of cellular functions, including transcription, translation, and DNA replication. This can occur by obstructing the machinery involved in these processes. The disruption of these functions results in the cell entering a dormant state, with reduced metabolic activity (Pu et al. 2019). This makes them less susceptible to antibiotics that target processes in actively dividing cells (Lewis 2010). The formation of protein aggregates may prolong the dormant state, thereby enabling cells to withstand hostile conditions. Once the aggregates have been dissolved, the cells are able to resume their normal cellular functions when the conditions have improved (Bollen et al. 2021).

1.4.1 Protein aggregation as a result of *tisB* expression

This chapter will mainly be an overview of the major insights of the study presented in chapter 2 “Protein aggregation is a consequence of the dormancy-inducing membrane toxin TisB in *Escherichia coli*” by Leinberger et al. (2024).

1.4.1.1 Moderate *tisB* expression as a model for studying dormancy and bacterial survival

One of the important advancements of this study is the development of a moderate expression system for the *tisB* gene. The system avoids the high levels of TisB toxicity, typically associated with overexpression, while still inducing dormancy. This contrasts with previous studies, such as Unoson & Wagner (2008), where overexpression of *tisB* from the active +42 mRNA led to excessive membrane disruption and cell death. By moderating expression levels, we achieve a more physiologically relevant model, allowing us to study the role of TisB in dormancy without

inducing high toxicity. This moderation is achieved by introducing an artificial 5' UTR that lacks a SD sequence.

Despite of the lacking SD sequence, TisB is still produced in sufficient amounts to cause depolarization, ATP depletion, growth inhibition, and persister formation, effects that were already described earlier (Berghoff et al. 2017, Dörr et al. 2010, Gurnev et al. 2012, Unoson & Wagner 2008). The disruption of the proton motive force and depletion of cellular energy underlie TisB-induced dormancy, reinforcing the toxin's role in promoting bacterial survival under stressful conditions such as antibiotic treatment.

1.4.1.2 TisB-dependent protein aggregation and its impact on dormancy duration

In response to TisB-induced stress, RNA-sequencing revealed the upregulation of several chaperone genes, including ibpAB and spy, confirming previous observations (Fozo et al. 2008, Spanka et al. 2019). These chaperones play an essential role in stabilizing misfolded proteins, which suggests that protein aggregation is a consequence of *tisB* expression.

A key novel contribution of our study is the demonstration that *tisB* expression indeed leads to protein aggregation in the cytoplasm. Using a fluorescent reporter system in which the small heat shock protein IbpA is fused to a monomeric superfolder green fluorescent protein (IbpA-msfGFP) constructed by Govers et al. (2018), we validate that cytoplasmic protein aggregation occurs in TisB-producing cells. This result builds upon previous work by Govers et al. (2018),who demonstrated that protein aggregates could serve as epigenetic markers of past stressful encounters in *E. coli*. Our findings confirm that TisB-induced aggregation is a functional response to severe intracellular stress.

Furthermore, we explore the interaction between the DNA-damaging antibiotic ciprofloxacin and TisB. It is already known that antibiotics like ciprofloxacin promote the formation of protein aggregates (Butler et al. 2023). We have now identified the TisB toxin as a molecular factor involved in this aggregation process.

It was established that the presence of protein aggregates correlates with an extended dormancy duration, supporting the idea that protein aggregates are integral to the maintenance of the TisB-dependent persister state. This finding is consistent with the work of Pu et al. (2019), who demonstrated that ATP-dependent protein aggregation regulates the depth of bacterial dormancy, which is crucial for antibiotic tolerance (Figure 8). Our study further highlights the functional importance of protein aggregates in controlling the duration of dormancy and their contribution to long-term bacterial survival. This is further validated by chaperone overexpression that leads to a reduced duration of dormancy and earlier recovery. These findings support the spiderweb hypothesis, suggesting that TisB-induced protein aggregation is one of several factors that together promote bacterial persistence Figure 3.

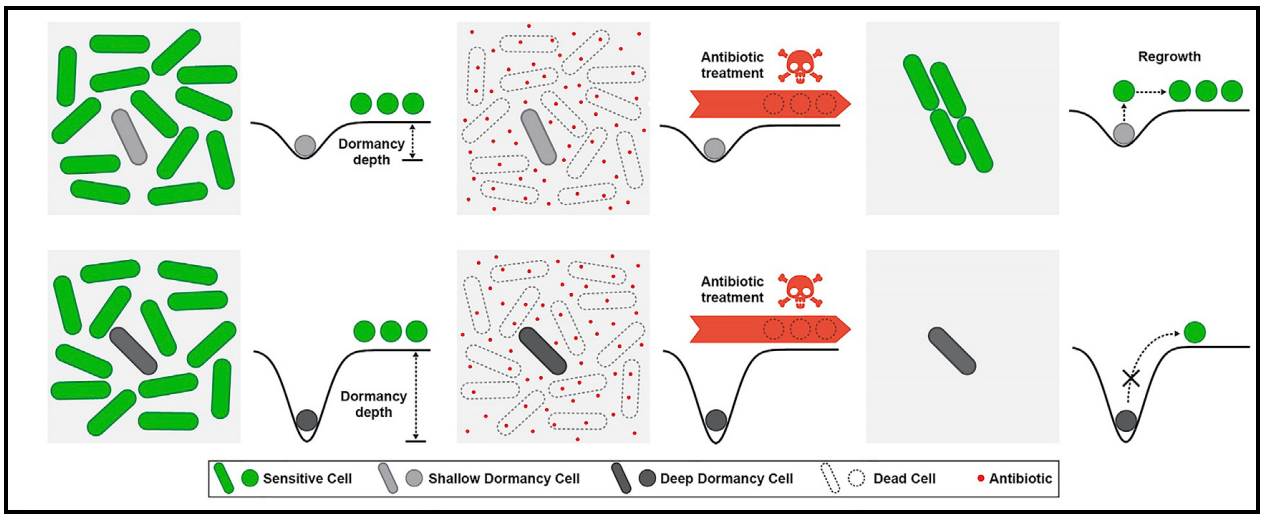

Figure 8: Bacterial dormancy depth affects antibiotic tolerance and regrowth
Active cells (green) are killed during antibiotic treatment, indicated by red dots. Dormant cells (grey) with different dormancy depth survive the treatment. Depending on the dormancy depth cells can regrow (light grey) or stay viable but non-culturable (VBNC) (dark grey).
(Pu et al. 2019)

1.4.1.3 Proteome analysis of TisB-dependent aggregates

To determine whether the protein aggregates in question were composed of specific proteins, a proteomic analysis was performed. We identified several proteins that were enriched in TisB-dependent protein aggregates, including chaperones IbpA and IbpB, which confirms a successful protein aggregation enrichment method. Moreover, a group of seven proteins from cryptic prophages was identified. It is currently unclear whether this has a biological function or if it is merely a random occurrence.

Aside from these findings, no unique characteristics of the aggregated proteins were detected that could provide further insights into the mechanisms of aggregate formation or their biological roles.

1.4.1.4 Recovery from TisB-induced dormancy

Our study offers crucial insights into the mechanisms through which TisB induces dormancy and persistence in *E. coli*, particularly through the induction of protein aggregation. These findings contribute to a broader understanding of the mechanisms by which bacterial cells survive during prolonged stress and highlight the multifaceted role of TisB in the persistence phenotype. But how do cells recover from TisB-induced dormancy? It is suggested that the recovery process is driven by a coordinated stress response, with chaperones playing a central role. This is supported by the reduced duration of dormancy when chaperons are overexpressed prior to the antibiotic treatment in this study. The significance of small heat shock proteins is further validated by the findings of Żwirowski et al. (2017). The authors demonstrated that ATP-independent chaperones form assemblies with misfolded proteins, preventing the formation of larger aggregates and marking the misfolded proteins for subsequent action by ATP-dependent chaperones for solubilization and refolding. This is consistent with the observation of ATP depletion upon TisB expression (Unoson & Wagner 2008), which limits the activity of ATP-dependent chaperones and could delay the disag-

gregation of protein aggregates. Only ATP-independent chaperones, such as Spy, IbpA, and IbpB, would be able to function under these conditions and mark misfolded proteins for subsequent action. After membrane repolarization, a crucial step in the awakening of persister cells (Wilmaerts et al. 2019), ATP-dependent chaperones could resume their role in solubilizing and refolding these marked aggregates, facilitating the awakening of persister cells.

1.5 Functional features of type I toxins

Given that toxins of type I TA systems typically integrate into the inner membrane, a transmembrane domain represents a crucial functional component. The domain is primarily composed of multiple hydrophobic amino acids. The hydrophobic nature of the amino acids in question compels the protein to exit the cytoplasm and enter the lipid bilayer. In the case of TisB, the amino acids that are predominantly present are leucine (L), alanine (A), valine (V), and isoleucine (I) (Figure 9A). It is postulated that the toxin initiates pore formation by binding to the negatively charged inner membrane via its positively charged C-terminus, thereby establishing an initial electrostatic interaction. Subsequently, hydrophobic interactions facilitate membrane integration as a result of the initial attachment (Scheglmann et al. 2002, Cao et al. 2023). Afterwards, oligomerization can occur. It seems reasonable to assume that amino acids with opposing properties form salt bridges or hydrogen bonds, and that this process is essential for oligomerization. During the process of oligomerization, the toxin forms a pore in the inner membrane (Geny & Popoff 2006). In the case of the toxin HokB a dimer is stabilized by a disulfide bridge which is catalyzed by a periplasmic oxidoreductase DsbA between two periplasmic cysteine (C46) residues (Wilmaerts et al. 2019).

1.5.1 Essential amino acids for cellular effects caused by TisB

This chapter will mainly be an overview of the major insights of the study presented in chapter 3 “Relevance of charged and polar amino acids for functionality of membrane toxin TisB” by Leinberger & Berghoff (2024).

1.5.1.1 Role of lysine 12 and glutamine 19

The study highlights the importance of lysine 12 (K12) and glutamine 19 (Q19) for the functionality of TisB. Both amino acids are integral to the transmembrane domain of TisB (Figure 9B). Substitution of either of these amino acids with leucine results in the complete loss of the ability of TisB to inhibit cell growth, deplete ATP, and cause protein aggregation. Lysine 12, in particular, is essential for maintaining TisB’s activity across several functional assays, including persistence after ciprofloxacin treatment. The importance of these amino acids is consistent with the “charge-zipper” model (Figure 9A) postulated by Schneider et al. (2019) and Steinbrecher et al. (2012), in which Q19 of two antiparallel TisB form a hydrogen bond and each K12 forms a salt bridge with D22. In this charged-zipper model, formation of a TisB tetramer, or more specifically a dimer of dimers, which would allow protons to pass across the inner membrane along a wire of water molecules within the pore, is postulated (Figure 9B).

However, the study also presents evidence that calls the above model into question. For example,

the substitution of K12D and D22K should have permitted the formation of compensatory salt bridges. Nevertheless, this TisB variant has lost all of its functional capabilities. Furthermore, the substitution of K12 with arginine, which possesses analogous amino acid properties, should have been capable of forming salt bridges. However, this TisB variant was also found to be non-functional.

The significance of K12 for the functionality of TisB is further highlighted when examining persister levels. The chromosomal substitution of this amino acid with leucine has the same effect as the complete deletion of *tisB*. The formation of persister cells is significantly decreased. Furthermore, the few persister cells that do form have a significant reduced appearance time after an antibiotic treatment, which indicates a reduced duration of dormancy.

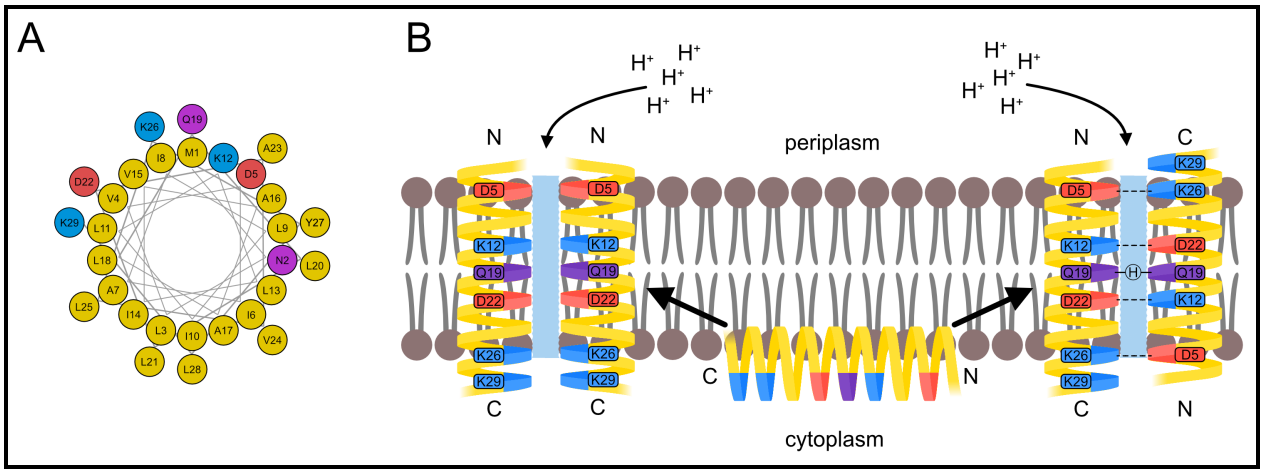

Figure 9: Parallel and antiparallel (charge-zipper) conformation of TisB
(A) Helical wheel projection of TisB. Amino acid color code: nonpolar (yellow), polar (purple), acidic (red), and basic (blue). (Leinberger et al. 2024) **(B)** Models of TisB pore formation. Same color code as in (a). The initial attachment of TisB to the inner membrane is followed by its insertion and oligomerization within the inner membrane, which ultimately leads to pore formation. In the context of the charge-zipper model (right), the formation of a tetramer (dimer of dimers) is proposed. The antiparallel orientation of the dimers is stabilized by salt bridges between opposing charges (dotted lines) and a Q19 hydrogen bond (H). The alternative model (left) postulates the oligomerization of an as yet unidentified number of monomers that are parallel to one another. This is caused by the C-terminal amino acids K26 and K29, which form an anker to the cytoplasm. In both models, protons from the periplasm can enter the cytoplasm along a wire of water molecules (light blue).

1.5.1.2 C-terminal lysines and their influence on TisB toxicity

In addition to K12 and Q19, the C-terminal lysins 26 and 29 (K26 and K29) appear to play a significant role in TisB functionality. A single substitution of one of these lysins has a minimal impact on TisB functionality. However, when both residues are substituted with leucine, TisB is rendered non-functional. This may reinforce the charge-zipper model, in which aspartic acid 5 (D5) can form a salt bridge with either of those amino acids. Furthermore, the substitution of both lysines with aspartic acid leads to a compromised protein that is not fully functional or even non-functional,

probably because the formation of D5-K26 and D5-K29 salt bridges is disrupted. However, mutation of D5 does not compromise TisB functionality, arguing against a major importance of D5-K26 and D5-K29 salt bridges.

Alternatively, the C-terminal lysines may play a key role in the initial contact of TisB with the negatively charged inner membrane. Similarly, substitution of the positively charged K29 of ZorO with a negatively charged glutamate has been observed to result in a loss of function (Bogati et al. 2022). This suggests that the C-terminus has potential to assist in membrane orientation (Scheglmann et al. 2002, Seppälä et al. 2010, Soutourina 2019), as has been suggested for other bacterial toxins, like Fst (Nonin-Lecomte et al. 2021). Furthermore, the positive inside rule could be interpreted as supporting the presented alternative TisB orientation (Figure 9). This rule is based on the observation that the majority of proteins have their positively charged residues located within the cytoplasm and that positive residues that are in closer proximity to the transmembrane domain have a more pronounced effect on the orientation of the protein (Fontaine et al. 2011). Given that TisB contains positively charged K26 and K29 residues within its C-terminal domain, the resulting C_{in} N_{out} orientation would be in accordance with the positive inside rule (Figure 9).

The conservation of specific amino acids across species provides preliminary evidence that some are more crucial for functionality than others. This study confirms the importance of the individual conserved amino acids mentioned above, specifically K12, Q19, K26, and K29. Additionally, our findings support and also challenge the charge-zipper model. Further investigation is required to ascertain the model's viability.

1.6 Conclusion

This thesis has established fundamental insights into the functionality of TisB in *E. coli*, specifically its role in stabilizing dormancy through promotion of protein aggregation. By utilizing a moderate expression system, this study enabled an in-depth exploration of TisB's physiological role while minimizing excessive toxicity. This approach uncovered how TisB influences the cellular stress response and enhances survival under antibiotic pressure.

Building upon these findings, future research should further investigate whether the proteins identified in TisB-dependent aggregates share common characteristics. In particular, it would be beneficial to determine if DNA-binding proteins play a role in forming protective aggregates around DNA to prevent further damage. This hypothesis provides a basis for investigating whether protein aggregation functions as an active adaptive mechanism to safeguard cellular structures or merely represents a passive strategy for stabilizing persistence.

Furthermore, additional investigation is required to elucidate the role of chaperones in response to TisB-induced stress. The observed upregulation of chaperone genes, such as ibpAB and spy, and the reduction in recovery time when these chaperones are overexpressed suggest that chaperones may play a role in the recovery from ciprofloxacin-induced stress. Chaperones such as IbpAB and Spy are likely to play an essential role in reducing the effects of TisB-dependent aggregation by assisting in the refolding or clearance of misfolded proteins, which ultimately promotes a faster exit from dormancy. Further investigation into the precise mechanisms by which other chaperones facilitate the management of TisB-induced stress could provide a deeper understanding of the cellular processes that support bacterial persistence and recovery. Moreover, an understanding of the potential interaction partners of TisB could provide crucial insights into its integration and stabilization within the inner membrane. For example, the identification of helper proteins that facilitate TisB's membrane assembly, stabilize its presence, or assist in pore disassembly could lead to significant advances in our understanding of regulation of toxin activity. An investigation of whether these interactions necessitate the specific amino acids identified as crucial for TisB functionality could clarify whether TisB operates independently or relies on other cellular factors.

A key task for future research is to verify or refute the charge-zipper model, which postulates salt bridges and hydrogen bonds as stabilizing forces within the TisB oligomer. In case that the model is disproven: What are the alternatives? A parallel orientation of TisB monomers is conceivable, and it would be important to investigate the stabilization mechanisms, such as potential unknown interaction partners that may be responsible for maintaining the oligomeric structure. The identification of any necessary amino acids for such interactions would provide further insight into the functional architecture of TisB within the membrane. By exploring these questions, future work can build on the findings of this thesis to uncover broader implications of TisB's role in bacterial dormancy and persistence, potentially informing new strategies to combat chronic bacterial infections.

1.7 List of references

Aakre, C. D., Phung, T. N., Huang, D. & Laub, M. T. (2013), 'A bacterial toxin inhibits dna replication elongation through a direct interaction with the sliding clamp', *Molecular Cell* **52**, 617–628.

Alekshun, M. N. & Levy, S. B. (2007), 'Molecular mechanisms of antibacterial multidrug resistance', *Cell* **128**, 1037–1050.

Ayrapetyan, M., Williams, T. C. & Oliver, J. D. (2015), 'Bridging the gap between viable but non-culturable and antibiotic persistent bacteria'.

Ayrapetyan, M., Williams, T. & Oliver, J. D. (2018), 'Relationship between the viable but nonculturable state and antibiotic persister cells', *Journal of Bacteriology* **200**.

Balaban, N. Q., Helaine, S., Lewis, K., Ackermann, M., Aldridge, B., Andersson, D. I., Brynildsen, M. P., Bumann, D., Camilli, A., Collins, J. J., Dehio, C., Fortune, S., Ghigo, J. M., Hardt, W. D., Harms, A., Heinemann, M., Hung, D. T., Jenal, U., Levin, B. R., Michiels, J., Storz, G., Tan, M. W., Tenson, T., Melderen, L. V. & Zinkernagel, A. (2019), 'Definitions and guidelines for research on antibiotic persistence', *Nature Reviews Microbiology* **17**, 441–448.

Balaban, N. Q., Merrin, J., Chait, R., Kowalik, L. & Leibler, S. (2004), 'Bacterial persistence as a phenotypic switch', *Science* **305**, 1622–1625.

Barrangou, R., Fremaux, C., Deveau, H., Richards, M., Boyaval, P., Moineau, S., Romero, D. A. & Horvath, P. (2007), 'Crispr provides acquired resistance against viruses in prokaryotes', *Science* **315**, 1709–1712.

Berghoff, B. A., Hoekzema, M., Aulbach, L. & Wagner, E. G. H. (2017), 'Two regulatory rna elements affect tisb-dependent depolarization and persister formation', *Molecular Microbiology* **103**, 1020–1033.

Berghoff, B. A. & Wagner, E. G. H. (2019), *Persister Formation Driven by TisB-Dependent Membrane Depolarization*, Springer International Publishing, pp. 77–97.

Bogati, B., Wadsworth, N., Barrera, F. & Fozo, E. M. (2022), 'Improved growth of escherichia coli in aminoglycoside antibiotics by the zor-orz toxin-antitoxin system', *Journal of Bacteriology* **204**.

Bollen, C., Dewachter, L. & Michiels, J. (2021), 'Protein aggregation as a bacterial strategy to survive antibiotic treatment', *Frontiers in Molecular Biosciences* **8**.

Brantl, S. (2009), 'Bacterial chromosome-encoded small regulatory rnas', *Future Microbiology* **4**, 85–103.

Brantl, S. (2012), 'Acting antisense: Plasmid- and chromosome-encoded srnas from gram-positive bacteria', *Future Microbiology* **7**, 853–871.

Butler, G., Bos, J., Austin, R. H., Amend, S. R. & Pienta, K. J. (2023), 'Escherichia coli survival in response to ciprofloxacin antibiotic stress correlates with increased nucleoid length and effective misfolded protein management', *Royal Society Open Science* **10**.

Cao, Z., Zhao, L., Yan, T. & Liu, L. (2023), 'Effects of c-terminal lys-arg residue of aapa1 protein on toxicity and structural mechanism', *Toxins* **15**.

Chen, Z., Yang, H. & Pavletich, N. P. (2008), 'Mechanism of homologous recombination from the reca-ssdna/dsdna structures', *Nature* **453**, 489–494.

Cheng, H. Y., Soo, V. W., Islam, S., McAnulty, M. J., Benedik, M. J. & Wood, T. K. (2014), 'Toxin ghot of the ghot/ghos toxin/antitoxin system damages the cell membrane to reduce adenosine triphosphate and to reduce growth under stress', *Environmental microbiology* **16**, 1741–1754.

Christensen, S. K., Mikkelsen, M., Pedersen, K. & Gerdes, K. (2001), 'Rele, a global inhibitor of translation, is activated during nutritional stress', *Proc Natl Acad Sci U S A* **98**, 14328–14333. **URL:** *www.pnas.orgcgidoi10.1073pnas.251327898*

Christensen, S. K., Pedersen, K., Hansen, F. G. & Gerdes, K. (2003), 'Toxin-antitoxin loci as stress-response-elements: Chpak/mazf and chpbk cleave translated rnas and are counteracted by tmrna', *Journal of Molecular Biology* **332**, 809–819.

Cox, M. M. (2007), 'Regulation of bacterial reca protein function', *Critical Reviews in Biochemistry and Molecular Biology* **42**, 41–63.

Dahl, J. U., Gray, M. J. & Jakob, U. (2015), 'Protein quality control under oxidative stress conditions', *Journal of Molecular Biology* **427**, 1549–1563.

Darfeuille, F., Unoson, C., Vogel, J. & Wagner, E. G. H. (2007), 'An antisense rna inhibits translation by competing with standby ribosomes', *Molecular Cell* **26**, 381–392.

D'Ari, R. (1985), 'The sos system', *BIOCHIMIE* **67**, 343–347.

De Smit, M. H. & Van Duin, J. (2003), 'Translational standby sites: How ribosomes may deal with the rapid folding kinetics of mrna', *Journal of Molecular Biology* **331**, 737–743.

Dougan, D. A., Mogk, A. & Bukau, B. (2002), 'Protein folding and degradation in bacteria: To degrade or not to degrade? that is the question', *CMLS, Cell. Mol. Life Sci* **59**, 1607–1616.

Durand, S., Gilet, L. & Condon, C. (2012), 'The essential function of b. subtilis rnase iii is to silence foreign toxin genes', *PLoS Genetics* **8**.

Duval, M., Korepanov, A., Fuchsbauer, O., Fechter, P., Haller, A., Fabbretti, A., Choulier, L., Micura, R., Klaholz, B. P., Romby, P., Springer, M. & Marzi, S. (2013), 'Escherichia coli ribosomal protein s1 unfolds structured mrnas onto the ribosome for active translation initiation', *PLoS Biology* **11**.

Dörr, T., Vulić, M. & Lewis, K. (2010), 'Ciprofloxacin causes persister formation by inducing the tisb toxin in escherichia coli', *PLoS Biology* **8**.

Edelmann, D., Leinberger, F. H., Schmid, N. E., Oberpaul, M., Schäberle, T. F. & Berghoff, B. A. (2021), 'Elevated expression of toxin tisb protects persister cells against ciprofloxacin but enhances susceptibility to mitomycin c', *Microorganisms* **9**.

El Mortaji, L., Tejada-Arranz, A., Rifflet, A., Boneca, I. G., Pehau-Arnaudet, G., Radicella, J. P., Marsin, S. & Reuse, H. D. (2020), 'A peptide of a type i toxinantitoxin system induces helicobacter pylori morphological transformation from spiral shape to coccoids', *PNAS* **117**, 31398–31409.
URL: *https://www.pnas.org/lookup/suppl/*

Fineran, P. C., Blower, T. R., Foulds, I. J., Humphreys, D. P., Lilley, K. S. & Salmond, G. P. C. (2009), 'The phage abortive infection system, toxin, functions as a protein-rna toxin-antitoxin pair'.
URL: *www.pnas.org/cgi/content/full/*

Fontaine, F., Fuchs, R. T. & Storz, G. (2011), 'Membrane localization of small proteins in escherichia coli', *Journal of Biological Chemistry* **286**, 32464–32474.

Fozo, E. M., Kawano, M., Fontaine, F., Kaya, Y., Mendieta, K. S., Jones, K. L., Ocampo, A., Rudd, K. E. & Storz, G. (2008), 'Repression of small toxic protein synthesis by the sib and ohsc small rnas', *Molecular Microbiology* **70**, 1076–1093.

Fozo, E. M., Makarova, K. S., Shabalina, S. A., Yutin, N., Koonin, E. V. & Storz, G. (2010), 'Abundance of type i toxin-antitoxin systems in bacteria: Searches for new candidates and discovery of novel families', *Nucleic Acids Research* **38**, 3743–3759.

Fraikin, N., Goormaghtigh, F. & Melderen, L. V. (2020), 'Type ii toxin-antitoxin systems: Evolution and revolutions', *Journal of Bacteriology* **202**.
URL: *https://doi.org/10.1128/jb.00763-19*

Geny, B. & Popoff, M. R. (2006), 'Bacterial protein toxins and lipids: pore formation or toxin entry into cells', *Biology of the Cell* **98**, 667–678.

Gerdes, K. (2024), 'Diverse genetic contexts of hica toxin domains propose a role in anti-phage defense', *mBio* **15**.

Gerdes, K., Bech1, F. W., Jorgensen', S. T., Lobner-Olesen, A., Rasmussen2, P. B., Atlung, T., Boe, L., Karlstrom1, O., Molin, S. & Meyenburg, K. V. (1986), 'Mechanism of postsegregational killing by the hok gene product of the parb system of plasmid rl and its homology with the relf gene product of the e. coli relb operon', *The EMBO Journal* **5**, 2023–2029.

Gerdes, K. & Rasmussen, P. B. (1986), 'Unique type of plasmid maintenance function: Postsegregational killing of plasmid-free cells (plasmid stabllity/parb+ of plasmid ri/regulated kilhing/phage a promoter pr)', *Biochemistry* **83**, 3116–3120.

Gerdes, K., Thisted, T. & Martinussen, J. (1990), 'Mechanism of post-segregational killing by the hoklsok system of plasmid r1: sok antisense rna regulates formation of a hok mrna species correlated with killing of plasmid-free cells', *Molecular Microbiology* **4**, 1807–1818.

Gerdes, K. & Wagner, E. G. H. (2007), 'Rna antitoxins', *Current Opinion in Microbiology* **10**, 117–124.

Germain-Amiot, N., Augagneur, Y., Camberlein, E., Nicolas, I., Lecureur, V., Rouillon, A. & Felden, B. (2019), 'A novel staphylococcus aureus cis-trans type i toxin-antitoxin module with dual effects on bacteria and host cells', *Nucleic Acids Research* **47**, 1759–1773.

Giese, K. C., Michalowski, C. B. & Little, J. W. (2008), 'Reca-dependent cleavage of lexa dimers', *Journal of Molecular Biology* **377**, 148–161.

Govers, S. K., Mortier, J., Adam, A. & Aertsen, A. (2018), 'Protein aggregates encode epigenetic memory of stressful encounters in individual escherichia coli cells', *PLoS Biology* **16**.

Guo, Y., Quiroga, C., Chen, Q., McAnulty, M. J., Benedik, M. J., Wood, T. K. & Wang, X. (2014), 'Ralr (a dnase) and rala (a small rna) form a type i toxin-antitoxin system in escherichia coli', *Nucleic Acids Research* **42**, 6448–6462.

Gurnev, P. A., Ortenberg, R., Dörr, T., Lewis, K. & Bezrukov, S. M. (2012), 'Persister-promoting bacterial toxin tisb produces anion-selective pores in planar lipid bilayers', *FEBS Letters* **586**, 2529–2534.

Hampton, H. G., Watson, B. N. & Fineran, P. C. (2020), 'The arms race between bacteria and their phage foes', *Nature* **577**, 327–336.

Harms, A., Brodersen, D. E., Mitarai, N. & Gerdes, K. (2018), 'Toxins, targets, and triggers: An overview of toxin-antitoxin biology', *Molecular Cell* **70**, 768–784.

Hayes, F. (2003), 'Toxins-antitoxins: Plasmid maintenance, programmed cell death, and cell cycle arrest', *Science* **301**, 1496–1499.
URL: *https://www.science.org*

Henestrosa, A. R. F. D., Ogi, T., Aoyagi, S., Chafin, D., Hayes, J. J., Ohmori, H. & Woodgate, R. (2000), 'Identification of additional genes belonging to the lexa regulon in escherichia coli', *Molecular Microbiology* **35**, 1560–1572.

Huerta, A. M. & Collado-Vides, J. (2003), 'Sigma70 promoters in escherichia coli: Specific transcription in dense regions of overlapping promoter-like signals', *Journal of Molecular Biology* **333**, 261–278.

Jurėnas, D., Fraikin, N., Goormaghtigh, F. & Melderen, L. V. (2022), 'Biology and evolution of bacterial toxin–antitoxin systems', *Nature Reviews Microbiology* **20**, 335–350.

Jurėnas, D. & Van Melderen, L. (2020), 'The variety in the common theme of translation inhibition by type ii toxin–antitoxin systems', *Frontiers in Genetics* **11**.

Kawano, M., Aravind, L. & Storz, G. (2007), 'An antisense rna controls synthesis of an sos-induced toxin evolved from an antitoxin', *Molecular Microbiology* **64**, 738–754.

Kawano, M., Oshima, T., Kasai, H. & Mori, H. (2002), 'Molecular characterization of long direct repeat (ldr) sequences expressing a stable mrna encoding for a 35-amino-acid cell-killing peptide and a cis-encoded small antisense rna in escherichia coli', *Molecular Microbiology* **45**, 333–349.

Kitagawa, M., Matsumura, Y. & Tsuchido, T. (2000), 'Small heat shock proteins, ibpa and ibpb, are involved in resistances to heat and superoxide stresses in escherichia coli', *FEMS Microbiology Letters* **184**, 165–171.

Kress, W., Željka Maglica & Weber-Ban, E. (2009), 'Clp chaperone-proteases: structure and function', *Research in Microbiology* **160**, 618–628.

Kuczyn, D., Ska-Wis, ., Ke, S., Matuszewska, E., Lund, P., Taylor, A., Lipin, B., Ska, . & Laskowska, E. (2002), 'The escherichia coli small heat-shock proteins ibpa and ibpb prevent the aggregation of endogenous proteins denatured in vivo during extreme heat shock', *Microbiology* **148**, 1757–1765.

Lee, K. Y. & Lee, B. J. (2016), 'Structure, biology, and therapeutic application of toxin-antitoxin systems in pathogenic bacteria', *Toxins* **8**.

Lehnherr, H., Maguin, E., Jafri, S. & Yarmolinsky, M. (1993), 'Plasmid addiction genes of bacteriophage p1: doc, which causes cell death on curing of prophage, and phd, which prevents host death when prophage is retained', *Journal of Molecular Biology* **233**, 414–428.

Leinberger, F. H. & Berghoff, B. A. (2024), 'Relevance of charged and polar amino acids for functionality of membrane toxin tisb', *Scientific Reports* **14**, 22998.
URL: *https://www.nature.com/articles/s41598-024-73879-7*

Leinberger, F. H., Cassidy, L., Edelmann, D., Schmid, N. E., Oberpaul, M., Blumenkamp, P., Schmidt, S., Natriashvili, A., Ulbrich, M. H., Tholey, A., Koch, H.-G. & Berghoff, B. A. (2024), 'Protein aggregation is a consequence of the dormancy-inducing membrane toxin tisb in escherichia coli', *mSystems* .
URL: *https://journals.asm.org/doi/10.1128/msystems.01060-24*

LeRoux, M. & Laub, M. T. (2022), 'Toxin-antitoxin systems as phage defense elements', *Annual Reviews* **76**, 21–43.
URL: *https://doi.org/10.1146/annurev-micro-020722-*

Lewis, K. (2010), 'Persister cells', *Annual Review of Microbiology* **64**, 357–372.

Li, M., Gong, L., Cheng, F., Yu, H., Zhao, D., Wang, R., Wang, T., Zhang, S., Zhou, J., Shmakov, S. A., Koonin, E. V. & Xiang, H. (2021), 'Toxin-antitoxin rna pairs safeguard crispr-cas systems', *Science* **372**.

Ling, J., Cho, C., Guo, L. T., Aerni, H. R., Rinehart, J. & Söll, D. (2012), 'Protein aggregation caused by aminoglycoside action is prevented by a hydrogen peroxide scavenger', *Molecular Cell* **48**, 713–722.

Little, J. W. (1991), 'Mechanism of specific lexa cleavage: autodigestion and the role of reca coprotease', *Biochimie* **73**, 411–422.

Manikandan, P., Sandhya, S., Nadig, K., Paul, S., Srinivasan, N., Rothweiler, U. & Singh, M. (2022), 'Identification, functional characterization, assembly and structure of toxin type iii toxin-antitoxin complex from e. coli', *Nucleic Acids Research* **50**, 1687–1700.

Marimon, O., Teixeira, J. M., Cordeiro, T. N., Soo, V. W., Wood, T. L., Mayzel, M., Amata, I., García, J., Morera, A., Gay, M., Vilaseca, M., Orekhov, V. Y., Wood, T. K. & Pons, M. (2016), 'An oxygen-sensitive toxin-antitoxin system', *Nature Communications* **7**.

Markossian, K. A. & Kurganov, B. I. (2004), 'Protein folding, misfolding, and aggregation. formation of inclusion bodies and aggresomes', *Biochemistry (Moscow)* **69**, 971–984.

Marzi, S., Myasnikov, A. G., Serganov, A., Ehresmann, C., Romby, P., Yusupov, M. & Klaholz, B. P. (2007), 'Structured mrnas regulate translation initiation by binding to the platform of the ribosome', *Cell* **130**, 1019–1031.

Masuda, H., Tan, Q., Awano, N., Wu, K. P. & Inouye, M. (2012), 'Yeeu enhances the bundling of cytoskeletal polymers of mreb and ftsz, antagonizing the cbta (yeev) toxicity in escherichia coli', *Molecular Microbiology* **84**, 979–989.

McKenzie, A. M., Henry, C., Myers, K. S., Place, M. M. & Keck, J. L. (2022), 'Identification of genetic interactions with prib links the pria/prib dna replication restart pathway to double-strand dna break repair in escherichia coli', *G3: Genes, Genomes, Genetics* **12**.

Meißner, C., Jahn, N. & Brantl, S. (2016), 'In vitro characterization of the type i toxin-antitoxin system bsre/sr5 from bacillus subtilis', *Journal of Biological Chemistry* **291**, 560–571.

Michaux, C., Hartke, A., Martini, C., Reiss, S., Albrecht, D., Budin-Verneuil, A., Sanguinetti, M., Engelmann, S., Hain, T., Verneuil, N. & Giard, J. C. (2014), 'Involvement of enterococcus faecalis small rnas in stress response and virulence', *Infection and Immunity* **82**, 3599–3611.

Mruk, I. & Kobayashi, I. (2014), 'To be or not to be: Regulation of restriction-modification systems and other toxin-antitoxin systems', *Nucleic Acids Research* **42**, 70–86.

Nielsen, A. K., Thorsted, P., Thisted, T., Wagner, E. G. & Gerdes, K. (1991), 'The rifampicin-inducible genes srn6 from f and pnd from r483 are regulated by antisense rnas and mediate plasmid maintenance by kiiling of plasmid-free segregants', *Molecular Microbiology* **5**, 1961–1973.

Nonin-Lecomte, S., Fermon, L., Felden, B. & Pinel-Marie, M. L. (2021), 'Bacterial type i toxins: Folding and membrane interactions', *Toxins* **13**.

Ogura, T. & Hiraga, S. (1983), 'Mini-f plasmid genes that couple host cell division to plasmid proliferation (stable maintenance of plasmid/plasmid partition/host-plasmid interaction/oric plasmid/sos-like function)', *Genetics* **80**, 4784–4788.

Ono, T., Akimoto, S., Ono, K. & Ohnishi, Y. (1986), 'Plasmid genes increase membrane permeability in escherichia coli', *Biochimica et Biophysica Acta (BBA) - Gene Structure and Expression*

867, 81–88.
URL: *https://linkinghub.elsevier.com/retrieve/pii/0167478186900679*

Panta, P. R. & Doerrler, W. T. (2021), 'A link between ph homeostasis and colistin resistance in bacteria', *Scientific Reports* **11**.

Peltier, J., Hamiot, A., Garneau, J. R., Boudry, P., Maikova, A., Hajnsdorf, E., Fortier, L. C., Dupuy, B. & Soutourina, O. (2020), 'Type i toxin-antitoxin systems contribute to the maintenance of mobile genetic elements in clostridioides difficile', *Communications Biology* **3**.

Pu, Y., Li, Y., Jin, X., Tian, T., Ma, Q., Zhao, Z., yuan Lin, S., Chen, Z., Li, B., Yao, G., Leake, M. C., Lo, C. J. & Bai, F. (2019), 'Atp-dependent dynamic protein aggregation regulates bacterial dormancy depth critical for antibiotic tolerance', *Molecular Cell* **73**, 143–156.e4.

Ramisetty, B. C. M. & Santhosh, R. S. (2015), 'Horizontal gene transfer of chromosomal type ii toxin-antitoxin systems of escherichia coli', *FEMS Microbiology Letters* **363**.

Romilly, C., Deindl, S., Gerhart, E. & Wagner, H. (2019), 'The ribosomal protein s1-dependent standby site in tisb mrna consists of a single-stranded region and a 5 structure element', *PNAS* **116**, 15901–15906.

Sayed, N., Nonin-Lecomte, S., Réty, S. & Felden, B. (2012), 'Functional and structural insights of a staphylococcus aureus apoptotic-like membrane peptide from a toxin-antitoxin module', *Journal of Biological Chemistry* **287**, 43454–43463.

Scheglmann, D., Werner, K., Eiselt, G. & Klinger, R. (2002), 'Role of paired basic residues of protein c-termini in phospholipid binding', *Protein Engineering* **15**, 521–527.
URL: *http://www.proteome.com/databases/*

Schneider, V., Wadhwani, P., Reichert, J., Bürck, J., Elstner, M., Ulrich, A. S. & Kubař, T. (2019), 'Tetrameric charge-zipper assembly of the tisb peptide in membranes - computer simulation and experiment', *Journal of Physical Chemistry B* **123**, 1770–1779.

Seppälä, S., Slusky, J. S., Lloris-Garcerá, P., Rapp, M. & Heijne, G. V. (2010), 'Control of membrane protein topology by a single c-terminal residue', *Science* **328**, 1698–1700.

Shore, S. F. H., Leinberger, F. H., Fozo, E. M. & Berghoff, B. A. (2024), 'Type i toxin-antitoxin systems in bacteria: from regulation to biological functions.', *EcoSal Plus* p. eesp00252022.

Singh, G., Yadav, M., Ghosh, C. & Rathore, J. S. (2021), 'Bacterial toxin-antitoxin modules: classification, functions, and association with persistence', *Current Research in Microbial Sciences* **2**.

Soutourina, O. (2019), 'Type i toxin-antitoxin systems in clostridia', *Toxins* **11**.

Spanka, D. T., Konzer, A., Edelmann, D. & Berghoff, B. A. (2019), 'High-throughput proteomics identifies proteins with importance to postantibiotic recovery in depolarized persister cells', *Frontiers in Microbiology* **10**.

Steinbrecher, T., Prock, S., Reichert, J., Wadhwani, P., Zimpfer, B., Bürck, J., Berditsch, M., Elstner, M. & Ulrich, A. S. (2012), 'Peptide-lipid interactions of the stress-response peptide tisb that induces bacterial persistence', *Biophysical Journal* **103**, 1460–1469.

Sterk, M., Romilly, C. & Wagner, E. G. H. (2018), 'Unstructured 5'-tails act through ribosome standby to override inhibitory structure at ribosome binding sites', *Nucleic Acids Research* **46**, 4188–4199.

Studer, S. M. & Joseph, S. (2006), 'Unfolding of mrna secondary structure by the bacterial translation initiation complex', *Molecular Cell* **22**, 105–115.

Su, W. L., Bredèche, M. F., Dion, S., Dauverd, J., Condamine, B., Gutierrez, A., Denamur, E. & Matic, I. (2022), 'Tisb protein protects escherichia coli cells suffering massive dna damage from environmental toxic compounds', *mBio* **13**.

Thisted, T. & Gerdes, K. (1992), 'Mechanism of post-segregational killing by the hok/sok system of plasmid rl sok antisense rna regulates hok gene expression indirectly through the overlapping mok gene', *J. Mol. Bid* **223**, 41–54.

Thompson, M. K., Nocedal, I., Culviner, P. H., Zhang, T., Gozzi, K. R. & Laub, M. T. (2022), 'Escherichia coli syme is a dna-binding protein that can condense the nucleoid', *Molecular Microbiology* **117**, 851–870.

Unoson, C. & Wagner, E. G. H. (2008), 'A small sos-induced toxin is targeted against the inner membrane in escherichia coli', *Molecular Microbiology* **70**, 258–270.

Van Melderen, L. & De Bast, M. S. (2009), 'Bacterial toxin-antitoxin systems: More than selfish entities?', *PLoS Genetics* **5**.

Ventura, S. & Villaverde, A. (2006), 'Protein quality in bacterial inclusion bodies', *Trends in Biotechnology* **24**, 179–185.

Verstraeten, N., Knapen, W. J., Kint, C. I., Liebens, V., den Bergh, B. V., Dewachter, L., Michiels, J. E., Fu, Q., David, C. C., Fierro, A. C., Marchal, K., Beirlant, J., Versées, W., Hofkens, J., Jansen, M., Fauvart, M. & Michiels, J. (2015), 'Obg and membrane depolarization are part of a microbial bet-hedging strategy that leads to antibiotic tolerance', *Molecular Cell* **59**, 9–21.

Vogel, J., Argaman, L., Wagner, E. G. H. & Altuvia, S. (2004), 'The small rna istr inhibits synthesis of an sos-induced toxic peptide', *Current Biology* **14**, 2271–2276.

Wagner, E. G. H. & Unoson, C. (2012), 'The toxin-antitoxin system tisb-istr1: Expression, regulation and biological role in persister phenotypes', *RNA Biology* **9**, 1513–1519.

Wang, X., Lord, D. M., Cheng, H. Y., Osbourne, D. O., Hong, S. H., Sanchez-Torres, V., Quiroga, C., Zheng, K., Herrmann, T., Peti, W., Benedik, M. J., Page, R. & Wood, T. K. (2012), 'A new type v toxin-antitoxin system where mrna for toxin ghot is cleaved by antitoxin ghos', *Nature Chemical Biology* **8**, 855–861.

Weaver, K. E., Weaver, D. M., Wells, C. L., Waters, C. M., Gardner, M. E. & Ehli, E. A. (2003), 'Enterococcus faecalis plasmid pad1-encoded fst toxin affects membrane permeability and alters cellular responses to lantibiotics', *Journal of Bacteriology* **185**, 2169–2177.

Weaver, K. & Tritle, D. (1994), 'Identification and characterization of an enterococcus faecalis plasmid pad1-encoded stability determinant which produces two small rna molecules necessary for its function', *PLASMID* **32**, 168–181.

Weel-Sneve, R., Kristiansen, K. I., Odsbu, I., Dalhus, B., Booth, J., Rognes, T., Skarstad, K. & Bjørås, M. (2013), 'Single transmembrane peptide dinq modulates membrane-dependent activities', *PLoS Genetics* **9**.

Wen, J., Won, D. & Fozo, E. M. (2014), 'The zoro-orzo type i toxin-antitoxin locus: Repression by the orzo antitoxin', *Nucleic Acids Research* **42**, 1930–1946.

Wilmaerts, D., Bayoumi, M., Dewachter, L., Knapen, W., Mika, J. T., Hofkens, J., Dedecker, P., Maglia, G., Verstraeten, N. & Michiels, J. (2018), 'The persistence-inducing toxin hokb forms dynamic pores that cause atp leakage', *mBio* **9**.

Wilmaerts, D., Dewachter, L., Loose, P. J. D., Bollen, C., Verstraeten, N. & Michiels, J. (2019), 'Hokb monomerization and membrane repolarization control persister awakening', *Molecular Cell* **75**, 1031–1042.e4.

Żwirowski, S., Kłosowska, A., Obuchowski, I., Nillegoda, N. B., Piróg, A., Ziętkiewicz, S., Bukau, B., Mogk, A. & Liberek, K. (2017), 'Hsp70 displaces small heat shock proteins from aggregates to initiate protein refolding', *The EMBO Journal* **36**, 783–796.

2

Protein aggregation is a consequence of the dormancy-inducing membrane toxin TisB in *Escherichia coli*

Florian H. Leinberger, Liam Cassidy, Daniel Edelmann, Nicole E. Schmid, Markus Oberpaul, Patrick Blumenkamp, Sebastian Schmidt, Ana Natriashvili, Maximilian H. Ulbrich, Andreas Tholey, Hans-Georg Koch, Bork A. Berghoff

AMERICAN SOCIETY FOR MICROBIOLOGY | mSystems

| Molecular and Cellular Biology | Research Article

Protein aggregation is a consequence of the dormancy-inducing membrane toxin TisB in *Escherichia coli*

Florian H. Leinberger,[1] Liam Cassidy,[2] Daniel Edelmann,[1] Nicole E. Schmid,[1] Markus Oberpaul,[3,4] Patrick Blumenkamp,[5] Sebastian Schmidt,[1] Ana Natriashvili,[6,7] Maximilian H. Ulbrich,[8,9] Andreas Tholey,[2] Hans-Georg Koch,[6] Bork A. Berghoff[1]

AUTHOR AFFILIATIONS See affiliation list on p. 21.

ABSTRACT Bacterial dormancy is a valuable strategy to survive stressful conditions. Toxins from chromosomal toxin-antitoxin systems have the potential to halt cell growth, induce dormancy, and eventually promote a stress-tolerant persister state. Due to their potential toxicity when overexpressed, sophisticated expression systems are needed when studying toxin genes. Here, we present a moderate expression system for toxin genes based on an artificial 5′ untranslated region. We applied the system to induce expression of the toxin gene *tisB* from the chromosomal type I toxin-antitoxin system *tisB/istR-1* in *Escherichia coli*. TisB is a small hydrophobic protein that targets the inner membrane, resulting in depolarization and ATP depletion. We analyzed TisB-producing cells by RNA-sequencing and revealed several genes with a role in recovery from TisB-induced dormancy, including the chaperone genes *ibpAB* and *spy*. The importance of chaperone genes suggested that TisB-producing cells are prone to protein aggregation, which was validated by an *in vivo* fluorescent reporter system. We moved on to show that TisB is an essential factor for protein aggregation upon DNA damage mediated by the fluoroquinolone antibiotic ciprofloxacin in *E. coli* wild-type cells. The occurrence of protein aggregates correlates with an extended dormancy duration, which underscores their importance for the life cycle of TisB-dependent persister cells.

IMPORTANCE Protein aggregates occur in all living cells due to misfolding of proteins. In bacteria, protein aggregation is associated with cellular inactivity, which is related to dormancy and tolerance to stressful conditions, including exposure to antibiotics. In *Escherichia coli*, the membrane toxin TisB is an important factor for dormancy and antibiotic tolerance upon DNA damage mediated by the fluoroquinolone antibiotic ciprofloxacin. Here, we show that TisB provokes protein aggregation, which, in turn, promotes an extended state of cellular dormancy. Our study suggests that protein aggregation is a consequence of membrane toxins with the potential to affect the duration of dormancy and the outcome of antibiotic therapy.

KEYWORDS toxin-antitoxin systems, type I toxins, protein aggregation, dormancy, antibiotics

Bacteria constantly encounter stressful conditions due to sudden changes in their environments. They can tolerate these stress conditions to some extent and can maintain cellular integrity by switching on designated response systems, which sense these conditions and adjust the expression of specific genes to counteract the harmful situation. Under extreme hostile conditions, however, regular stress response systems may fail to protect cells from lethal damages, a situation that is unpredictable and demands alternative survival strategies. One possibility is the formation of dormant cells, which are characterized by reduced cellular activity, growth arrest, and the ability to withstand even extreme stress conditions (1, 2). Dormancy typically occurs only in a

Editor Danielle Tullman-Ercek, Northwestern University, Evanston, Illinois, USA

Address correspondence to Bork A. Berghoff, bork.berghoff@uni-ulm.de.

The authors declare no conflict of interest.

See the funding table on p. 21.

Received 8 August 2024
Accepted 6 September 2024
Published 8 October 2024

fraction of cells and, therefore, represents an example of phenotypic heterogeneity that is considered a bet-hedging strategy for survival in unpredictable environments: some bacteria sacrifice their own propagation to ensure continuity of the genotype in case of extreme hostile conditions (3).

Bacterial dormancy occurs in different shapes and degrees and may therefore be defined as a "multidimensional trait space" (4). In its broadest definition, dormancy is "any rest period or reversible interruption of the phenotypic development of an organism" (5), which also includes myxospores within fruiting bodies of myxobacteria or endospores of some gram-positive bacteria, which may reside in dormant state for many years (6, 7). In contrast to these extreme morphotypes, bacterial populations almost constantly generate cells that are morphologically similar to their siblings but have entered a transient state of reduced activity from which they can rapidly recover. A prominent example are so-called persister cells, which are well known for their ability to survive antibiotic treatments (8–10). They have gained increasing attention as they may cause infection relapse or serve as a reservoir for antibiotic resistance development (11–13). As it stands right now, there are many ways into the persister state, including spontaneous events (14, 15), nutrient limitation and starvation (16, 17), metabolic perturbations (18), oxidative stress (19, 20), and low energy levels (21, 22). However, it is not entirely clear whether a combination of these events is necessary to reduce cellular activity to such an extent that persister formation is promoted. In this respect, not every dormant cell is a persister cell, but dormancy increases the likelihood of reaching the persister state (23).

Another possibility to induce dormancy is toxin-antitoxin (TA) systems, which are ubiquitously found in bacteria and contribute to stress responses or stabilization of mobile genetic elements (24, 25). Different TA system types have been identified, but they all have in common that the antitoxin inhibits toxin activity or prevents toxin production, which likely restricts toxin-dependent effects to specific (stress) conditions (24–28). Whether or not toxins from TA systems induce a persister state is subject to current debate (29, 30), but the contribution of toxins to bacterial dormancy and condition-dependent persister formation seems plausible (26, 31–33). One well-studied toxin with a potential influence on dormancy and persistence is TisB from the type I TA system *tisB/istR-1* in *Escherichia coli* (34–36). TisB is a small hydrophobic protein that targets the inner membrane and leads to membrane depolarization, ATP depletion, and further secondary effects, such as reactive oxygen species formation and inhibition of translation (31, 37–40). The reduced energy level in TisB-producing cells is expected to support persister formation, especially under conditions of DNA damage, when the corresponding *tisB* toxin gene is strongly induced upon auto-cleavage of the LexA repressor as part of the SOS response (33, 39, 41, 42). However, transcription of *tisB* is not sufficient to produce the TisB protein because the primary *tisB* mRNA (+1 mRNA) is translationally inactive due to an inhibitory secondary structure in its 5′ part. The +1 mRNA needs to undergo processing into the active +42 mRNA to be translated (43). Translation of the +42 mRNA depends on a non-canonical translation initiation mechanism that involves a single-stranded ribosome standby site (RSS), a 5′ pseudoknot structure, and ribosomal protein S1 (44, 45). However, the translation of +42 mRNA is efficiently inhibited by the RNA antitoxin IstR-1 (42, 43). Hence, two regulatory RNA elements (secondary structure in the +1 mRNA and antitoxin IstR-1) limit *tisB* expression to SOS conditions and set a threshold for TisB production in individual cells, thereby causing phenotypic heterogeneity (39, 46).

An early transcriptome study demonstrated that the heterologous production of TisB and other membrane toxins led to the induction of several stress response genes (47), indicating that these toxins cause stress due to primary and secondary effects (31, 40). However, heterologous toxin expression systems tend to produce excessive effects. In the current study, we aimed to construct a moderate expression system to study the TisB-dependent stress response. We observed that moderate *tisB* expression elicits a stress response that contributes to recovery from TisB-induced dormancy. Upregulation

of several chaperone genes suggested that TisB provokes protein aggregation, which was validated using a fluorescent reporter system. Intriguingly, we found that the DNA-damaging antibiotic ciprofloxacin causes protein aggregation in a TisB-dependent manner and that protein aggregates affect the dormancy duration of persister cells. Our study supports the view that TisB—and probably other type I toxins—affect dormancy and persistence through a variety of downstream effects, including protein aggregation.

RESULTS

A moderate expression system for investigation of TisB-induced dormancy

Production of the membrane toxin TisB from the type I TA system *tisB/istR-1* inflicts a stressful situation, including perturbation of membrane functioning, energy depletion, and further secondary effects (31, 48). Recent work on TisB has highlighted the importance of particular stress-related proteins in the context of TisB-dependent persistence, such as superoxide dismutases and alkyl hydroperoxide reductase (40, 49). To grasp the global response to TisB-mediated stress, we aimed to construct an inducible expression system that provokes TisB-dependent effects but avoids high TisB levels and concomitant TisB toxicity (37, 50). In *E. coli*, pBAD plasmids are applied for controllable gene expression from the P_{BAD} promoter using L-arabinose (L-ara) as an inducer. When using the pBAD derivative p+42-*tisB* (37), transcription from the P_{BAD} promoter produces the native *tisB* +42 mRNA, which is translationally active due to its accessible RSS and the existence of a Shine-Dalgarno (SD) sequence (Fig. 1A). However, *tisB* induction from p+42-*tisB* reduces the number of colony forming units (CFU) by at least 10-fold, indicating TisB toxicity and probably cell death (37). Since *tisB* expression from its chromosomal gene copy is not expected to cause cell death (37), but rather supports stabilization of a growth-arrested state (31), p+42-*tisB* does probably not represent a suitable expression system to study authentic TisB effects.

Expression strength can be modulated by plasmid copy number and promoter strength (51). Alternatively, the efficiency of translation can be modulated. We followed the latter strategy and tested an artificial 5′ UTR with a length of 20 bp that lacks an SD sequence (52) (Fig. 1A). The artificial 5′ UTR was fused to the *syfp2* open reading frame to analyze single-cell *syfp2* expression levels by flow cytometry. The SD-free 5′ UTR decreased the sYFP2 fluorescence by approximately 180-fold in comparison to an SD-containing 5′ UTR (Fig. S1). Importantly, the SD-free 5′ UTR did not introduce an expression heterogeneity among the population (Fig. S1). To test its suitability for moderate *tisB* expression, the native *tisB* 5′ UTR was replaced by the SD-free 5′ UTR to yield plasmid p0SD-*tisB*. Using 3×FLAG fusions and western blot analysis, we compared the p+42-*tisB* and p0SD-*tisB* systems by assessing 3×FLAG-TisB protein levels in *E. coli* wild-type (WT) MG1655 (Fig. 1B). 3×FLAG-TisB levels were reduced by ~10-fold using the p0SD-*tisB* system, which was presumably due to lower efficiency of translation initiation but might also be partly attributable to lower steady-state levels of the *0SD-3×FLAG-tisB* mRNA (Fig. S1). Optical density (OD_{600}) measurements demonstrated that TisB induction from plasmid p0SD-*tisB* by L-ara was sufficient to halt cell growth during the exponential phase, while an empty pBAD control showed normal growth (Fig. 1C). There was, however, a short delay for growth inhibition with p0SD-*tisB* when compared to p+42-*tisB*. The primary effect of TisB is depolarization of the inner membrane (38, 39). We assessed depolarization by the potential-sensitive probe $DiBAC_4(3)$ after 1 hour of L-ara treatment during the exponential phase. Expression from both p+42-*tisB* and p0SD-*tisB* caused an increase in intracellular $DiBAC_4(3)$ fluorescence in comparison to the empty pBAD control as assessed by flow cytometry (Fig. 1D). While the main population was similarly shifted with both expression systems, a second population with an increased $DiBAC_4(3)$ fluorescence occurred, which was especially prominent with the p+42-*tisB* system. Whether this subpopulation represents extremely damaged or even dead cells remains unknown. Importantly, after 1 hour of L-ara treatment, 66% of cells were able to form colonies with the p0SD-*tisB* system, while this value dropped to 1% with p+42-*tisB* (Fig.

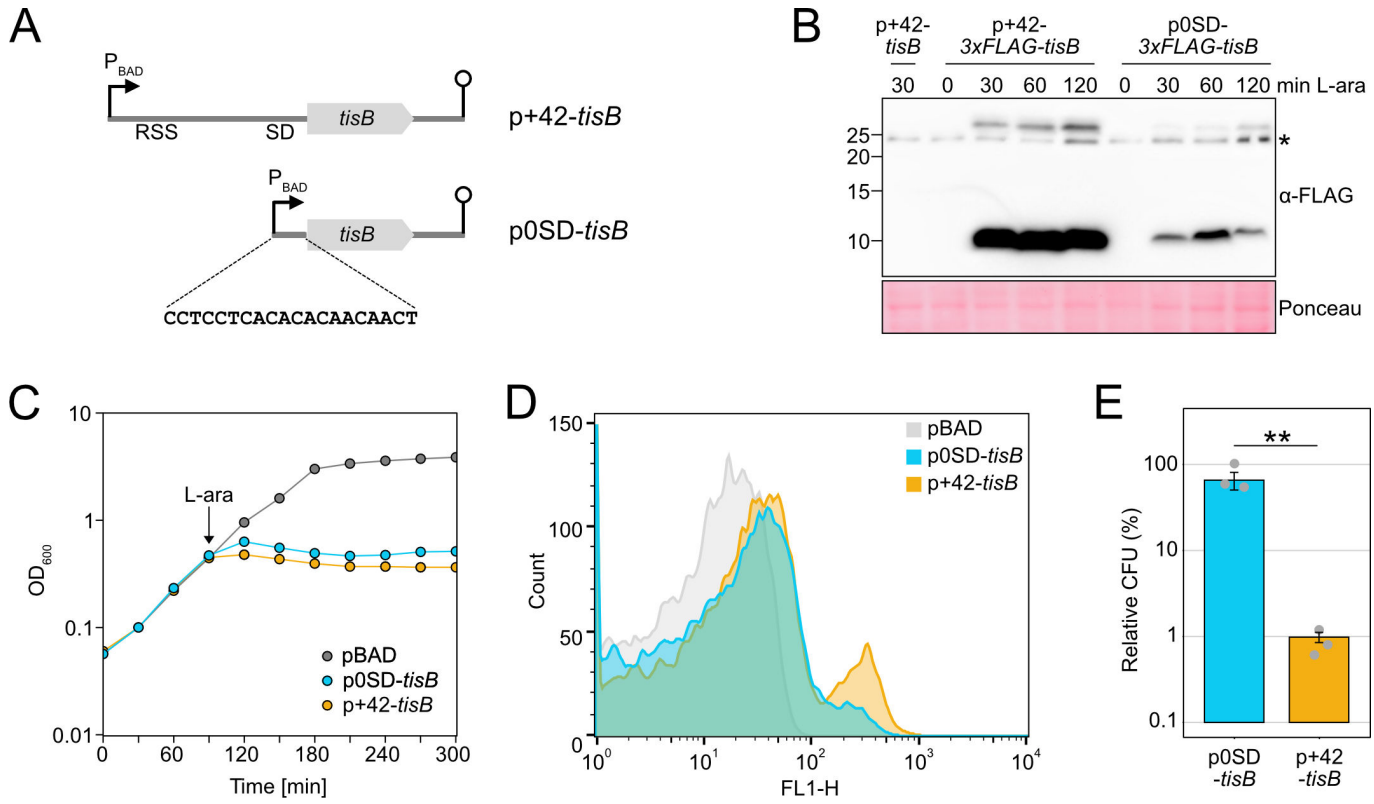

FIG 1 Characterization of a moderate *tisB* expression system. (A) Schematic representation of different *tisB* expression systems. The p+42-*tisB* plasmid contains the native *tisB* 5′ UTR, including a RSS and a SD sequence. Transcription from the P_{BAD} promoter starts at the *tisB* +42 position. The p0SD-*tisB* plasmid contains the *tisB* coding sequence preceded by an artificial 20 bp 5′ UTR. Lollipop structures indicate Rho-independent terminators. (B) Detection of 3×FLAG-TisB. Wild-type MG1655 harboring 3×FLAG-tag variants of p+42-*tisB* and p0SD-*tisB* were grown to an OD_{600} of ~0.4 (exponential phase) and treated with L-ara (0.2%). Samples were collected at the indicated time points. Total protein was separated using Tricine-SDS-PAGE and transferred to PVDF membranes by electro-blotting. 3×FLAG-TisB was detected using an HRP-conjugated monoclonal α-FLAG antibody. As a negative control, p+42-*tisB* was used. Two TisB-specific bands are visible, one at ~10 kDa and one above 25 kDa. The asterisk indicates an unspecific band. Ponceau staining is shown as loading control. (C) Growth inhibition by TisB. Wild-type MG1655, harboring p0SD-*tisB*, p+42-*tisB* or an empty pBAD plasmid, was treated with the inducer L-ara (0.2%) at an OD_{600} of ~0.4 (exponential phase; arrow). The OD_{600} was measured over time. Data points indicate the mean of three biological replicates. (D) TisB-dependent membrane depolarization. Wild-type MG1655 cells, harboring p0SD-*tisB*, p+42-*tisB* or an empty pBAD plasmid, were treated with the inducer L-ara (0.2%) for 1 hour when an OD_{600} of ~0.4 was reached (exponential phase). Staining with the potential-sensitive probe $DiBAC_4(3)$ was applied to assess depolarization. $DiBAC_4(3)$ fluorescence was measured using flow cytometry and the FL1-H detector. 10,000 events are displayed for each strain. (E) TisB toxicity with different expression systems. Wild-type MG1655, harboring p0SD-*tisB* or p+42-*tisB* was treated with L-ara (0.2%) during the exponential phase (OD_{600} ~0.4) for 1 hour. Pre- and post-treatment samples were used to determine relative CFU (%). Bars represent the mean of three biological replicates and error bars indicate the standard deviation. Dots show individual data points. ANOVA with post-hoc Tukey HSD test was performed (**$P < 0.01$).

1E). These findings indicate that p0SD-*tisB* largely avoids TisB toxicity and, therefore, represents a suitable expression system to study TisB-induced dormancy.

Dynamic phenotypic features upon moderate *tisB* expression

Elevated toxin levels were shown to increase phenotypic heterogeneity with respect to growth-arrest duration and persistence time (39, 53). The duration of toxin-induced growth arrest is reflected by the time that is needed by single cells to form colonies on agar plates, which can be quantified using the ScanLag method (54, 55). When *E. coli* wild-type MG1655, containing p0SD-*tisB*, was grown to an OD_{600} of ~0.4 (exponential phase) and plated on regular LB agar plates without L-ara (T0; Fig. 2A), the median colony appearance time was 820 min (Fig. 2B). The narrow appearance-time distribution indicated homogeneous lag times, as expected from exponentially growing populations. By contrast, when cultures were treated with L-ara for 30 min to induce TisB-dependent growth arrest before cells were spread on agar plates (T30; Fig. 2A), the median colony

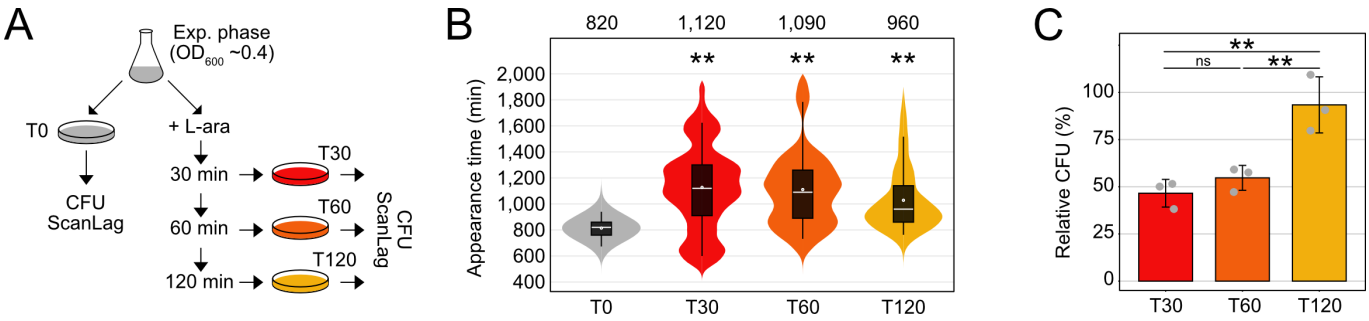

FIG 2 Dynamic phenotypic features upon moderate *tisB* expression. (A) Schematic representation of the performed experiment. Wild-type MG1655, harboring the p0SD-*tisB* plasmid, was treated with L-ara (0.2%) in the exponential phase (OD_{600} ~0.4). At the indicated time points (T30, T60, and T120), cells were plated on LB agar without L-ara and colony growth was analyzed using the ScanLag method (see Material and Methods). As a control, cells were analyzed before L-ara was added (T0). (B) ScanLag analysis was applied to determine the colony appearance time after *tisB* expression. For each time point, colony appearance times are illustrated as violin box plots. Colonies from three biological replicates were combined (T0: *n* = 154; T30: *n* = 59; T60: *n* = 103; T120: *n* = 124). The white dot indicates the mean. The respective median appearance time (white bar) is shown on top of each plot. L-ara-treated samples were compared to the control (T0) using a pairwise Wilcoxon rank-sum test (**$P < 0.0001$). (C) Colony counts increase upon progressing *tisB* expression. LB agar plates from panel B were used to determine colony counts. Pre-treatment (T0) and post-treatment (T30, T60, and T120) samples were used to determine relative CFU (%). Bars represent the mean of three biological replicates and error bars indicate the standard deviation. Dots show individual data points. ANOVA with *post hoc* Tukey HSD test was performed (**$P < 0.01$; ns: not significant).

appearance time shifted to 1,120 min. In other words, cells needed on average 5 hours longer to form colonies. Furthermore, heterogeneity of colony appearance was clearly increased (Fig. 2B). Since the speed of colony growth could not account for the 5-hour shift (Fig. S2), we concluded that TisB production from the p0SD-*tisB* system generated populations with very heterogeneous growth-arrest durations. While results for a 60 min L-ara treatment (T60) were comparable to the 30-min time point, the median colony appearance time was only 960 min after 120 min of L-ara treatment (T120), which was also accompanied by a more homogeneous distribution (Fig. 2B). Intriguingly, relative CFU counts stayed at ~50% during the first 60 min of L-ara treatment but increased to more than 90% after 120 min (Fig. 2C). Hence, cells regained their ability to form colonies at later stages of the experiment. Even though the p0SD-*tisB* plasmid was stable over the whole duration of the experiment (Fig. S1), we observed changes in 3×FLAG-TisB levels, with a peak at 60 min and a decline at 120 min (Fig. 1B), which was mirrored at the mRNA level (Fig. S1). This might represent an inconsistent expression strength introduced by the p0SD-*tisB* system itself. Alternatively, the decline in TisB protein levels and the improved ability to form colonies at the 120 min time point indicate an adaptation, probably through activation of a stress response that limits further TisB production.

A global transcriptome analysis reveals TisB-dependent upregulation of stress-related genes

It has already been observed that type I toxins cause upregulation of several stress-related genes (47), and we have shown that *tisB* expression provokes superoxide formation and upregulation of *soxS* and the SoxRS regulon (40). To reveal the response to TisB on a global scale, transcriptome analysis of MG1655 p0SD-*tisB* was performed. Cultures were grown to an OD_{600} of ~0.4 (exponential phase) and treated with L-ara for 30 min. Samples before and after L-ara treatment were collected and analyzed by RNA-seq, which identified 67 upregulated and 66 downregulated genes (log_2 fold change > 2 and < −2, *P*-value < 0.01; Data Set S1). We specifically focused on upregulated genes, as they might represent an active response to TisB. As expected, *tisB* and *soxS* were among the genes with the strongest upregulation (Fig. 3A). To select candidates for further analysis, we compared the set of upregulated genes from our RNA-seq analysis to (i) microarray data of heterologous *tisB* expression (47), (ii) proteome data of a de-regulated *tisB* strain (49), and (iii) transcriptional regulation data from the RegulonDB database

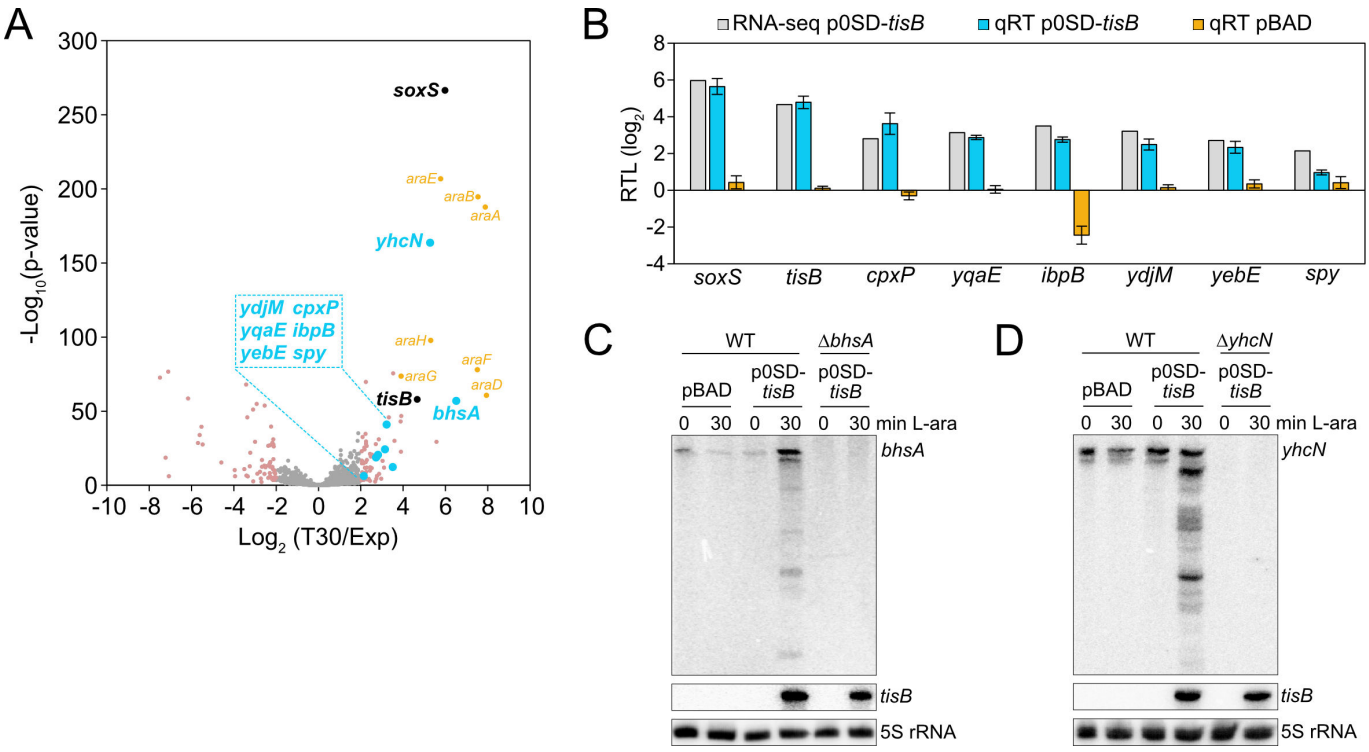

FIG 3 Identification of TisB-responsive genes by RNA-seq. (A) Global response to *tisB* expression. Wild-type MG1655, harboring the p0SD-*tisB* plasmid, was treated with L-ara (0.2%) during the exponential phase (OD_{600} ~0.4) for 30 min. RNA samples extracted before (Exp) and after treatment (T30) were analyzed using RNA-seq. The volcano plot illustrates the $\log_2$ fold change on the *x*-axis and the $-\log_{10}$(*P*-value) on the *y*-axis. Differentially expressed genes ($\log_2$ fold change > 2 or < −2, *P*-value < 0.01) are shown in pink. Selected candidates are highlighted in blue, while genes affected by L-ara are shown in orange (*araBAD*, *araE*, *araFGH*), and *tisB* and *soxS* are shown in black. (B) Confirmation of RNA-seq using qRT-PCR. Wild-type MG1655, harboring p0SD-*tisB* (blue bars) or an empty pBAD plasmid (orange bars), was treated with L-ara (0.2%) during exponential phase (OD_{600} ~0.4) for 30 min. Relative transcript levels (RTL; $\log_2$) were assessed by qRT-PCR (qRT). Log_2 fold changes from the RNA-seq analysis are shown for comparison (gray bars). Bars represent the mean of three biological replicates, with two technical replicates each, and error bars indicate the standard deviation. (C, D) Confirmation of RNA-seq using northern blot analysis. Wild-type MG1655, harboring p0SD-*tisB* or an empty pBAD plasmid, was treated with L-ara (0.2%) during the exponential phase (OD_{600} ~0.4) for 30 min. Total RNA was separated using urea-polyacrylamide gels and blotted onto nylon membranes. Radioactive probes binding to the coding region of (C) *bhsA* or (D) *yhcN* were applied for the detection of transcripts. Corresponding deletion mutants (Δ*bhsA* or Δ*yhcN*) were used to show the specificity of the probes. A *tisB* probe was applied to verify *tisB* induction from p0SD-*tisB*, and 5S rRNA was probed as loading control.

(56). The regulon analysis highlighted genes that are transcriptionally regulated by CpxR, the response regulator from the CpxAR two-component system (Fig. S3). The Cpx system belongs to the envelope stress response and is mainly involved in sensing misfolded proteins in the inner membrane and periplasm (57). In total, we selected four CpxR-dependent genes: *cpxP*, *spy*, *yebE,* and *yqaE* (Fig. 3A). Importantly, *cpxP*, *spy,* and *yebE* were found in the transcriptome study by Fozo et al. (47), and *spy* and *yebE* were also found in the proteome study by Spanka et al. (49). CpxP and Spy are located in the periplasm and have chaperone functions; YebE and YqaE are poorly characterized inner membrane proteins. In addition, we selected *ydjM* (Fig. 3A), encoding another poorly characterized inner membrane protein. Like *tisB*, *ydjM* belongs to the LexA regulon and might have an important function during the SOS response. The transcriptome study by Fozo et al. showed that the *ibpAB* operon is upregulated upon type I toxin expression (47). Both *ibpA* and *ibpB* encode small heat-shock proteins (sHSPs) with chaperone functions in the cytoplasm. Since *ibpB* showed stronger induction than *ibpA* in our RNA-seq data (Data Set S1), we selected *ibpB* for further analysis (Fig. 3A). We applied quantitative reverse transcription PCR (qRT-PCR) to verify TisB-dependent induction of the selected genes. *soxS* and *tisB* were used as positive controls (Fig. 3B). To exclude that upregulation of stress-related genes was due to the L-ara treatment, wild-type MG1655

containing an empty pBAD plasmid was analyzed by qRT-PCR, clearly showing that L-ara alone was not sufficient to cause induction of the stress-related genes (Fig. 3B). Finally, *bhsA* and *yhcN* were selected because they were among the genes with the strongest upregulation (Fig. 3A). Both genes encode DUF1471 domain-containing proteins that are located in the cell envelope and have a putative role in stress responses and/or biofilm formation (58–60). Since qRT-PCR analysis did not produce reliable results for *bhsA* and *yhcN*, northern blot analysis was performed, which confirmed their TisB-dependent induction (Fig. 3C and D). We note, however, that *tisB* expression caused accumulation of several mRNA degradation products, which was particularly evident for *yhcN* (Fig. 3D). Strong *tisB* expression causes rRNA degradation in less than 1 hour (37, 40, 50), but this was not observed when using the p0SD-*tisB* system (Fig. S1), suggesting that global RNA decay cannot account for *bhsA* and *yhcN* degradation. Degradation of *bhsA* and *yhcN* might have a biological function, such as the generation of regulatory RNAs, but this needs further investigation.

Stress-related genes support recovery from TisB-induced dormancy

To evaluate the function of the selected candidates with respect to TisB-induced dormancy, we deleted the corresponding genes and transferred the p0SD-*tisB* plasmid to the resulting mutants. As expected, all mutants showed L-ara-induced and TisB-dependent growth inhibition (Fig. S4). In a subsequent experiment, mutants were grown to an OD_{600} of ~0.4 (exponential phase) and tested for their ability to form colonies after 1 hour of L-ara treatment. The relative CFU counts for the mutants ranged between 43% and 111%, which was not strikingly different when compared to the wild type (70%; Fig. 4A). We concluded that each gene only had a minor influence on the ability of TisB-producing cells to form colonies on LB agar plates. We reasoned that the stress-related genes might rather influence the growth-arrest duration by supporting the recovery from TisB-mediated stress (40, 49). Indeed, when using ScanLag, seven out of eight mutants showed a delayed recovery and significantly increased growth-arrest duration in comparison to the wild type, with Δ*bhsA* being the only exception (Fig. 4B). The growth-arrest duration, as measured by the colony appearance time, was prolonged by at least 80 min (Δ*ibpB*) and up to 220 min (Δ*yebE* and Δ*cpxP*). To exclude that the gene deletion itself and/or the L-ara treatment would affect the colony appearance time, an empty pBAD plasmid was transferred to the mutants. The resulting strains were grown to the exponential phase, treated with L-ara for 1 hour, and analyzed by ScanLag. In this control experiment, none of the mutants showed a delayed colony appearance in comparison to the wild type (Fig. S5), clearly indicating that the stress-related genes have a particular function upon TisB-mediated stress and probably support the recovery process. Since four of the eight candidates belong to the CpxR regulon (Fig. 4A), we constructed a *cpxR* deletion mutant, transferred the p0SD-*tisB* plasmid, and induced *tisB* expression by L-ara. However, neither CFU counts nor colony appearance were significantly different in the *cpxR* mutant when compared to the wild type (Fig. S6), probably due to the dual regulatory function of CpxR and the complex features found within the CpxR regulon (61).

TisB causes intracellular ATP depletion and protein aggregation

The importance of proteins with chaperone activity during recovery from TisB-induced growth arrest (Fig. 4) suggested that unfolded proteins and protein aggregates impose a challenge for TisB-producing cells. It was previously demonstrated that due to ATP depletion, protein aggregates form and affect the dormancy of bacterial cells (62, 63). Since TisB is expected to decrease the intracellular ATP concentration due to depolarization of the inner membrane and breakdown of the proton motive force (33, 35, 37), intracellular ATP concentrations were measured before and after L-ara treatment in wild-type MG1655 containing either p0SD-*tisB* or an empty pBAD plasmid. In the TisB-producing strain, a 60-min treatment with L-ara caused a ~32-fold ATP reduction, while the ATP concentration remained unchanged in the control strain (Fig. 5A). To assess

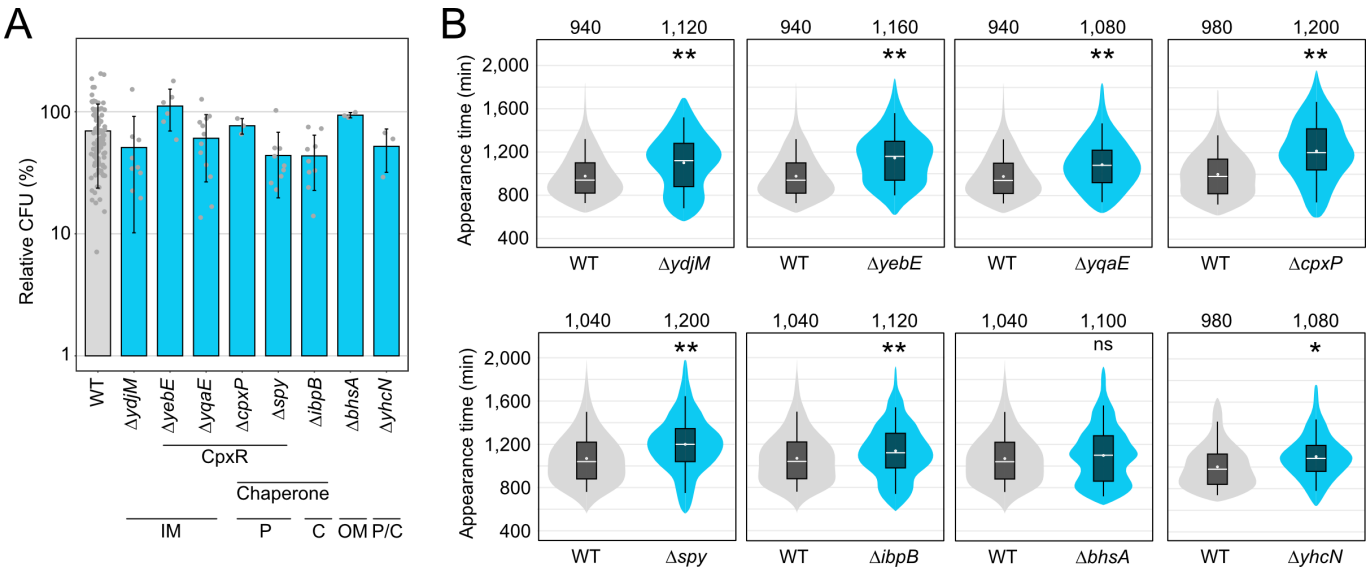

FIG 4 TisB-responsive genes mainly affect the recovery after *tisB* expression. (A) TisB toxicity in selected deletion mutants. WT MG1655 and deletion mutants, harboring the p0SD-*tisB* plasmid, were treated with L-ara (0.2%) during the exponential phase (OD_{600} ~0.4) for 1 hour. Pre- and post-treatment samples were used to determine relative CFU (%). Bars represent the mean of at least three biological replicates and error bars indicate the standard deviation. Dots show individual data points (WT: *n* = 102; Δ*ydjM*: *n* = 9; Δ*yebE*: *n* = 6; Δ*yqaE*: *n* = 12; Δ*cpxP*: *n* = 3; Δ*spy*: *n* = 9; Δ*ibpB*: *n* = 9; Δ*bhsA*: *n* = 3; Δ*yhcN*: *n* = 3). ANOVA with post hoc Tukey HSD was performed (no significant difference between deletion mutants and the wild type was detected). It is indicated whether the genes are CpxR-dependent or have a chaperone activity. Their proposed cellular localization is given (C: cytoplasm, IM: inner membrane, P: periplasm, OM: outer membrane). (B) ScanLag analysis of selected deletion mutants. WT MG1655 and deletion mutants, harboring the p0SD-*tisB* plasmid, were treated with L-ara (0.2%) during the exponential phase (O_{D600} ~0.4) for 1 hour. ScanLag was applied to determine the colony appearance time after *tisB* expression. For each deletion mutant, colony appearance times are illustrated as violin box plots and compared to a corresponding wild type. Colonies from at least three biological replicates were combined (WT: *n* ≥ 192; Δ*ydjM*: *n* = 452; Δ*yebE*: *n* = 383; Δ*yqaE*: *n* = 393; Δ*cpxP*: *n* = 252; Δ*spy*: *n* = 356; Δ*ibpB*: *n* = 682; Δ*bhsA*: *n* = 365; Δ*yhcN*: *n* = 192). The white dot indicates the mean. The respective median appearance time (white bar) is shown on top of each plot. Deletion mutants were compared to wild-type MG1655 using a pairwise Wilcoxon rank-sum test (*P < 0.001, **P < 0.0001, ns: not significant). It should be noted that ScanLag results vary between individual runs. For every mutant, statistical testing refers to the corresponding control strain (WT) from the same experimental run.

cytosolic protein aggregation as a likely consequence of ATP depletion, we applied a reporter strain that chromosomally expresses a monomeric superfolder green fluorescent protein (msfGFP) fused to the C-terminus of the sHSP IbpA (64). As expected, cytosolic msfGFP fluorescence changed from a diffuse to a punctuated pattern (i.e., formation of foci) after 15 min of heat shock at 47°C (Fig. S7). Since IbpA localizes to protein aggregates, the msfGFP foci clearly indicated the formation of protein aggregates in the cytoplasm due to elevated temperature (63, 64). We performed a U-Net analysis (65) to count msfGFP foci in individual cells (Fig. S7). Expression of *tisB* from p0SD-*tisB* in the *ibpA-msfGFP* reporter background (60-min L-ara treatment) led to the formation of foci, with ~48% of cells having three foci and ~20% having two or four foci (Fig. 5B). As a control, the empty pBAD plasmid was transferred to the *ibpA-msfGFP* reporter background, and the resulting strain was treated with L-ara. However, L-ara alone was not sufficient to cause foci formation (Fig. 5B). To demonstrate that functional TisB was needed for ATP depletion and foci formation, plasmid p0SD-*tisB-K12L* was applied for production of the TisB-K12L variant. TisB-K12L has central lysine 12 replaced with leucine, leading to attenuated TisB activity without affecting membrane localization (40). As expected, TisB-K12L did not cause major ATP depletion (Fig. 5A). More intriguingly, a reporter strain containing p0SD-*tisB-K12L* displayed mainly cells without foci (~83%) after 60 min of L-ara treatment (Fig. 5B). This control experiment demonstrated that production of a small membrane protein (TisB-K12L) is not sufficient to cause cytosolic protein aggregation, but rather that functional TisB toxin triggers the formation of protein aggregates, probably due to strong intracellular ATP depletion.

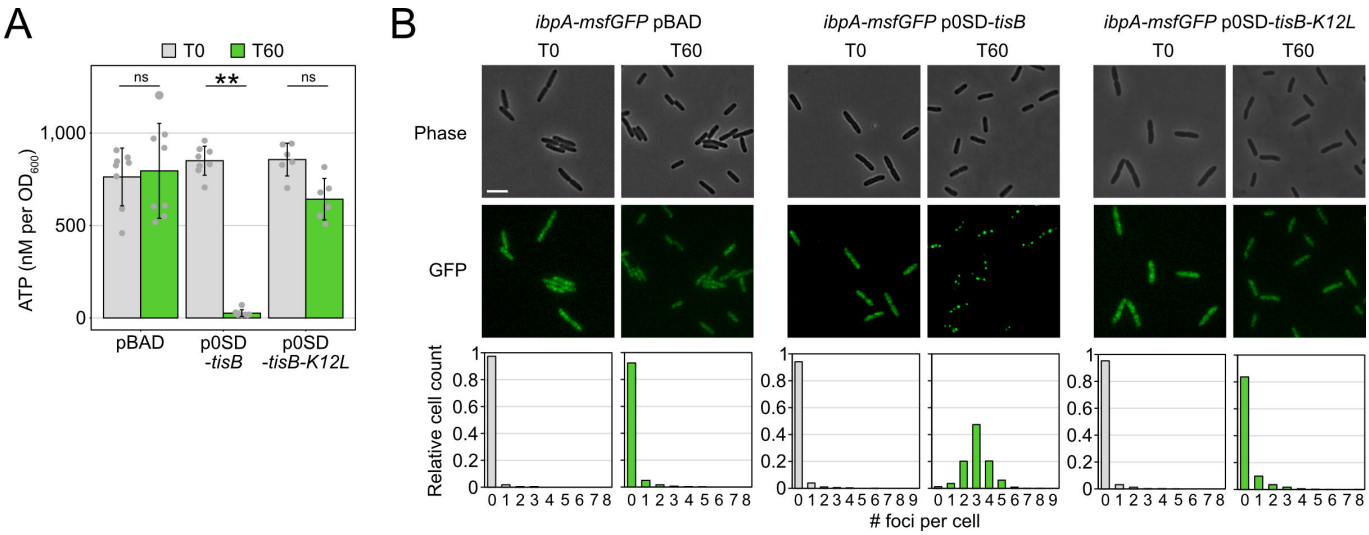

FIG 5 Expression of *tisB* causes cytoplasmic protein aggregation. (A) TisB-dependent ATP depletion. Wild-type MG1655, harboring either an empty pBAD plasmid, the p0SD-*tisB* plasmid, or the p0SD-*tisB-K12L* variant, was treated with L-ara (0.2%) during the exponential phase (OD_{600} ~0.4) for 60 min. A luciferase-based assay was applied to measure cellular ATP levels (nM per OD_{600}) before (T0) and after L-ara treatment (T60). Bars represent the mean of at least six biological replicates and error bars indicate the standard deviation. Dots show individual data points (pBAD: *n* = 8; p0SD-*tisB*: *n* = 8; p0SD-*tisB-K12L*: *n* = 6). ANOVA with post hoc Tukey HSD test was performed (**P < 0.01; ns: not significant). (B) TisB-dependent protein aggregation in the cytoplasm. Strain MG1655 *ibpA-msfGFP*, harboring an empty pBAD plasmid, the p0SD-*tisB* plasmid, or the p0SD-*tisB-K12L* variant, was treated with L-ara (0.2%) during exponential phase (T0; OD_{600} ~0.4) for 60 min (T60). Phase contrast images are displayed together with corresponding fluorescence images (GFP). White bars represent a length scale of 2 µm. Representative images from three biological replicates are shown. In the lower panel, msfGFP foci were quantified from three biological replicates. All images were evaluated using a U-Net neural network analysis and in-house image processing tools to automatically count msfGFP foci per cell. At least 507 cells were analyzed for each condition (pBAD T0: *n* = 507; pBAD T60: *n* = 3,019; p0SD-*tisB* T0: *n* = 730; p0SD-*tisB* T60: *n* = 1,474; p0SD-*tisB-K12L* T0: *n* = 1,405; p0SD-*tisB-K12L* T60: *n* = 1,896).

Ciprofloxacin provokes TisB-dependent protein aggregation

So far, we have shown that *tisB* expression from plasmid p0SD-*tisB* induces several stress-related genes, encoding—among others—the chaperones CpxP, Spy, and IbpB. Deletion of these genes delays the recovery of cells following TisB-mediated stress. Furthermore, we have observed strong ATP depletion and protein aggregation upon *tisB* expression from plasmid p0SD-*tisB*. While these experiments are helpful in appreciating the cellular consequences of *tisB* expression, they do not provide direct evidence for the consequences of *tisB* expression in wild-type cells. In wild-type cells, *tisB* transcription is strongly induced upon DNA damage through UV light or DNA-damaging agents, such as mitomycin C or ciprofloxacin (39, 41, 42, 66). When using the gyrase inhibitor ciprofloxacin (CIP), most TisB-dependent effects are observed only after approximately 3 hours of a high-dose treatment (31). We, therefore, treated wild-type MG1655 and a corresponding *tisB* deletion mutant with CIP at a high concentration (10 µg/mL), which was 1,000× higher than the minimum inhibitory concentration (MIC). Intracellular ATP concentrations were determined over 6 hours. In wild-type cultures, a ~1.7-fold drop of ATP was only observed after four hours of CIP, while ATP concentrations even significantly increased in the *tisB* deletion mutant (Fig. 6A). It should be noted that the drop of ATP in CIP-treated wild-type cultures was not comparable to the drastic ATP depletion observed upon *tisB* expression from plasmid p0SD-*tisB* (Fig. 5A). However, ~66% of wild-type cells displayed one or two IbpA-msfGFP foci after 6 hours of CIP, indicating protein aggregation, which was not observed in the *tisB* deletion background (Fig. 6B). This led us to conclude (i) that TisB-dependent protein aggregation occurs in wild-type cells after prolonged DNA-damage stress and (ii) that ATP depletion is likely not the determining factor for TisB-dependent protein aggregation upon CIP treatment.

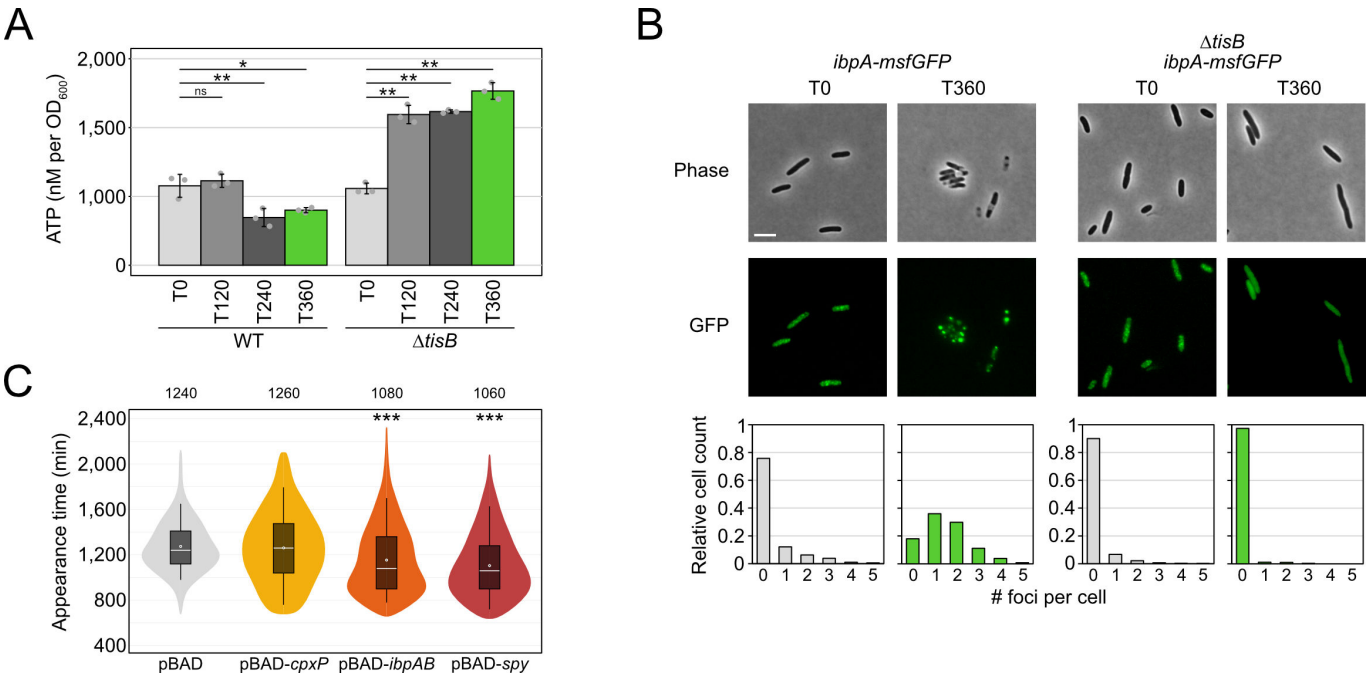

FIG 6 Analysis of TisB-dependent protein aggregates in wild-type cultures upon CIP treatment. (A) WT MG1655 and a *tisB* deletion mutant were treated with CIP (10 µg/mL; 1,000× MIC) during the exponential phase (OD_{600} ~0.4) for 360 min. A luciferase-based assay was applied to measure cellular ATP levels (nM per OD_{600}) before (T0) and after 120 min (T120), 240 min (T240), and 360 min (T360) of L-ara treatment. Bars represent the mean of three biological replicates, with two technical replicates each, and error bars indicate the standard deviation. Dots show individual data points. ANOVA with post hoc Tukey HSD test was performed (*P < 0.05, **P < 0.01, ns: not significant). (B) Strain MG1655 *ibpA-msfGFP* and Δ*tisB ibpA-msfGFP* were treated with CIP (10 µg/mL; 1,000× MIC) during exponential phase (T0; OD_{600} ~0.4) for 360 min (T360). Phase contrast images are displayed together with corresponding fluorescence images (GFP). White bars represent a length scale of 2 µm. Representative images from three biological replicates are shown. In the lower panel, msfGFP foci were quantified from three biological replicates. All images were evaluated using a U-Net neural network analysis and in-house image processing tools to automatically count msfGFP foci per cell. At least 577 cells were analyzed for each condition (*ibpA-msfGFP* T0: n = 766; *ibpA-msfGFP* T360: n = 577; Δ*tisB ibpA-msfGFP* T0: n = 1,621; Δ*tisB ibpA-msfGFP* T360: n = 901). (C) Influence of chaperone overexpression on recovery. Wild-type MG1655, harboring pBAD-*cpxP*, pBAD-*ibpAB*, pBAD-*spy,* or an empty pBAD plasmid, was pre-treated with the inducer L-ara (0.2%) for 30 min prior to the addition of CIP (10 µg/mL; 1,000× MIC) during exponential phase (OD_{600} ~0.4) for 6 hours. ScanLag was applied to determine the colony appearance time after CIP treatment. Colony appearance times are illustrated as violin box plots. Colonies from at least six biological replicates were combined (pBAD: n = 471; pBAD-*cpxP*: n = 266; pBAD-*ibpAB*: n = 479; pBAD-*cpxP*: n = 373). The white dot indicates the mean. The respective median appearance time (white bar) is shown on top of each plot. The chaperone overexpression strains were compared to the empty pBAD plasmid using a pairwise Wilcoxon rank-sum test (***P < 0.0001).

Since single deletions of the chaperone genes *cpxP*, *ibpB*, and *spy* extended the recovery time following plasmid-based *tisB* expression (Fig. 4B), we tested whether the corresponding gene deletions would also affect the recovery time of *E. coli* MG1655 following treatment with CIP. However, neither single nor double gene deletions affected recovery (data not shown). However, when expression of the *ibpAB* operon or the *spy* gene was induced from a plasmid 30 min prior to CIP treatment, the appearance time in ScanLag experiments was reduced by 160–180 min (Fig. 6C), indicating that increased IbpAB and Spy levels supported the recovery after CIP-induced stress.

Proteome analysis of aggregates

To further analyze TisB-dependent protein aggregates, wild-type cultures were treated with CIP, and aggregate-containing pellet fractions (PF) were separated from supernatants (SN) according to an established procedure (63) (Fig. 7A). The *tisB* deletion mutant was analyzed in parallel as a control for TisB-independent effects. The approach was initially validated by western blot analysis using the *ibpA-msfGFP* reporter background and detection of IbpA-msfGFP, confirming that the procedure was suitable to specifically enrich protein aggregates in wild-type PF samples (Fig. 7B). We then

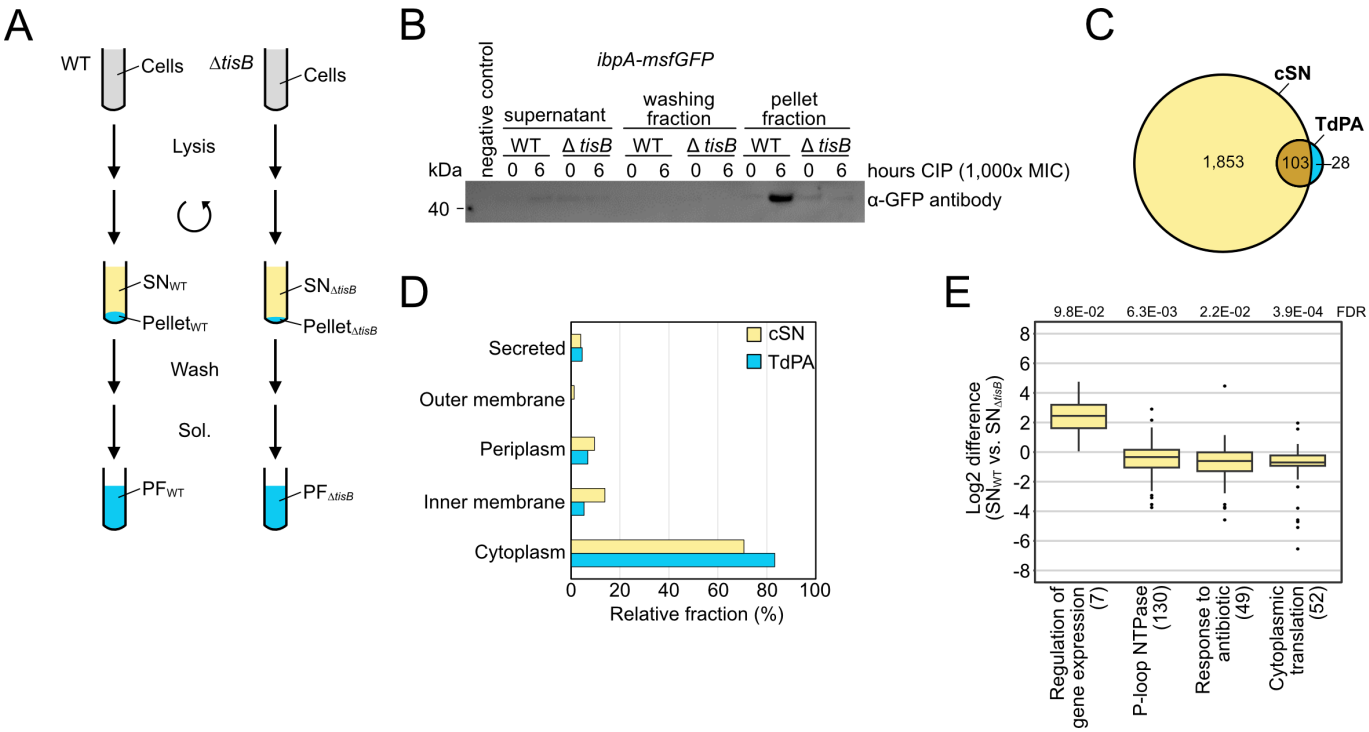

FIG 7 Proteome analysis of aggregates. (A) Schematic representation of the protein aggregate purification procedure. WT MG1655 and a *tisB* deletion mutant (Δ*tisB*) were treated with CIP (10 µg/mL; 1,000× MIC) during the exponential phase (OD_{600} ~0.4) for 6 hours. After cell lysis and centrifugation, SNs were collected for LC-MS analysis. The pellet fractions were washed three times and solubilized (Sol.) to receive pellet fractions (PF) for LC-MS analysis. (B) Western blot validation of protein aggregate purification. WT MG1655 *ibpA-msfGFP* and Δ*tisB ibpA-msfGFP* were treated with CIP (10 µg/mL; 1,000× MIC) during exponential phase (OD_{600} of ~0.4) and samples were collected at the indicated time points as described in Materials and Methods. A western blot was performed to detect IbpA-msfGFP using an α-GFP antibody. (C) Euler diagram of proteins identified by LC-MS. All proteins that were identified in at least two biological replicates of either wild-type or Δ*tisB* supernatant samples were combined (combined supernatant; cSN) and used as a reference data set. All proteins that were exclusively present or enriched in wild-type pellet fractions in comparison to Δ*tisB* were defined as TisB-dependent protein aggregates (TdPA). (D) Protein localization was predicted using LocTree3. The relative fractions of different protein localizations are shown for the combined supernatant (cSN) and TisB-dependent protein aggregates (TdPA). (E) 1D annotation enrichment results of differentially abundant proteins in the SN_{WT} versus $SN_{\Delta tisB}$ (number of enriched terms in brackets; Benjamini-Hochberg FDR provided on top).

performed the experiment in wild-type MG1655 and the corresponding *tisB* deletion mutant and analyzed SN and PF samples by liquid chromatography-mass spectrometry (LC-MS). The combined supernatant (cSN) of wild-type and Δ*tisB* cultures comprised 1,956 proteins in total, which was used as a reference data set (Fig. 7C). Analysis of the PF samples identified 29 proteins that were significantly enriched in wild-type PF samples in comparison to Δ*tisB* (log_2 fold change > 1 and Welch's *t*-test with Benjamini-Hochberg FDR < 0.05; Data Set S2). The sHSPs IbpA (log_2 fold change of 5.6) and IbpB (log_2 fold change of 3.2) were among the proteins with the highest enrichment factor, which confirmed a successful purification of protein aggregates in wild-type PF samples. Furthermore, we identified 102 proteins that were only present in wild-type PF samples but absent from Δ*tisB* PF samples (Data Set S2). The combination of both groups (131 proteins in total) was defined as "TisB-dependent protein aggregates" (TdPA; Fig. 7C). There was no intriguing difference between TdPA and cSN proteins concerning molecular weight or isoelectric point (Fig. S8). We speculated that TisB interferes with the export of outer membrane proteins (OMPs) and/or membrane insertion of inner membrane proteins (IMPs) (67). However, there was no enrichment of OMPs or IMPs in the TdPA data set (Fig. 7D). In support of this finding, *in vitro* experiments showed that inner membrane vesicles from CIP-treated wild-type cultures were not compromised in the transport of the outer membrane protein OmpA (Fig. S8). Finally, a STRING database search (68) revealed that no specific functional protein groups were enriched within

the TdPA data set, despite the occurrence of seven proteins that are encoded in the *E. coli* K-12 cryptic prophages, including integrases IntA, IntF, and IntE, excisionase XisE, repressor YmfK, cell division inhibitor YmfM, and transcriptional regulator YmfT (Fig. S8). In summary, we were not able to identify striking features of the TdPA proteins.

To learn more about the CIP-induced and TisB-dependent stress response, we compared SN samples by label-free quantification, revealing four functional categories that showed either increased or decreased protein abundance in the wild type as compared to the Δ*tisB* mutant (Fig. 7E). Among the category with increased protein abundance ("regulation of gene expression"), we found several cold-shock proteins (CspA, CspC, CspD, and CspE). The remaining categories contained proteins with decreased abundance, including 130 P-loop NTPases, 49 proteins with a potential role in response to antibiotic, and 52 ribosomal subunit proteins ("cytoplasmic translation"). The decreased abundance of ATP-utilizing NTPases and ribosomal subunit proteins suggests that TisB-producing cells reduce energy-consuming core processes, such as replication and translation, upon CIP-induced stress.

Protein aggregates determine the dormancy duration of persister cells after ciprofloxacin treatment

We asked the question of whether protein aggregation affects the state of persister cells upon treatment with CIP. Since the *tisB* deletion mutant does not form protein aggregates at the regular incubation temperature of 37°C, we applied heat stress at 46°C to induce aggregation (Fig. 8A). After 6 hours of CIP treatment at 37°C, survival was reduced by ~20-fold in Δ*tisB* as compared to the wild type (Fig. 8B). This is in agreement with previous results showing that TisB is an important factor for persister cell survival upon CIP treatment (33, 39). At 46°C, however, survival was comparable between both strains (Fig. 8B). A transcriptional *ibpB-syfp2* fusion confirmed that both strains showed similar induction of the heat shock response (Fig. S9). When applying the ScanLag method for cultures that were treated with CIP at 37°C, we observed that colonies of the Δ*tisB* mutant appeared on average 300 min earlier than wild-type colonies (Fig. 8C), indicating a reduced dormancy duration of Δ*tisB* cells, probably because aggregates were absent.

(Continued on next page)

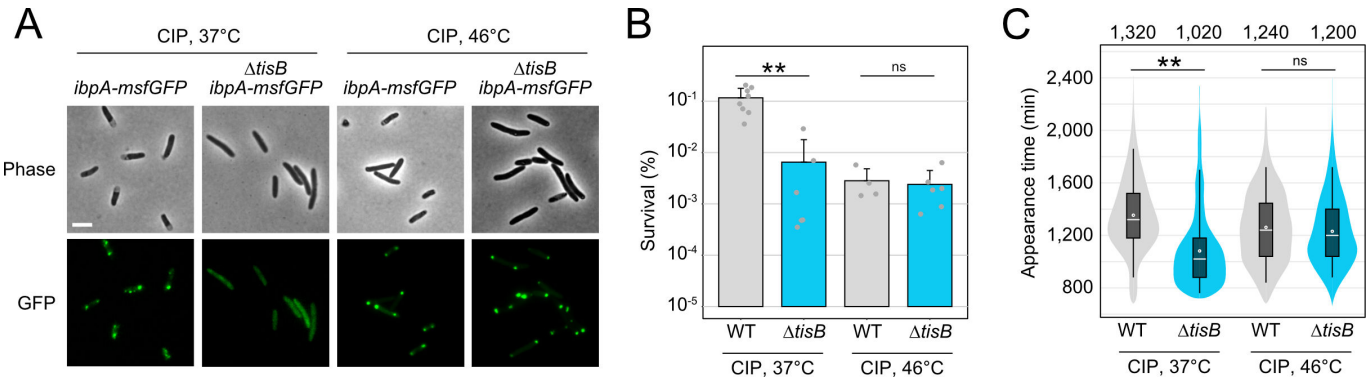

FIG 8 Heat-induced protein aggregates affect recovery from CIP. (A) Strain MG1655 *ibpA-msfGFP* and Δ*tisB ibpA-msfGFP* were treated with CIP (10 µg/mL; 1,000× MIC) during the exponential phase (OD_{600} ~0.4) for 6 hours at 37°C or 46°C. Phase contrast images are displayed together with corresponding fluorescence images (GFP). White bars represent a length scale of 2 µm. (B) WT MG1655 and a *tisB* deletion mutant were treated with ciprofloxacin (10 µg/mL; 1,000× MIC) during the exponential phase (OD_{600} ~0.4) for 6 hours at 37°C or 46°C. Pre- and post-treatment samples were used to determine relative CFU (%). Bars represent the mean of at least four biological replicates and error bars indicate the standard deviation. Dots show individual data points (WT 37°C: n = 8; Δ*tisB* 37°C: n = 6; WT 46°C: n = 4; Δ*tisB* 46°C: n = 6). ANOVA with post-hoc Tukey HSD was performed (**P < 0.01, ns: not significant). (C) WT MG1655 and a *tisB* deletion mutant were treated with ciprofloxacin (10 µg/mL; 1,000×MIC) during exponential phase (OD_{600} ~0.4) for 6 hours at 37°C or 46°C. ScanLag was applied to determine the colony appearance time after CIP treatment. Colony appearance times are illustrated as violin box plots. Colonies from at least three biological replicates were combined (WT 37°C: n = 1,431; Δ*tisB* 37°C: n = 272; WT 46°C: n = 476; Δ*tisB* 46°C: n = 1,026). The white dot indicates the mean. The respective median appearance time (white bar) is shown on top of each plot. The Δ*tisB* mutant was compared to the corresponding wild type MG1655 using a pairwise Wilcoxon rank-sum test (**P < 0.0001, ns: not significant).

When CIP was applied at 46°C, colony appearance times were comparable, suggesting that heat-induced protein aggregation has the potential to delay the recovery of Δ*tisB* persisters.

DISCUSSION

Dormancy is an efficient strategy to survive harmful situations. It is, therefore, not surprising that microorganisms have evolved different mechanisms to induce dormancy. A hallmark of toxins from chromosomal TA systems is their ability to halt cell growth, induce dormancy, and eventually promote persistence, especially when toxins are expressed from plasmids (32, 33, 39, 69–72). However, strong toxin expression from plasmids does not necessarily reflect the natural situation, potentially limiting the validity of the obtained effects. Here, we introduce an inducible system for moderate *tisB* expression that avoids toxic effects but retains the dormancy-promoting feature. Instead of manipulating transcription initiation (38, 51), we manipulated translation initiation by introducing an artificial SD-free 5′ UTR to the *tisB* gene on the pBAD expression plasmid. In *E. coli*, native transcripts without canonical SD sequences are not necessarily compromised in translation efficiency, suggesting that an SD sequence is not mandatory for efficient translation initiation (73). Here, we observed that the artificial SD-free 5′ UTR reduced TisB protein levels by ~10-fold in comparison to the native *tisB* 5′ UTR. We suggest that the SD-free 5′ UTR used in this study is a valuable genetic element that enables moderate expression of toxic genes, which may be especially useful when the resulting proteins have the potential to cause cell lysis or DNA damage (74–76). However, in the case of *tisB*, we observed inconsistent expression levels after extended cultivation, which might limit the use of the system to short-term experiments. Whether this represents a gene-specific feature requires further investigation.

The moderate *tisB* expression system was applied to reveal the response to TisB-mediated stress in *E. coli*. Our RNA-seq data are in good agreement with an earlier transcriptome study of a *tisB* overexpression strain (47). When comparing both analyses, the most prominent upregulated features are (i) the oxidative stress regulator gene *soxS*, (ii) the *ibpAB* operon, and (iii) CpxR-dependent genes, such as the chaperone genes *spy* and *cpxP*. It has been demonstrated that TisB provokes the formation of the reactive oxygen species superoxide, leading to strong *soxS* induction (40). The ability to detoxify superoxide by the superoxide dismutases SodA and SodB is important for recovery from TisB-induced dormancy (40). Here, we observed a similar pattern: the absence of stress-related proteins (e.g., chaperones IbpB, CpxP, or Spy) delayed the recovery from TisB-induced dormancy. We conclude that the TisB-dependent stress response mainly promotes the recovery process by repairing damages and restoring cellular integrity, as we have already speculated earlier (49). Recovery from TisB-induced dormancy would not only demand factors that cope with the cellular stress but also mechanistic means to remove the toxin and repolarize the inner membrane. In the case of membrane toxin HokB in *E. coli*, it has been observed that HokB pores are disassembled and targeted for degradation by DegQ protease, followed by membrane repolarization mediated by the electron transport chain (77). Whether similar mechanisms initiate the recovery from TisB-induced dormancy is currently unknown.

Chaperones are universal to all living cells and play important roles in protein quality control and disaggregation of protein aggregates (78, 79). The sHSPs IbpA and IbpB are chaperones that initiate the disaggregation process in the cytoplasm. Further components with a pivotal role in disaggregation and ATP-dependent protein re-folding are the DnaK-DnaJ-GrpE chaperone system, the ClpB disaggregase, chaperonins GroES and GroEL, and the ATP-dependent protease HslUV. Besides *ibpAB*, both our RNA-seq approach and proteome analysis revealed TisB-dependent upregulation of *clpB*, *groL,* and *hslU*, albeit they did not match our cutoff criteria. The prevalence of chaperone genes led to the hypothesis that *tisB* expression provokes protein aggregation, and indeed, cytosolic aggregates were observed upon *tisB* expression using an established fluorescent reporter system. Besides cytosolic chaperones, our data highlight

the functional importance of the periplasmic chaperones Spy and CpxP, both belonging to the CpxR regulon. While Spy is an ATP-independent chaperone that protects OMPs from folding stress (80, 81), CpxP might have a dual function by both regulating the Cpx response and acting as a chaperone (57, 82). Although not further investigated here, we suggest that *tisB* expression leads to protein folding stress in the cell envelope, thereby activating the Cpx response.

The membrane toxin TisB is well studied with regard to its inducing condition (i.e., SOS response following DNA damage) (33, 39, 42). TisB-dependent effects can, therefore, be revealed upon treatment with the DNA-damaging antibiotic CIP (31). Antibiotics have already been associated with an increased abundance of heat shock proteins and chaperones, as, for example, observed in *Pseudomonas aeruginosa* treated with the aminoglycoside tobramycin (83), *Streptococcus pneumoniae* treated with the β-lactam penicillin (84), or *Acinetobacter baumannii* treated with different classes of antibiotics (85). In *E. coli*, the deletion of heat shock proteins and chaperones resulted in reduced survival upon treatment with levofloxacin (86), a fluoroquinolone (FQ) antibiotic that is functionally related to CIP. The authors assumed that FQ antibiotics induce the formation of cytosolic protein aggregates, which need to be disassembled by heat shock proteins and chaperones (86). Intriguingly, we can demonstrate that protein aggregation occurs upon treatment with CIP and that this process depends on TisB, suggesting that TisB is the foremost factor for protein aggregation in response to FQ-induced DNA damage. The question remains how a membrane toxin provokes aggregation. Hypothetically, TisB accumulates in the cytoplasm and initiates a nucleation process that leads to aggregate formation (87). However, cellular fractionation experiments combined with western blot analysis indicate that TisB does not accumulate in the cytoplasm but rather completely localizes to the membrane (our unpublished results). Furthermore, we show here that the production of the attenuated toxin TisB-K12L does not trigger aggregation. We conclude that aggregation is a downstream effect of TisB and its function as a pore-forming toxin. Strong ATP depletion might be the crucial factor that drives TisB-dependent protein aggregation when *tisB* is expressed from the p0SD-*tisB* systems (62, 63). However, strong ATP depletion was not observed in CIP-treated wild-type cells and therefore fails to convincingly explain the CIP-induced protein aggregation. The primary action of TisB is the breakdown of the proton motive force (39), which is similar to the action of protonophores and leads to disturbance of pH homeostasis and acidification of the cytoplasm (88–90). Potentially, the drop in intracellular pH initiates the aggregation process (91), but this needs further investigation. Interestingly, it was observed only recently that TisB is the major factor for cytoplasmic condensation upon treatment with the DNA-damaging antibiotic ofloxacin (90). Whether cytoplasmic condensation and protein aggregation are intertwined processes remains an exciting issue for future studies.

Analysis of TisB-dependent protein aggregates revealed the enrichment of proteins from cryptic prophages, and it remains an open question whether this is coincidental or has a biological meaning. *E. coli* K-12 harbors nine cryptic prophages, and—albeit their functions remain largely unknown—it has been observed that they contribute to survival under antibiotic stress, including the DNA-damaging quinolone nalidixic acid (92). Potentially, the prophage proteins contribute to the aggregation process, which, in turn, affects antibiotic tolerance, but this needs further investigation.

Our data indicate that the occurrence of protein aggregates correlates well with an increased dormancy duration, which is in accordance with previous observations (62, 63). The dormancy duration might also ultimately affect persister levels. The wild-type had ~20-fold more persister cells than the *tisB* deletion mutant when treated with CIP at 37°C, corroborating former results (33, 39), but persister levels were comparable at 46°C. This apparent discrepancy can be solved when persister levels are seen as a dynamic measure that is mainly determined by the dormancy duration or, in other words, by the "kinetics of awakening" (93). At 37°C, the *tisB* deletion strain does not form protein aggregates, wakes up early, is killed by CIP and, hence, has a reduced persister level as

compared to the wild type. At 46°C, however, both strains form aggregates and wake up with the same kinetics, resulting in comparable persister levels. These considerations may also help to solve a recurrent discrepancy in the literature regarding TisB-dependent persistence. When *E. coli* is treated with CIP while growing in complex media, such as LB or Mueller-Hinton broth, a *tisB* deletion strain scores fewer persister cells than a wild type (33, 39). By contrast, when a MOPS-based minimal medium and ofloxacin are applied, a *tisB* deletion strain and a wild type have similar persister levels (90, 94). We assume that in MOPS medium wake-up kinetics are comparable between both strains, resulting in similar killing kinetics and, hence, persister levels. However, we cannot exclude that the antibiotic of choice (CIP versus ofloxacin) may have contributed to the conflicting results obtained in different laboratories. In conclusion, we propose that the primary function of the membrane toxin TisB is the establishment of a dormant state through energy depletion, but that secondary effects and environmental conditions determine the dormancy duration, which, in turn, affects long-term survival.

MATERIALS AND METHODS

Growth conditions

E. coli strains were grown in lysogeny broth (LB) medium at 37°C and 180 rpm. If temperature-sensitive plasmids were present, strains were grown at 30°C and 180 rpm. Pre-cultures were cultivated in the presence of antibiotics if applicable (50 µg/mL kanamycin, 15 µg/mL chloramphenicol, 200 µg/mL ampicillin, and 6 µg/mL tetracycline). Pre-cultures were diluted 100-fold into fresh LB medium and grown until the exponential phase was reached. Growth curves were recorded in 30-min time intervals with a cell density meter model 40 (Fisher Scientific).

Construction of strains and plasmids

E. coli strains used in this study are derivatives of K-12 wild-type MG1655 and are listed in Table S1. Chromosomal deletion or transcriptional fusion mutants were constructed using the λ red methodology (95). A selection marker (*cat* or *kan* gene) was amplified via PCR using primers with specific 40 bp overhangs, matching the desired deletion locus. An *E. coli* MG1655 strain, that provides the heat-inducible λ red genes on plasmid pSIM5-tet (96), was grown at 30°C in the presence of tetracycline (3 µg/mL) until an OD_{600} of ~0.4 was reached. After a 15-min heat shock at 42°C, electrocompetent cells were prepared and PCR products were transformed via electroporation. Clones were selected on LB agar plates containing the appropriate antibiotic (12.5 µg/mL chloramphenicol or 50 µg/µL kanamycin), and gene deletions were subsequently verified by colony PCR. After two incubations at 42°C, loss of the heat-sensitive plasmid pSIM5-tet was verified by tetracycline sensitivity. If necessary, deletion constructs were transduced into new strain backgrounds using P1 phages according to standard protocols.

Expression plasmid p0SD-*tisB* was generated by AQUA cloning (97). The *tisB* insert was amplified by PCR using primer pair AQ-0ATG-2-f/NES-rev and plasmid p+42-*tisB* as a template. Primer AQ-0ATG-2-f provides both a 20 bp artificial 5′ UTR (lacking a Shine-Dalgarno sequence) and a 20 bp overhang for AQUA cloning. The pBAD backbone was amplified by PCR using primer pair AQ-topo-f/AQ-topo-rev to generate matching overhangs for the *tisB* insert. Purified amplification products were mixed in a final volume of 10 µL, applying a molecular ratio of 7:1 (insert to backbone; 100 ng backbone). Mixtures were incubated at 25°C for 1 hour. Afterward, mixtures were transformed into chemically competent MG1655 cells and clones were selected on LB agar containing ampicillin (200 µg/mL). In a similar way, plasmid p0SD-*3xFLAG-tisB* was generated with primer pair AQ-0ATG-3x-f/NES-rev using plasmid p+42–*3xFLAG-tisB* as a template for amplification of the *3×FLAG-tisB* insert. Plasmid p0SD-*tisB-K12L* was generated by site-directed mutagenesis PCR using primer pair K12L-for/K12L-rev and plasmid p0SD-*tisB* as template. After PCR, parental plasmids were digested with DpnI (Thermo Fisher Scientific), and the linear PCR product was transformed into chemically

competent MG1655 cells. Clones were selected on LB agar containing ampicillin (200 µg/mL). For the generation of *cpxP*, *ibpAB*, and *spy* overexpression plasmids, the corresponding genes were amplified via PCR using primers containing BbsI recognition sites for the generation of specific overhangs. PCR products were cloned into plasmid pSL0002 using Golen Gate cloning as described elsewhere (98). For the generation of plasmid p0SD-*syfp2*, the pBAD backbone (37) and the *syfp2* open reading frame were amplified via PCR with primers introducing recognition sites for EcoRI and HindIII, followed by restriction and ligation. The forward primer for *syfp2* contained a sequence for the 20 bp artificial 5′ UTR. The ligation product was transformed into electrocompetent *E. coli* MG1655 cells. Clones were selected on LB agar containing ampicillin (200 µg/mL). All plasmids were verified by Sanger sequencing (Microsynth SeqLab, Göttingen, Germany) and are listed in Table S2. Primers used for cloning procedures are listed in Table S3.

Determination of relative colony counts and persister levels

Exponential-phase cultures (OD_{600} ~ 0.4) were treated with L-ara (0.2%) for 1 hour or with CIP (10 µg/µL; 1,000× MIC) for 6 hours at 37°C and 180 rpm. Pre- and post-treatment samples were serially diluted and plated on LB agar plates. In the case of L-ara treatment, cells were diluted with NaCl (0.9%). In the case of CIP treatment, cells were washed two times and diluted with 20 mM $MgSO_4$. Colonies were counted after ~20 hours (pre-treatment) or ~40 hours (post-treatment). Colony counts were used to determine CFU per milliliter. The ratio between treated and untreated samples represents either the relative CFU count (L-ara) or persister level (CIP). *P*-values were calculated using an ANOVA with a post hoc Tukey HSD test in R statistical language (https://www.r-project.org/).

Analysis of colony growth

Colony growth was analyzed using the ScanLag method (55). Agar plates from L-ara or CIP treatments (see "Determination of relative CFU counts and persister levels") were covered with black felt, placed on scanners, and incubated at 37°C. Epson Perfection V39 scanners were used to record a time series of images controlled by the ScanningManager application. Images (TIFF files) were taken every 20 min for a total period of 40 hours. Image processing was performed using MatLab (MathWorks) with functions PreparePictures, setMaskApp, TimeLapse, and ScanLagApp (54). After image processing, the appearance and growth times were extracted. The appearance time is defined by a colony size of 10 pixels, whereas the growth time is defined as the time that is needed to cause a colony size increase from 80 to 160 pixels. Growth data were used to create violin box plots with Power BI Desktop (Microsoft). *P*-values were calculated using a pairwise Wilcoxon rank-sum test in R statistical language (https://www.r-project.org/).

Membrane depolarization measurements

Exponential-phase cultures (OD_{600} ~0.4) were treated with 0.2% L-ara for 1 hour at 37°C and 180 rpm. Samples were withdrawn before and after the addition of L-ara and adjusted to an OD_{600} of 0.5. $DiBAC_4(3)$ (Sigma-Aldrich) was added at a final concentration of 1 µg/mL, followed by incubation for 20 min in the dark at room temperature. $DiBAC_4(3)$ fluorescence was measured via flow cytometry using a FACSCalibur (BD) and the FL1-H detector (ex: 488 ± 10 nm, em: 530 ± 30 nm). CellQuest Pro 4.0.2 (BD) was applied as an operating system. Data were analyzed with FlowJo v.10 (FlowJo LLC). Cell counts were normalized to ~10,000 events by application of the DownSample plugin.

ATP measurements

Cultures were grown to exponential phase (OD_{600} ~0.4) and treated with L-ara (0.2%) for 1 hour or with CIP (10 µg/µL; 1,000× MIC) for up to 6 hours. Samples (1 mL) were withdrawn before and after treatment. Cell pellets were collected by centrifugation (13,000 rpm, 3 min) and supernatants were discarded. Cells were washed with 1 mL NaCl (0.9%) and resuspended in 1 mL LB medium. 100 µL of samples was mixed

with 100 µL BacTiter-Glo reagent (Promega) and incubated for 5 min in the dark. The luminescence was measured using an Infinite M Nano+ microplate reader (Tecan). Values were transformed to nM, using the slope formula of an ATP calibration curve, and normalized to the OD_{600}. *P*-values were calculated using an ANOVA with a post-hoc Tukey HSD test in R statistical language (https://www.r-project.org/).

Fluorescence microscopy

Cultures were grown to exponential phase (OD_{600} ~0.4) and treated with L-ara (0.2%) for 1 hour or with CIP (10 µg/µL; 1,000× MIC) for 6 hours at 37°C or 46°C. Samples before and after treatment were transferred onto agarose pads (1% agarose in 1× PBS) on top of a microscopy slide with a cover slip on top of the cells. Images were recorded with a Leica DMI 6000 B inverse microscope (Leica Camera AG) using an HCX PL APO 100×/1.4 phase contrast objective, a pco.edge sCMOS camera (PCO AG), and software VisiView version 4.3.0 (Visitron Systems GmbH). For fluorescence images (GFP), a custom filter set (T495lpxr, EX470/40 m; EM525/50; Chroma Technology) was used. The exposure time was set to 50 ms with a binning of 2 and an offset of 0.0. Images were saved as TIFF and further processed with the open-source software ImageJ version 1.53 k.

Automated focus analysis

For U-Net training and segmentation, phase contrast images of *E. coli* cells were used. The software used was the U-Net plugin for ImageJ, available from the website of the Computer Vision Group at the University of Freiburg (65). For training, 906 cells in eight images were annotated. To enhance segmentation quality and facilitate the separation of cell aggregates into individual cells, one label was used for the circumference of the cells and one for their inside. A training with 2,000 iterations and a learning rate of 1E−4 yielded segmentations that were very close to the training annotation. With post-processing using a custom Wolfram Mathematica script, the segmentations were further refined and crooked, very small, very large features or cells at the image border were excluded. Visual inspection of all segmentations confirmed that the vast majority of cells were properly identified. The extracted cell shapes were used as masks for the GFP image channel. Spatial filtering, peak finding, and thresholding yielded the foci.

Preparation of RNA-sequencing samples

Exponential-phase cultures (OD_{600} ~ 0.4) of strain MG1655 p0SD-*tisB* were treated with 0,2% L-ara to induce *tisB* expression for 30 min. Samples from biological triplicates were withdrawn before (samples "Exp") and after L-ara treatment (samples "T30") and immediately inactivated by adding 200 µL stop solution (95% ethanol, 5% phenol) to 1 mL cell culture on ice. Total RNA was isolated according to the hot acid-phenol method as described (41). DNA was removed using the TURBO DNA-*free* kit (Invitrogen) according to the "rigorous treatment" instructions. The final clean-up was performed using phenol/chloroform/isoamyl alcohol (25:24:1) mixed with the sample in a 1:1 ratio, followed by chloroform treatment and precipitation as before. RNA quality was assessed on an 8% polyacrylamide gel containing 1× TBE and 7 M urea. Aliquots of approximately 3.5 µg of total RNA were prepared and stored at −80°C until further analysis.

RNA-sequencing and data analysis

RNA-sequencing was performed by vertis Biotechnologie AG. For cDNA synthesis, all RNA samples were first fragmented using ultrasound (4 pulses of 30 seconds, each at 4°C). Then, an oligonucleotide adapter was ligated to the 3′ end of the RNA molecules. First-strand cDNA synthesis was performed using M-MLV reverse transcriptase and the 3′ adapter as a primer. The first-strand cDNA was purified and the 5′ Illumina TruSeq sequencing adapter was ligated to the 3′ end of the antisense cDNA. The resulting cDNA was PCR-amplified to about 10–20 ng/µL using a high-fidelity DNA polymerase for 12 cycles. The TruSeq barcode sequences, which are part of the 5′ and 3′ TruSeq

sequencing adapters, were used. The cDNA was purified using the Agencourt AMPure XP kit (Beckman Coulter Genomics) and analyzed by capillary electrophoresis. For Illumina NextSeq sequencing, the samples were pooled in approximately equimolar amounts. The cDNA pool in the size range of 200–550 bp was eluted from a preparative agarose gel. An aliquot of the size-fractionated pool was analyzed by capillary electrophoresis. The cDNA pool was single-read sequenced on an Illumina NextSeq 500 system using 75 bp read length.

Quality and adapter trimming was performed with Trim Galore (Version 0.6.5) (https://github.com/FelixKrueger/TrimGalore) with Cutadapt Version 2.7 (http://dx.doi.org/10.14806/ej.17.1.200) using the parameters "--quality 20 --length 20" and default adapter detection and trimming. MultiQC (Version 1.8) (99) and FastQC (Version 0.11.8) (http://www.bioinformatics.babraham.ac.uk/projects/fastqc/) were used for quality control. The preprocessed reads were aligned with Bowtie2 (Version 2.3.5) (100) using the '--mm" and "--very-sensitive" settings and GCF_000005845.2 (NCBI; downloaded 25.11.2019) as a reference genome. For post-processing of the alignments, gene counting and data analysis, Samtools (Version 1.9) (101), featureCounts (Version 1.6.4) (102), and DESeq2 (Version 1.26) (103) were applied, respectively. All bioinformatic calculations were performed using Curare (Version 0.1.1) (https://github.com/pblumenkamp/Curare) and R statistical language (https://www.r-project.org/). Processed RNA-seq data are available as Data Set S1 and have been deposited together with raw data files on the NCBI Gene Expression Omnibus (GEO) under the accession number GSE255764.

Northern blot analysis

Cultures were grown to exponential phase (OD_{600} ~0.4) and treated with L-ara (0.2%) for 30 min. Total RNA for northern blot analysis was isolated using the hot acid-phenol method as described (41). Northern blot analysis was performed with 5–10 µg of total RNA. The RNA was separated using 10% polyacrylamide gels containing 1× TBE and 7 M urea at 300 V for approximately 3 hours. The RNA was transferred to a RotiNylon plus membrane (Roth) by semi-dry electroblotting at 250 mA for 3 hours. After UV-crosslinking, the membrane was pre-hybridized using Church buffer (0.5 M phosphate buffer [pH 7.2], 1% [wt/vol] bovine serum albumin, 1 mM EDTA, 7% [wt/vol] SDS) at 42°C for 1 hour. Hybridization with probes for detection was performed overnight. Specific probes were generated by end-labeling of oligodeoxyribonucleotides (Table S3) using T4 Polynucleotide Kinase (New England Biolabs) and [γ-^{32}P]ATP (Hartmann Analytic). Membranes were washed (5× SSC, 0.01% SDS) and exposed to phosphorimaging screens (Bio-Rad). Screens were analyzed using a Molecular Imager FX and the Quantity One 1-D Analysis Software (Bio-Rad).

Quantitative reverse transcription-PCR

Cultures were grown to exponential phase (OD_{600} ~0.4) and treated with L-ara (0.2%) 30 min. Total RNA for quantitative reverse transcription PCR (qRT-PCR) was isolated using the NucleoSpin RNA Kit (Macherey-Nagel), including DNA digestion. RNA concentrations were measured using a spectrophotometer (NanoDrop 1000) and subsequently adjusted to a concentration of 5 ng/µL. For reverse transcription and amplification of gene-specific fragments, 10 µL of reaction mixtures was prepared with the Brilliant III Ultra-Fast SYBR Green qRT-PCR Master Mix (Agilent) in technical duplicates for each sample. Reaction mixtures contained 1 ng/µL of total RNA and 0.5 µM of each primer (Table S3). Reverse transcription and amplification were performed on a CFX Connect Real-Time System (Bio-Rad). Reverse transcription was carried out at 50°C for 10 min followed by 95°C for 3 min. For amplification, 45 cycles were applied at 95°C for 5 seconds, 56°C for 10 seconds and 72°C for 10 seconds (*tisB* gene), or at 95°C for 5 seconds and 60°C for 10 seconds (all remaining genes). Amplification curves were recorded with the CFX Maestro software (Bio-Rad). Cq values were used to calculate fold changes according to Pfaffl (104). The *hcaT* gene was used as a reference for normalization (41).

Western blot analysis

For the detection of 3×FLAG-TisB, strains were grown to the exponential phase. Samples were withdrawn in a defined volume (equivalent to an OD_{600} of 10) and centrifuged at 10,000 rpm and 4°C for 10 min. Cell pellets were resuspended in 50 µL SDS sample buffer (12% SDS, 6% β-mercaptoethanol, 30% glycerol, 0.05% Coomassie blue, 150 mM Tris/HCl, pH 7.0). For protein separation, a Tricine-SDS-PAGE was applied with 16% polyacrylamide (105). Samples were incubated at 95°C for 10 min before loading onto the gel. An initial voltage of 60 V was applied until samples entered the separation gel. Afterward, electrophoresis was carried out at 100 V for about 3 hours. Proteins were transferred onto a PVDF membrane by semi-dry electroblotting overnight at 0.4 mA/cm^2. Membranes were stained with Ponceau S and documented before blocking with 5% milk powder in 1× PBST (PBS + 0.1% Tween20) for 1 hour. For detection of 3×FLAG-TisB, membranes were incubated with an HRP-conjugated monoclonal IgG α-FLAG antibody (Sigma-Aldrich) in 3% BSA in PBST at room temperature for 90 min. Using the Lumi-Light Western Blotting Substrate (Roche), 3×FLAG-TisB was visualized and documented in a chemiluminescence imager (PeqLab) with the FusionCapt Advance software (Vilber Lourmat).

Purification of protein aggregates

Protein aggregates were purified according to a published protocol (63) with minor modifications. Strains were grown to the exponential phase (OD_{600} ~0.4) and treated with CIP (10 µg/mL; 1,000× MIC) for 6 hours. Cells (38 mL culture volume) were harvested and centrifuged at 4,000 × *g* and 4°C for 30 min. Cells were resuspended in 10 mL washing buffer I (300 mM NaCl, 5 mM β-mercaptoethanol, 1 mM EDTA, 50 mM HEPES, pH 7.5) and centrifuged as before. The cell pellet was dissolved in 10 mL lysis buffer [washing buffer I containing 1 µg/mL leupeptin and 0.1 mg/mL 4-(2-aminoethyl)benzenesulfonyl fluoride hydrochloride (AEBSF)]. Cells were lysed in three cycles with a cell homogenizer at 1,380 to 1,725 bar, followed by centrifugation at 11,000 × *g* and 4°C for 30 min to clear the lysates. SNs were stored at −80°C until LC-MS analysis. Pellets were resuspended in 2 mL washing buffer II (washing buffer I containing 0.8% Triton X-100 and 0.1% sodium deoxycholate) and centrifuged as before. The washing step was repeated two more times. After the final washing step, pellets were resuspended in 1 mL solubilization buffer (1% SDS, 1× SigmaFast Protease Inhibitor [Sigma-Aldrich], 50 mM HEPES, pH 8.0). Pellet fractions (PF) were stored at −80°C until LC-MS analysis.

LC-MS-based proteome analysis

Samples generated via the purification of protein aggregates, that is, lysate supernatants and the protein aggregate pellets, were processed following the SP3 protocol (106). For the lysate supernatants and protein aggregate samples, 50 µg of each was analyzed. Briefly, all samples (in triplicate) were resuspended in 75 µL of 100 mM ammonium bicarbonate (ABC) buffer (pH 7.4). Samples were reduced in the presence of tris(2-carboxyethyl)phosphine (5 mM) (1 hour, 56°C), before alkylation was performed with chloroacetamide (50 mM) (room temperature [RT] in the dark, 30 min). Beads (SpeedBeads Magnetic Carboxylate) were washed twice with Milli-Q water, and 100 µg of beads in 250 mM ABC buffer were added to each sample (final volume of 100 µL per sample). Precipitation of the proteins onto the beads was initiated via the addition of 100 µL of ethanol, the samples were gently shaken (5 min, 800 rpm) before a further 300 µL of ethanol was added and the samples were gently shaken (800 rpm) for an additional 20 min (final concentration of ca. 80% ethanol). The bead-associated precipitated proteins were pelleted by centrifugation (21,100 × *g*, 5 min, RT) with magnet-assisted isolation to assist aspiration of the solution. The beads were then washed twice with 80% ethanol, with centrifugation (21,100 × *g*, 5 min, RT) and magnet-assisted aspiration to remove all liquid. The samples were briefly sonicated in a sonication bath between washes to aid in the re-solubilization of the protein-associated beads. Following the final wash, the beads were suspended in 100 µL of 100 mM ABC buffer containing

trypsin (0.4 µg in total per sample, enzyme to protein ratio of 1:125), the samples were briefly sonicated to ensure no aggregation of the beads, then incubated overnight (37°C, shaking at 1,300 rpm). Following overnight digestion, the samples were centrifuged (21,100 × *g*, 5 min), before magnet-assisted collection of the peptide-containing supernatant was performed. The peptides were cleaned up via solid phase extraction (SPE) using Pierce C18 Tips 100 µL (as per the manufacturer's protocol). Following cleanup, the supernatants were dried down via vacuum centrifugation and stored at −20°C. On the day of MS analysis, peptides were resuspended in 20 µL of HPLC loading buffer (3% acetonitrile and 0.1% trifluoroacetic acid).

Chromatographic separation was performed on a Dionex U3000 Nano-HPLC system equipped with an Acclaim PepMap 100 C18 column (2 µm particle size, 75 µm × 500 mm) coupled online to a mass spectrometer. The eluents used were as follows: eluent A (0.05% formic acid) and eluent B (80% acetonitrile and 0.04% formic acid). The separation was performed over a programmed 120 min run. Initial chromatographic conditions were 4% eluent B for 4 min followed by linear gradients from 4% to 50% eluent B over 90 min, then 50% to 95% over 8 min, and 8 min at 95% eluent B. Following this, an inter-run equilibration of the column was performed (20 min at 4% eluent B). A 300 nL/min flow rate and 1 µL of sample were injected per run. Two wash runs (loading buffer injections) were performed between each sample. Data acquisition following separation was performed on a Q Exactive Plus mass spectrometer (Thermo Fisher Scientific). A full scan MS acquisition was performed (350–1,000 *m/z*, resolution 70,000) with the subsequent data-dependent MS/MS acquisition for the top 15 most intense ions via HCD activation at NCE 26 (resolution 17,500); an isolation window of 3 *m/z* was employed with apex trigger (3–15 s) and dynamic exclusion (30 s duration) enabled.

Bottom-up proteomic data analysis was performed using Proteome Discoverer (Ver. 3.0.1.27) (Thermo Fisher Scientific), and the Chimerys search algorithm. In addition, the Minora node was included to enable label-free quantification. Raw data files were searched against a protein FASTA database containing the complete UniProt *E. coli* (K-12 substrain MG1655) protein FASTA (accessed from UniProt 2023.04.11) plus the list of common laboratory contaminants (cRAP47). The searches were conducted with trypsin specificity, allowing a maximum of two missed cleavages. Strict parsimony criteria were applied with high stringency at both the protein and peptide levels (protein level false discovery rate [FDR] < 1%), and at least one high unique confidence peptide (PSM level FDR < 1%). Statistical assessment of the data was performed using the Perseus software package (Ver. 2.0.10.0). The Welch's *t*-test was performed with a minimum of two valid quantification values required for each protein in both groups, and Benjamini-Hochberg FDR calculation was performed at both medium (FDR < 5%) and high (FDR < 1%) cut-off levels. In addition, an abundance fold change of greater than 2 (i.e., $\log_2$ difference < −1 or > 1) was required. Further assessment of potentially enriched protein categories was performed via 1D annotation enrichment (Benjamini-Hochberg FDR < 0.1) for the SN samples. The mass spectrometry proteomics data have been deposited to the ProteomeXchange Consortium (107) via the PRIDE partner repository with the data set identifier PXD049478.

Bioinformatics data analysis

For bioinformatics data analysis of protein aggregates, two different data sets were defined. All proteins, that were identified in at least two biological replicates of either wild-type or Δ*tisB* supernatant samples, were used as reference and referred to as combined supernatant. All proteins, that were exclusively present or enriched in wild-type pellet fractions in comparison to Δ*tisB* pellet fractions, were defined as TisB-dependent protein aggregates (TdPA). For the prediction of protein localization, LocTree3 was used (108). The file 83333_Escherichia_coli.bact.lc3 was retrieved from Bacteria.zip and used to assign the localization to each identified protein. For protein-protein association networks and functional enrichment analyses, a multi-protein search in the STRING database was performed (68).

ACKNOWLEDGMENTS

We are grateful to Niklas Philipp for his help with data analysis. We would like to thank Nasrine Bekhedda and Dana Sensen for their experimental support. Abram Aertsen is acknowledged for providing the *ibpA-msfGFP* reporter strain. We further thank Liliya Chernova for the discussion on protein aggregation and Kai Thormann for support with microscopy.

Work in the group of B.A.B. was supported by the German Research Council (DFG) in the framework of the SPP2002 (BE 5210/3-1 and BE 5210/3-2) and by Fonds der Chemischen Industrie (material cost allowance). A.T. and L.C. were supported by DFG in the framework of the SPP2002, project Z2 (TH872/10-2). H.-G.K. was supported by the DFG in the framework of the SPP2002 (KO2184/9.1 and KO2184/9.2) and by the SFB1381 (Project ID 403222702).

AUTHOR AFFILIATIONS

[1]Institute for Microbiology and Molecular Biology, Justus-Liebig-Universität, Giessen, Germany
[2]Systematic Proteome Research & Bioanalytics, Institute for Experimental Medicine, Christian-Albrechts-Universität, Kiel, Germany
[3]Branch for Bioresources of the Fraunhofer IME, Fraunhofer Institute for Molecular Biology and Applied Ecology IME, Giessen, Germany
[4]Department of Insect Biotechnology, Justus-Liebig-Universität, Giessen, Germany
[5]Bioinformatics and Systems Biology, Justus-Liebig-Universität, Giessen, Germany
[6]Institute of Biochemistry and Molecular Biology, ZBMZ, Faculty of Medicine, Albert-Ludwigs-Universität, Freiburg, Germany
[7]Faculty of Biology, Albert-Ludwigs-Universität, Freiburg, Germany
[8]Internal Medicine IV, Department of Medicine, University Medical Center, and Faculty of Medicine, Albert-Ludwigs-Universität, Freiburg, Germany
[9]BIOSS Centre for Biological Signalling Studies, Albert-Ludwigs-Universität, Freiburg, Germany

PRESENT ADDRESS

Bork A. Berghoff, Institute of Molecular Biology and Biotechnology of Prokaryotes, University of Ulm, Ulm, Germany

AUTHOR ORCIDs

Andreas Tholey http://orcid.org/0000-0002-8687-6817
Hans-Georg Koch http://orcid.org/0000-0001-5913-0334
Bork A. Berghoff http://orcid.org/0000-0002-6299-419X

FUNDING

Funder	Grant(s)	Author(s)
Deutsche Forschungsgemeinschaft (DFG)	BE 5210/3-1,BE 5210/3-2	Bork A. Berghoff
Fonds der Chemischen Industrie (FCI)	material cost allowance	Bork A. Berghoff
Deutsche Forschungsgemeinschaft (DFG)	TH872/10-2	Liam Cassidy Andreas Tholey
Deutsche Forschungsgemeinschaft (DFG)	KO2184/9.1, KO2184/9.2, SFB1381 (Project ID 403222702)	Hans-Georg Koch

AUTHOR CONTRIBUTIONS

Florian H. Leinberger, Conceptualization, Data curation, Formal analysis, Investigation, Validation, Visualization, Writing – original draft | Liam Cassidy, Data curation, Formal analysis, Investigation, Methodology, Validation, Visualization, Writing – original draft | Daniel Edelmann, Conceptualization, Formal analysis, Investigation | Nicole E. Schmid, Formal analysis, Investigation | Markus Oberpaul, Formal analysis, Investigation, Methodology | Patrick Blumenkamp, Data curation, Formal analysis | Sebastian Schmidt, Investigation | Ana Natriashvili, Formal analysis, Investigation | Maximilian H. Ulbrich, Data curation, Formal analysis, Methodology, Visualization | Andreas Tholey, Formal analysis, Funding acquisition, Project administration, Supervision | Hans-Georg Koch, Conceptualization, Funding acquisition, Project administration, Supervision | Bork A. Berghoff, Conceptualization, Formal analysis, Funding acquisition, Project administration, Supervision, Visualization, Writing – original draft

DATA AVAILABILITY

Processed RNA-seq data are available as Data Set S1 and have been deposited together with raw data files on the NCBI Gene Expression Omnibus (GEO) under the accession number GSE255764. The mass spectrometry proteomics data have been deposited to the ProteomeXchange Consortium (107) via the PRIDE partner repository with the data set identifier PXD049478.

ADDITIONAL FILES

The following material is available online.

Supplemental Material

Data Set S1 (mSystems01060-24-s0001.xlsx). RNA-seq results.
Data Set S2 (mSystems01060-24-s0002.xlsx). Proteomics data.
Supplemental Figures (mSystems01060-24-s0003.pdf). Figures S1 to S9.
Supplemental Tables (mSystems01060-24-s0004.xlsx). Tables S1 to S3.

REFERENCES

1. Ayrapetyan M, Williams T, Oliver JD. 2018. Relationship between the viable but nonculturable state and antibiotic persister cells. J Bacteriol 200:e00249-18. https://doi.org/10.1128/JB.00249-18
2. Lewis K. 2007. Persister cells, dormancy and infectious disease. Nat Rev Microbiol 5:48–56. https://doi.org/10.1038/nrmicro1557
3. Veening J-W, Smits WK, Kuipers OP. 2008. Bistability, epigenetics, and bet-hedging in bacteria. Annu Rev Microbiol 62:193–210. https://doi.org/10.1146/annurev.micro.62.081307.163002
4. McDonald MD, Owusu-Ansah C, Ellenbogen JB, Malone ZD, Ricketts MP, Frolking SE, Ernakovich JG, Ibba M, Bagby SC, Weissman JL. 2024. What is microbial dormancy? Trends Microbiol 32:142–150. https://doi.org/10.1016/j.tim.2023.08.006
5. Lennon JT, Jones SE. 2011. Microbial seed banks: the ecological and evolutionary implications of dormancy. Nat Rev Microbiol 9:119–130. https://doi.org/10.1038/nrmicro2504
6. Checinska A, Paszczynski A, Burbank M. 2015. *Bacillus* and other spore-forming genera: variations in responses and mechanisms for survival. Annu Rev Food Sci Technol 6:351–369. https://doi.org/10.1146/annurev-food-030713-092332
7. Muñoz-Dorado J, Marcos-Torres FJ, García-Bravo E, Moraleda-Muñoz A, Pérez J. 2016. Myxobacteria: moving, killing, feeding, and surviving together. Front Microbiol 7:781. https://doi.org/10.3389/fmicb.2016.00781
8. Lewis K. 2010. Persister cells. Annu Rev Microbiol 64:357–372. https://doi.org/10.1146/annurev.micro.112408.134306
9. Lewis K. 2008. Multidrug tolerance of biofilms and persister cells, p 107–131. In Current topics in microbiology and immunology
10. Balaban NQ, Helaine S, Lewis K, Ackermann M, Aldridge B, Andersson DI, Brynildsen MP, Bumann D, Camilli A, Collins JJ, Dehio C, Fortune S, Ghigo J-M, Hardt W-D, Harms A, Heinemann M, Hung DT, Jenal U, Levin BR, Michiels J, Storz G, Tan M-W, Tenson T, Van Melderen L, Zinkernagel A. 2019. Definitions and guidelines for research on antibiotic persistence. Nat Rev Microbiol 17:441–448. https://doi.org/10.1038/s41579-019-0196-3
11. Liu J, Gefen O, Ronin I, Bar-Meir M, Balaban NQ. 2020. Effect of tolerance on the evolution of antibiotic resistance under drug combinations. Science 367:200–204. https://doi.org/10.1126/science.aay3041
12. Levin-Reisman I, Ronin I, Gefen O, Braniss I, Shoresh N, Balaban NQ. 2017. Antibiotic tolerance facilitates the evolution of resistance. Science 355:826–830. https://doi.org/10.1126/science.aaj2191
13. Windels EM, Michiels JE, Fauvart M, Wenseleers T, Van den Bergh B, Michiels J. 2019. Bacterial persistence promotes the evolution of antibiotic resistance by increasing survival and mutation rates. ISME J 13:1239–1251. https://doi.org/10.1038/s41396-019-0344-9
14. Balaban NQ, Merrin J, Chait R, Kowalik L, Leibler S. 2004. Bacterial persistence as a phenotypic switch. Science 305:1622–1625. https://doi.org/10.1126/science.1099390
15. Johnson PJT, Levin BR. 2013. Pharmacodynamics, population dynamics, and the evolution of persistence in *Staphylococcus aureus*. PLoS Genet 9:e1003123. https://doi.org/10.1371/journal.pgen.1003123
16. Pontes MH, Groisman EA. 2019. Slow growth determines nonheritable antibiotic resistance in *Salmonella enterica*. Sci Signal 12:eaax3938. https://doi.org/10.1126/scisignal.aax3938
17. Korch SB, Henderson TA, Hill TM. 2003. Characterization of the *hipA7* allele of *Escherichia coli* and evidence that high persistence is governed

by (p)ppGpp synthesis. Mol Microbiol 50:1199–1213. https://doi.org/10.1046/j.1365-2958.2003.03779.x
18. Radzikowski JL, Vedelaar S, Siegel D, Ortega ÁD, Schmidt A, Heinemann M. 2016. Bacterial persistence is an active σ^S stress response to metabolic flux limitation. Mol Syst Biol 12:882. https://doi.org/10.15252/msb.20166998
19. Wu Y, Vulić M, Keren I, Lewis K. 2012. Role of oxidative stress in persister tolerance. Antimicrob Agents Chemother 56:4922–4926. https://doi.org/10.1128/AAC.00921-12
20. Hernandez-Morfa M, Reinoso-Vizcaíno NM, Olivero NB, Zappia VE, Cortes PR, Jaime A, Echenique J. 2022. Host cell oxidative stress promotes intracellular fluoroquinolone persisters of *Streptococcus pneumoniae*. Microbiol Spectr 10:e0436422. https://doi.org/10.1128/spectrum.04364-22
21. Shan Y, Brown Gandt A, Rowe SE, Deisinger JP, Conlon BP, Lewis K. 2017. ATP-dependent persister formation in *Escherichia coli*. mBio 8:e02267-16. https://doi.org/10.1128/mBio.02267-16
22. Conlon BP, Rowe SE, Gandt AB, Nuxoll AS, Donegan NP, Zalis EA, Clair G, Adkins JN, Cheung AL, Lewis K. 2016. Persister formation in *Staphylococcus aureus* is associated with ATP depletion. Nat Microbiol 1:16051. https://doi.org/10.1038/nmicrobiol.2016.51
23. Orman MA, Brynildsen MP. 2013. Dormancy is not necessary or sufficient for bacterial persistence. Antimicrob Agents Chemother 57:3230–3239. https://doi.org/10.1128/AAC.00243-13
24. Harms A, Brodersen DE, Mitarai N, Gerdes K. 2018. Toxins, targets, and triggers: an overview of toxin-antitoxin biology. Mol Cell 70:768–784. https://doi.org/10.1016/j.molcel.2018.01.003
25. Jurėnas D, Fraikin N, Goormaghtigh F, Van Melderen L. 2022. Biology and evolution of bacterial toxin-antitoxin systems. Nat Rev Microbiol 20:335–350. https://doi.org/10.1038/s41579-021-00661-1
26. Ronneau S, Helaine S. 2019. Clarifying the link between toxin–antitoxin modules and bacterial persistence. J Mol Biol 431:3462–3471. https://doi.org/10.1016/j.jmb.2019.03.019
27. Shore SFH, Leinberger FH, Fozo EM, Berghoff BA. 2024. Type I toxin-antitoxin systems in bacteria: from regulation to biological functions. EcoSal Plus:eesp00252022. https://doi.org/10.1128/ecosalplus.esp-0025-2022
28. Page R, Peti W. 2016. Toxin-antitoxin systems in bacterial growth arrest and persistence. Nat Chem Biol 12:208–214. https://doi.org/10.1038/nchembio.2044
29. Van Melderen L, Wood TK. 2017. Commentary: what is the link between stringent response, endoribonuclease encoding type II toxin-antitoxin systems and persistence? Front Microbiol 8:191. https://doi.org/10.3389/fmicb.2017.00191
30. Goormaghtigh F, Fraikin N, Putrinš M, Hallaert T, Hauryliuk V, Garcia-Pino A, Sjödin A, Kasvandik S, Udekwu K, Tenson T, Kaldalu N, Van Melderen L. 2018. Reassessing the role of type II toxin-antitoxin systems in formation of *Escherichia coli* type II persister cells. mBio 9:e00640-18. https://doi.org/10.1128/mBio.00640-18
31. Edelmann D, Berghoff BA. 2022. A shift in perspective: a role for the type I toxin TisB as persistence-stabilizing factor. Front Microbiol 13:871699. https://doi.org/10.3389/fmicb.2022.871699
32. Helaine S, Cheverton AM, Watson KG, Faure LM, Matthews SA, Holden DW. 2014. Internalization of *Salmonella* by macrophages induces formation of nonreplicating persisters. Science 343:204–208. https://doi.org/10.1126/science.1244705
33. Dörr T, Vulić M, Lewis K. 2010. Ciprofloxacin causes persister formation by inducing the TisB toxin in *Escherichia coli*. PLoS Biol 8:e1000317. https://doi.org/10.1371/journal.pbio.1000317
34. Wagner EGH, Unoson C. 2012. The toxin-antitoxin system *tisB-istR1*: expression, regulation, and biological role in persister phenotypes. RNA Biol 9:1513–1519. https://doi.org/10.4161/rna.22578
35. Berghoff BA, Wagner EGH. 2019. Persister formation driven by TisB-dependent membrane depolarization, p 77–97. In Lewis K (ed), Persister cells and infectious disease. Springer International Publishing, Cham.
36. Berghoff BA, Wagner EGH. 2017. RNA-based regulation in type I toxin-antitoxin systems and its implication for bacterial persistence. Curr Genet 63:1011–1016. https://doi.org/10.1007/s00294-017-0710-y
37. Unoson C, Wagner EGH. 2008. A small SOS-induced toxin is targeted against the inner membrane in *Escherichia coli*. Mol Microbiol 70:258–270. https://doi.org/10.1111/j.1365-2958.2008.06416.x
38. Gurnev PA, Ortenberg R, Dörr T, Lewis K, Bezrukov SM. 2012. Persister-promoting bacterial toxin TisB produces anion-selective pores in planar lipid bilayers. FEBS Lett 586:2529–2534. https://doi.org/10.1016/j.febslet.2012.06.021
39. Berghoff BA, Hoekzema M, Aulbach L, Wagner EGH. 2017. Two regulatory RNA elements affect TisB-dependent depolarization and persister formation. Mol Microbiol 103:1020–1033. https://doi.org/10.1111/mmi.13607
40. Edelmann D, Berghoff BA. 2019. Type I toxin-dependent generation of superoxide affects the persister life cycle of *Escherichia coli*. Sci Rep 9:14256. https://doi.org/10.1038/s41598-019-50668-1
41. Berghoff BA, Karlsson T, Källman T, Wagner EGH, Grabherr MG. 2017. RNA-sequence data normalization through *in silico* prediction of reference genes: the bacterial response to DNA damage as case study. BioData Min 10:30. https://doi.org/10.1186/s13040-017-0150-8
42. Vogel J, Argaman L, Wagner EGH, Altuvia S. 2004. The small RNA IstR inhibits synthesis of an SOS-induced toxic peptide. Curr Biol 14:2271–2276. https://doi.org/10.1016/j.cub.2004.12.003
43. Darfeuille F, Unoson C, Vogel J, Wagner EGH. 2007. An antisense RNA inhibits translation by competing with standby ribosomes. Mol Cell 26:381–392. https://doi.org/10.1016/j.molcel.2007.04.003
44. Romilly C, Lippegaus A, Wagner EGH. 2020. An RNA pseudoknot is essential for standby-mediated translation of the *tisB* toxin mRNA in *Escherichia coli*. Nucleic Acids Res 48:12336–12347. https://doi.org/10.1093/nar/gkaa1139
45. Romilly C, Deindl S, Wagner EGH. 2019. The ribosomal protein S1-dependent standby site in *tisB* mRNA consists of a single-stranded region and a 5′ structure element. Proc Natl Acad Sci U S A 116:15901–15906. https://doi.org/10.1073/pnas.1904309116
46. Edelmann D, Oberpaul M, Schäberle TF, Berghoff BA. 2021. Post-transcriptional deregulation of the *tisB/istR-1* toxin–antitoxin system promotes SOS-independent persister formation in *Escherichia coli*. Environ Microbiol Rep 13:159–168. https://doi.org/10.1111/1758-2229.12919
47. Fozo EM, Kawano M, Fontaine F, Kaya Y, Mendieta KS, Jones KL, Ocampo A, Rudd KE, Storz G. 2008. Repression of small toxic protein synthesis by the Sib and OhsC small RNAs. Mol Microbiol 70:1076–1093. https://doi.org/10.1111/j.1365-2958.2008.06394.x
48. Brielle R, Pinel-Marie M-L, Felden B. 2016. Linking bacterial type I toxins with their actions. Curr Opin Microbiol 30:114–121. https://doi.org/10.1016/j.mib.2016.01.009
49. Spanka D-T, Konzer A, Edelmann D, Berghoff BA. 2019. High-throughput proteomics identifies proteins with importance to postantibiotic recovery in depolarized persister cells. Front Microbiol 10:378. https://doi.org/10.3389/fmicb.2019.00378
50. Edelmann D, Leinberger FH, Schmid NE, Oberpaul M, Schäberle TF, Berghoff BA. 2021. Elevated expression of toxin TisB protects persister cells against ciprofloxacin but enhances susceptibility to mitomycin C. Microorganisms 9:943. https://doi.org/10.3390/microorganisms9050943
51. Lutz R, Bujard H. 1997. Independent and tight regulation of transcriptional units in *Escherichia coli* via the LacR/O, the TetR/O and AraC/I1-I2 regulatory elements. Nucleic Acids Res 25:1203–1210. https://doi.org/10.1093/nar/25.6.1203
52. Osterman IA, Evfratov SA, Sergiev PV, Dontsova OA. 2013. Comparison of mRNA features affecting translation initiation and reinitiation. Nucleic Acids Res 41:474–486. https://doi.org/10.1093/nar/gks989
53. Rotem E, Loinger A, Ronin I, Levin-Reisman I, Gabay C, Shoresh N, Biham O, Balaban NQ. 2010. Regulation of phenotypic variability by a threshold-based mechanism underlies bacterial persistence. Proc Natl Acad Sci U S A 107:12541–12546. https://doi.org/10.1073/pnas.1004333107
54. Levin-Reisman I, Fridman O, Balaban NQ. 2014. ScanLag: high-throughput quantification of colony growth and lag time. J Vis Exp e51456:51456. https://doi.org/10.3791/51456
55. Levin-Reisman I, Gefen O, Fridman O, Ronin I, Shwa D, Sheftel H, Balaban NQ. 2010. Automated imaging with ScanLag reveals previously

undetectable bacterial growth phenotypes. Nat Methods 7:737–739. https://doi.org/10.1038/nmeth.1485
56. Santos-Zavaleta A, Salgado H, Gama-Castro S, Sánchez-Pérez M, Gómez-Romero L, Ledezma-Tejeida D, García-Sotelo JS, Alquicira-Hernández K, Muñiz-Rascado LJ, Peña-Loredo P, Ishida-Gutiérrez C, Velázquez-Ramírez DA, Del Moral-Chávez V, Bonavides-Martínez C, Méndez-Cruz CF, Galagan J, Collado-Vides J. 2019. RegulonDB v 10.5: tackling challenges to unify classic and high throughput knowledge of gene regulation in *E. coli* K-12. Nucleic Acids Res 47:D212–D220. https://doi.org/10.1093/nar/gky1077
57. Grabowicz M, Silhavy TJ. 2017. Envelope stress responses: an interconnected safety net. Trends Biochem Sci 42:232–242. https://doi.org/10.1016/j.tibs.2016.10.002
58. Lee J, Hiibel SR, Reardon KF, Wood TK. 2010. Identification of stress - related proteins in *Escherichia coli* using the pollutant *cis* - dichloroethylene. J Appl Microbiol 108:2088–2102. https://doi.org/10.1111/j.1365-2672.2009.04611.x
59. Zhang X-S, García-Contreras R, Wood TK. 2007. YcfR (BhsA) influences *Escherichia coli* biofilm formation through stress response and surface hydrophobicity. J Bacteriol 189:3051–3062. https://doi.org/10.1128/JB.01832-06
60. Mermod M, Magnani D, Solioz M, Stoyanov JV. 2012. The copper-inducible ComR (YcfQ) repressor regulates expression of ComC (YcfR), which affects copper permeability of the outer membrane of *Escherichia coli*. Biometals 25:33–43. https://doi.org/10.1007/s10534-011-9510-x
61. Zhao Z, Xu Y, Jiang B, Qi Q, Tang Y-J, Xian M, Wang J, Zhao G. 2022. Systematic identification of CpxRA-regulated genes and their roles in *Escherichia coli* stress response. mSystems 7:e0041922. https://doi.org/10.1128/msystems.00419-22
62. Pu Y, Li Y, Jin X, Tian T, Ma Q, Zhao Z, Lin S-Y, Chen Z, Li B, Yao G, Leake MC, Lo C-J, Bai F. 2019. ATP-dependent dynamic protein aggregation regulates bacterial dormancy depth critical for antibiotic tolerance. Mol Cell 73:143–156. https://doi.org/10.1016/j.molcel.2018.10.022
63. Dewachter L, Bollen C, Wilmaerts D, Louwagie E, Herpels P, Matthay P, Khodaparast L, Khodaparast L, Rousseau F, Schymkowitz J, Michiels J. 2021. The dynamic transition of persistence toward the viable but nonculturable state during stationary phase is driven by protein aggregation. mBio 12:e0070321. https://doi.org/10.1128/mBio.00703-21
64. Govers SK, Mortier J, Adam A, Aertsen A. 2018. Protein aggregates encode epigenetic memory of stressful encounters in individual *Escherichia coli* cells. PLoS Biol 16:e2003853. https://doi.org/10.1371/journal.pbio.2003853
65. Falk T, Mai D, Bensch R, Çiçek Ö, Abdulkadir A, Marrakchi Y, Böhm A, Deubner J, Jäckel Z, Seiwald K, Dovzhenko A, Tietz O, Dal Bosco C, Walsh S, Saltukoglu D, Tay TL, Prinz M, Palme K, Simons M, Diester I, Brox T, Ronneberger O. 2019. U-Net: deep learning for cell counting, detection, and morphometry. Nat Methods 16:67–70. https://doi.org/10.1038/s41592-018-0261-2
66. Courcelle J, Khodursky A, Peter B, Brown PO, Hanawalt PC. 2001. Comparative gene expression profiles following UV exposure in wild-type and SOS-deficient *Escherichia coli*. Genetics 158:41–64. https://doi.org/10.1093/genetics/158.1.41
67. Wagner S, Baars L, Ytterberg AJ, Klussmeier A, Wagner CS, Nord O, Nygren P-A, van Wijk KJ, de Gier J-W. 2007. Consequences of membrane protein overexpression in *Escherichia coli*. Mol Cell Proteomics 6:1527–1550. https://doi.org/10.1074/mcp.M600431-MCP200
68. Szklarczyk D, Kirsch R, Koutrouli M, Nastou K, Mehryary F, Hachilif R, Gable AL, Fang T, Doncheva NT, Pyysalo S, Bork P, Jensen LJ, von Mering C. 2023. The STRING database in 2023: protein-protein association networks and functional enrichment analyses for any sequenced genome of interest. Nucleic Acids Res 51:D638–D646. https://doi.org/10.1093/nar/gkac1000
69. Harrison JJ, Wade WD, Akierman S, Vacchi-Suzzi C, Stremick CA, Turner RJ, Ceri H. 2009. The chromosomal toxin gene *yafQ* is a determinant of multidrug tolerance for *Escherichia coli* growing in a biofilm. Antimicrob Agents Chemother 53:2253–2258. https://doi.org/10.1128/AAC.00043-09
70. Singh R, Barry CE, Boshoff HIM. 2010. The three RelE homologs of *Mycobacterium tuberculosis* have individual, drug-specific effects on bacterial antibiotic tolerance. J Bacteriol 192:1279–1291. https://doi.org/10.1128/JB.01285-09
71. Korch SB, Hill TM. 2006. Ectopic overexpression of wild-type and mutant *hipA* genes in *Escherichia coli*: effects on macromolecular synthesis and persister formation. J Bacteriol 188:3826–3836. https://doi.org/10.1128/JB.01740-05
72. Chowdhury N, Kwan BW, Wood TK. 2016. Persistence increases in the absence of the alarmone guanosine tetraphosphate by reducing cell growth. Sci Rep 6:20519. https://doi.org/10.1038/srep20519
73. Ludwig P, Huber M, Lehr M, Wegener M, Zerulla K, Lange C, Soppa J. 2018. Non-canonical *Escherichia coli* transcripts lacking a Shine–Dalgarno motif have very different translational efficiencies and do not form a coherent group. Microbiol (Reading) 164:646–658. https://doi.org/10.1099/mic.0.000619
74. Mutschler H, Gebhardt M, Shoeman RL, Meinhart A. 2011. A novel mechanism of programmed cell death in bacteria by toxin-antitoxin systems corrupts peptidoglycan synthesis. PLoS Biol 9:e1001033. https://doi.org/10.1371/journal.pbio.1001033
75. Bahassi EM, O'Dea MH, Allali N, Messens J, Gellert M, Couturier M. 1999. Interactions of CcdB with DNA gyrase. Inactivation of GyrA, poisoning of the gyrase-DNA complex, and the antidote action of CcdA. J Biol Chem 274:10936–10944. https://doi.org/10.1074/jbc.274.16.10936
76. Critchlow SE, O'Dea MH, Howells AJ, Couturier M, Gellert M, Maxwell A. 1997. The interaction of the F plasmid killer protein, CcdB, with DNA gyrase: induction of DNA cleavage and blocking of transcription. J Mol Biol 273:826–839. https://doi.org/10.1006/jmbi.1997.1357
77. Wilmaerts D, Dewachter L, De Loose P-J, Bollen C, Verstraeten N, Michiels J. 2019. HokB monomerization and membrane repolarization control persister awakening. Mol Cell 75:1031–1042. https://doi.org/10.1016/j.molcel.2019.06.015
78. Schramm FD, Schroeder K, Jonas K. 2020. Protein aggregation in bacteria. FEMS Microbiol Rev 44:54–72. https://doi.org/10.1093/femsre/fuz026
79. Mogk A, Bukau B, Kampinga HH. 2018. Cellular handling of protein aggregates by disaggregation machines. Mol Cell 69:214–226. https://doi.org/10.1016/j.molcel.2018.01.004
80. He W, Yu G, Li T, Bai L, Yang Y, Xue Z, Pang Y, Reichmann D, Hiller S, He L, Liu M, Quan S. 2021. Chaperone spy protects outer membrane proteins from folding stress via dynamic complex formation. mBio 12:e0213021. https://doi.org/10.1128/mBio.02130-21
81. Mitra R, Wu K, Lee C, Bardwell JCA. 2022. ATP-independent chaperones. Annu Rev Biophys 51:409–429. https://doi.org/10.1146/annurev-biophys-090121-082906
82. DiGiuseppe PA, Silhavy TJ. 2003. Signal detection and target gene induction by the CpxRA two-component system. J Bacteriol 185:2432–2440. https://doi.org/10.1128/JB.185.8.2432-2440.2003
83. Wu X, Held K, Zheng C, Staudinger BJ, Chavez JD, Weisbrod CR, Eng JK, Singh PK, Manoil C, Bruce JE. 2015. Dynamic proteome response of *Pseudomonas aeruginosa* to tobramycin antibiotic treatment. Mol Cell Proteomics 14:2126–2137. https://doi.org/10.1074/mcp.M115.050161
84. Tran TDH, Kwon HY, Kim EH, Kim KW, Briles DE, Pyo S, Rhee DK. 2011. Decrease in penicillin susceptibility due to heat shock protein ClpL in *Streptococcus pneumoniae*. Antimicrob Agents Chemother 55:2714–2728. https://doi.org/10.1128/AAC.01383-10
85. Cardoso K, Gandra RF, Wisniewski ES, Osaku CA, Kadowaki MK, Felipach-Neto V, Haus L-Á, Simão R de C. 2010. DnaK and GroEL are induced in response to antibiotic and heat shock in *Acinetobacter baumannii*. J Med Microbiol 59:1061–1068. https://doi.org/10.1099/jmm.0.020339-0
86. Yamaguchi Y, Tomoyasu T, Takaya A, Morioka M, Yamamoto T. 2003. Effects of disruption of heat shock genes on susceptibility of *Escherichia coli* to fluoroquinolones. BMC Microbiol 3:1–8. https://doi.org/10.1186/1471-2180-3-16
87. Khodaparast L, Khodaparast L, Gallardo R, Louros NN, Michiels E, Ramakrishnan R, Ramakers M, Claes F, Young L, Shahrooei M, Wilkinson H, Desager M, Mengistu Tadesse W, Nilsson KPR, Hammarström P, Aertsen A, Carpentier S, Van Eldere J, Rousseau F, Schymkowitz J. 2018. Aggregating sequences that occur in many proteins constitute weak

spots of bacterial proteostasis. Nat Commun 9:866. https://doi.org/10.1038/s41467-018-03131-0
88. Michels M, Bakker EP. 1985. Generation of a large, protonophore-sensitive proton motive force and pH difference in the acidophilic bacteria *Thermoplasma acidophilum* and *Bacillus acidocaldarius*. J Bacteriol 161:231–237. https://doi.org/10.1128/jb.161.1.231-237.1985
89. Krulwich TA, Sachs G, Padan E. 2011. Molecular aspects of bacterial pH sensing and homeostasis. Nat Rev Microbiol 9:330–343. https://doi.org/10.1038/nrmicro2549
90. Cayron J, Oms T, Schlechtweg T, Zedek S, Van Melderen L. 2024. TisB protein is the single molecular determinant underlying multiple downstream effects of ofloxacin in *Escherichia coli*. Sci Adv 10:eadk1577. https://doi.org/10.1126/sciadv.adk1577
91. Van Tartwijk FW, Kaminski CF. 2022. Protein condensation, cellular organization, and spatiotemporal regulation of cytoplasmic properties. Adv Biol 6:e2101328. https://doi.org/10.1002/adbi.202101328
92. Wang X, Kim Y, Ma Q, Hong SH, Pokusaeva K, Sturino JM, Wood TK. 2010. Cryptic prophages help bacteria cope with adverse environments. Nat Commun 1:147. https://doi.org/10.1038/ncomms1146
93. Jõers A, Kaldalu N, Tenson T. 2010. The frequency of persisters in *Escherichia coli* reflects the kinetics of awakening from dormancy. J Bacteriol 192:3379–3384. https://doi.org/10.1128/JB.00056-10
94. Goormaghtigh F, Van Melderen L. 2019. Single-cell imaging and characterization of *Escherichia coli* persister cells to ofloxacin in exponential cultures. Sci Adv 5:eaav9462. https://doi.org/10.1126/sciadv.aav9462
95. Datsenko KA, Wanner BL. 2000. One-step inactivation of chromosomal genes in *Escherichia coli* K-12 using PCR products. Proc Natl Acad Sci U S A 97:6640–6645. https://doi.org/10.1073/pnas.120163297
96. Datta S, Costantino N, Court DL. 2006. A set of recombineering plasmids for Gram-negative bacteria. Gene 379:109–115. https://doi.org/10.1016/j.gene.2006.04.018
97. Beyer HM, Gonschorek P, Samodelov SL, Meier M, Weber W, Zurbriggen MD. 2015. AQUA cloning: a versatile and simple enzyme-free cloning approach. PLoS One 10:e0137652. https://doi.org/10.1371/journal.pone.0137652
98. Köbel TS, Melo Palhares R, Fromm C, Szymanski W, Angelidou G, Glatter T, Georg J, Berghoff BA, Schindler D. 2022. An easy-to-use plasmid toolset for efficient generation and benchmarking of synthetic small RNAs in bacteria. ACS Synth Biol 11:2989–3003. https://doi.org/10.1021/acssynbio.2c00164
99. Ewels P, Magnusson M, Lundin S, Käller M. 2016. MultiQC: summarize analysis results for multiple tools and samples in a single report. Bioinformatics 32:3047–3048. https://doi.org/10.1093/bioinformatics/btw354
100. Langmead B, Salzberg SL. 2012. Fast gapped-read alignment with Bowtie 2. Nat Methods 9:357–359. https://doi.org/10.1038/nmeth.1923
101. Danecek P, Bonfield JK, Liddle J, Marshall J, Ohan V, Pollard MO, Whitwham A, Keane T, McCarthy SA, Davies RM, Li H. 2021. Twelve years of SAMtools and BCFtools. Gigascience 10:1–4. https://doi.org/10.1093/gigascience/giab008
102. Liao Y, Smyth GK, Shi W. 2014. featureCounts: an efficient general purpose program for assigning sequence reads to genomic features. Bioinformatics 30:923–930. https://doi.org/10.1093/bioinformatics/btt656
103. Love MI, Huber W, Anders S. 2014. Moderated estimation of fold change and dispersion for RNA-seq data with DESeq2. Genome Biol 15:550. https://doi.org/10.1186/s13059-014-0550-8
104. Pfaffl MW. 2001. A new mathematical model for relative quantification in real-time RT-PCR. Nucleic Acids Res 29:e45. https://doi.org/10.1093/nar/29.9.e45
105. Schägger H. 2006. Tricine–SDS-PAGE. Nat Protoc 1:16–22. https://doi.org/10.1038/nprot.2006.4
106. Hughes CS, Moggridge S, Müller T, Sorensen PH, Morin GB, Krijgsveld J. 2019. Single-pot, solid-phase-enhanced sample preparation for proteomics experiments. Nat Protoc 14:68–85. https://doi.org/10.1038/s41596-018-0082-x
107. Vizcaíno JA, Deutsch EW, Wang R, Csordas A, Reisinger F, Ríos D, Dianes JA, Sun Z, Farrah T, Bandeira N, Binz PA, Xenarios I, Eisenacher M, Mayer G, Gatto L, Campos A, Chalkley RJ, Kraus HJ, Albar JP, Martinez-Bartolomé S, Apweiler R, Omenn GS, Martens L, Jones AR, Hermjakob H. 2014. ProteomeXchange provides globally coordinated proteomics data submission and dissemination. Nat Biotechnol 32:223–226. https://doi.org/10.1038/nbt.2839
108. Goldberg T, Hecht M, Hamp T, Karl T, Yachdav G, Ahmed N, Altermann U, Angerer P, Ansorge S, Balasz K, et al. 2014. LocTree3 prediction of localization. Nucleic Acids Res 42:W350–W355. https://doi.org/10.1093/nar/gku396

2.1

Supplement

Protein aggregation is a consequence of the dormancy-inducing membrane toxin TisB in *Escherichia coli*

Supplemental Figures

Protein aggregation is a consequence of the dormancy-inducing membrane toxin TisB in *Escherichia coli*

Florian H. Leinberger, Liam Cassidy, Daniel Edelmann, Nicole E. Schmid, Markus Oberpaul, Patrick Blumenkamp, Sebastian Schmidt, Ana Natriashvili, Maximilian H. Ulbrich, Andreas Tholey, Hans-Georg Koch and Bork A. Berghoff

This file contains:

Figures S1 to S9

Figure S1

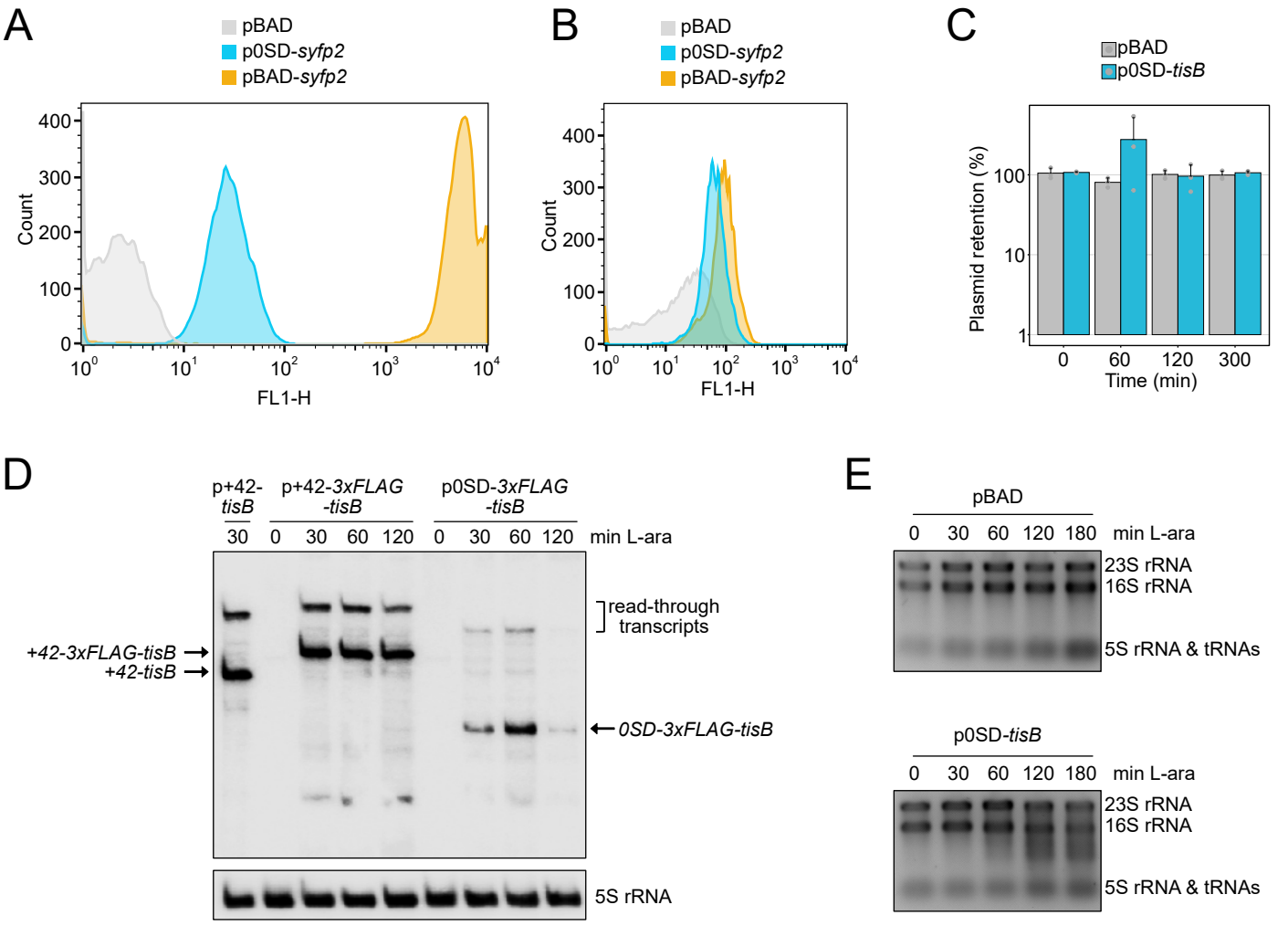

Figure S1. Evaluation of the p0SD-*tisB* expression system.

(A) Translational efficiency of the SD-free 5' UTR (0SD). Wild type MG1655, harboring either an empty pBAD plasmid, p0SD-*syfp2* or pBAD-*syfp2*, was treated with L-ara (0.2%) during the exponential phase (OD_{600} ~ 0.4) for 1 hour. Samples were resuspended in 100 µl paraformaldehyde (2% in 1x PBS) and incubated in the dark at room temperature for 10 minutes. Samples were washed two times with 200 µl 1x PBS before resuspended in 250 µl 1x PBS. The sYFP2 fluorescence was measured using flow cytometry and detecteor FL1-H. **(B)** Same samples as in (A). sYFP2 fluorescence was measured using flow cytometry at various detector intensities to ensure that the data is centered: empty pBAD plasmid (grey | 999), p0SD-*syfp2* (blue | 774) and pBAD-*syfp2* (orange | 412). **(C)** Plasmid stability. Wild type MG1655, harboring either p0SD-*tisB* or an empty pBAD plasmid, was treated with L-ara (0.2%) during the exponential phase (OD_{600} ~ 0.4). Samples were collected at specified time points and plated on LB agar plates, both with and without 200 µg/ml ampicillin. Cell counts were used to calculate the relative plasmid retention. Bars represent the mean of three biological replicates and error bars indicate the standard deviation. Dots show individual data points. **(D)** Northern blot analysis of different *tisB* expression systems. Wild type MG1655, harboring pBAD derivatives with different *tisB* fragments with and without 3xFLAG sequence, was grown to an OD_{600} of ~0.4 (exponential phase) and treated with L-arabinose (L-ara; 0.2 %) as inducer. Samples were collected at the indicated time points for total RNA isolation and subsequent northern blot analysis. A radioactively labelled probe, targeted against the *tisB* open reading frame, was used for detection of *tisB* transcripts. 5S rRNA was probed as loading control. **(E)** Integrity of abundant RNAs. Wild type MG1655, harboring an empty pBAD plasmid or p0SD-*tisB*, were grown to an OD_{600} of ~0.4 (exponential phase) and treated with L-ara (0.2 %). Samples were collected at the indicated time points for total RNA isolation and subsequent quality analysis on 1% agarose gels, containing 1x TBE and 25 mM guanidinium thiocyanate.

Figure S2

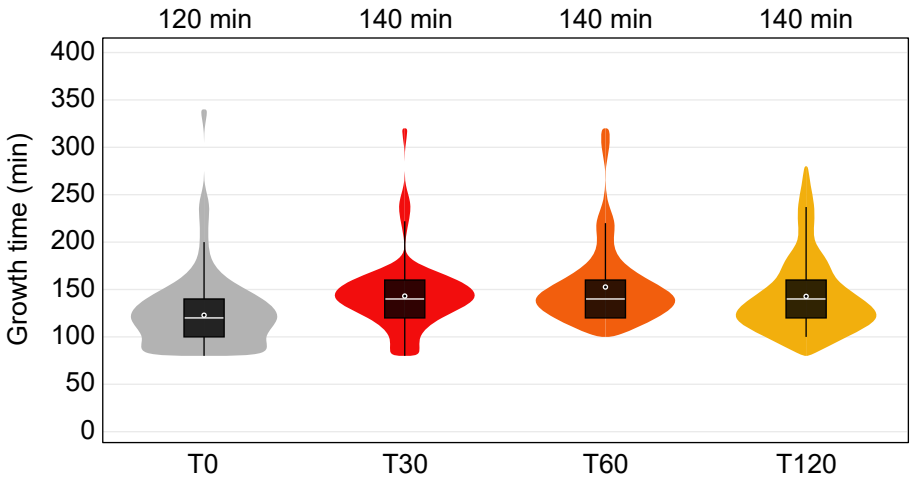

Figure S2. Colony growth time analysis by ScanLag.

ScanLag analysis was applied to determine the colony growth time after *tisB* expression. For each time point, colony growth times are illustrated as violin box plots. Colonies from three biological replicates were combined (T0: n=154; T30: n=59; T60: n=103; T120: n=124). The white dot indicates the mean. The corresponding median appearance time (white bar) is shown on top of each plot.

Figure S3

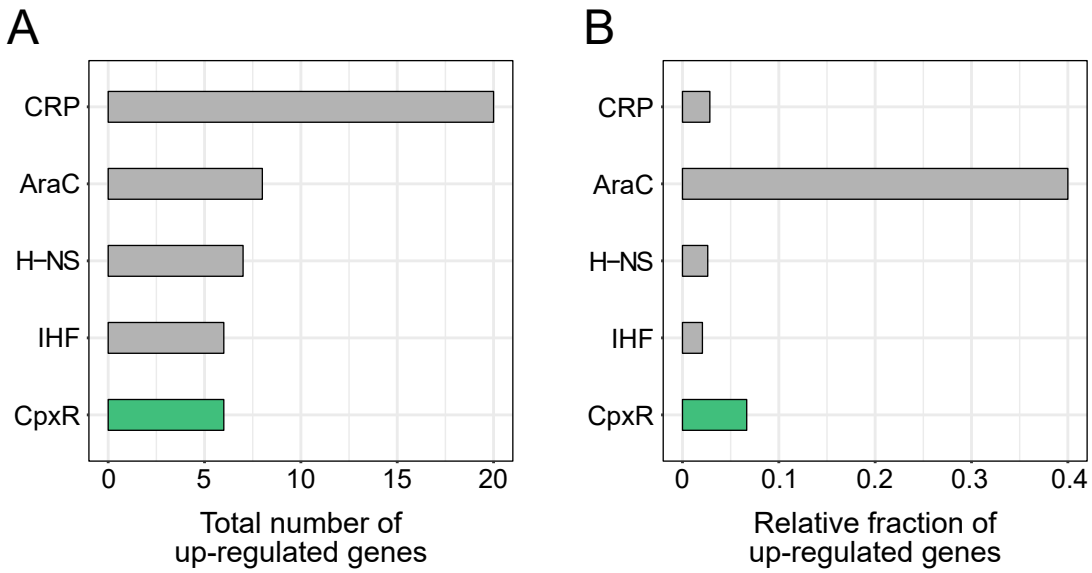

Figure S3. Regulon analysis of TisB-responsive genes.

RNA-seq identified 67 genes that were up-regulated upon *tisB* expression using the p0SD-*tisB* system (log_2 fold change >2 and p-value <0.01). These genes were subjected to a regulon analysis using Bioconductor package regutools (R package for data extraction from RegulonDB). **(A)** Top-5 regulons according to total numer of up-regulated genes. **(B)** Top-5 regulons according to the numer of up-regulated genes in relation to the regulon size.

Figure S4

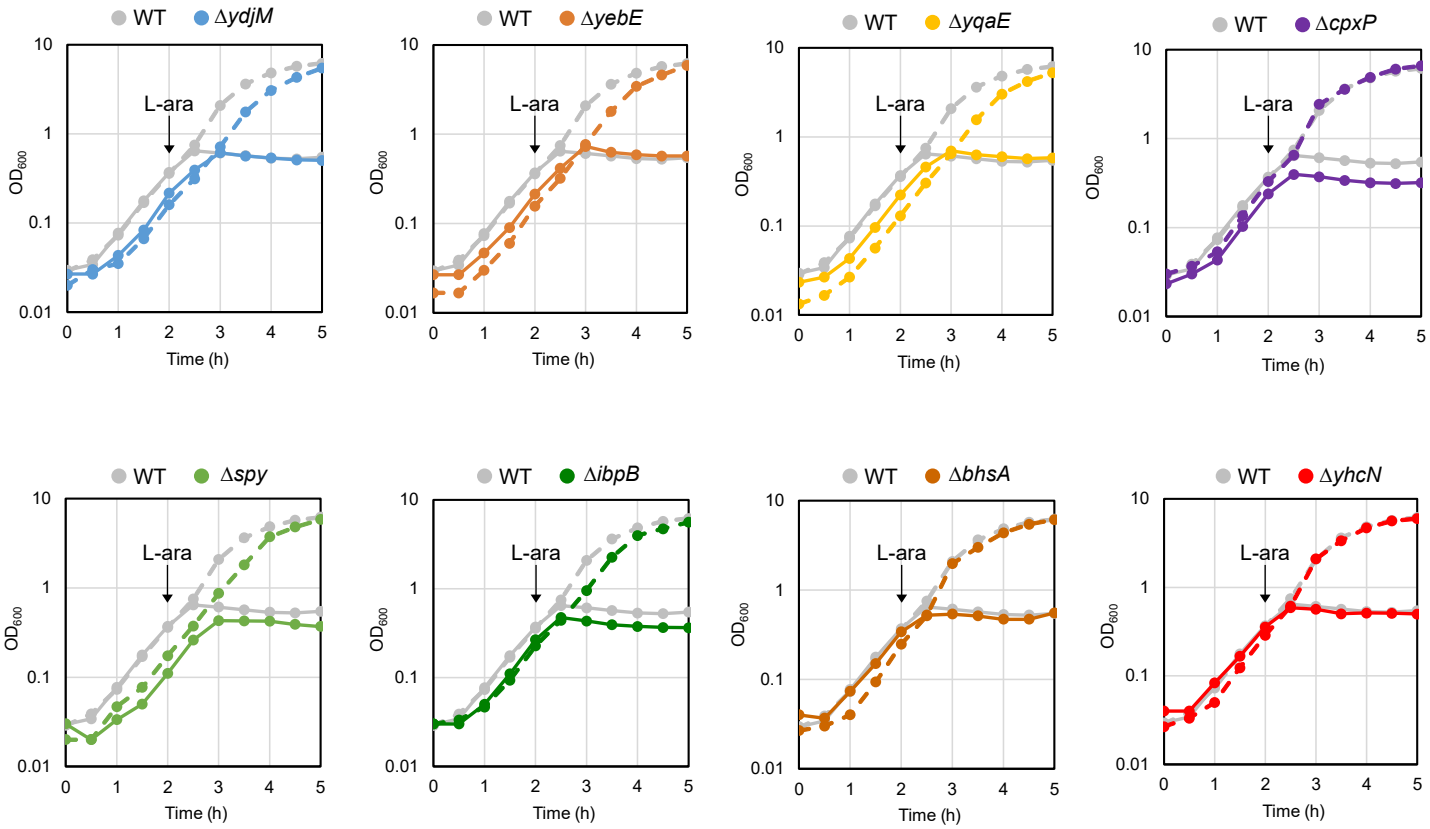

Figure S4. TisB-induced growth inhibition in different deletion mutants.

MG1655 wild type (WT) and isogenic deletion mutants, containing either an empty pBAD plasmid (dashed curves) or p0SD-*tisB* (solid curves), were grown in LB medium at 37°C. The OD_{600} was monitored over time. At the indicated time point during exponential phase, cultures were treated with L-arabinose (L-ara; 0.2%) as inducer.

Figure S5

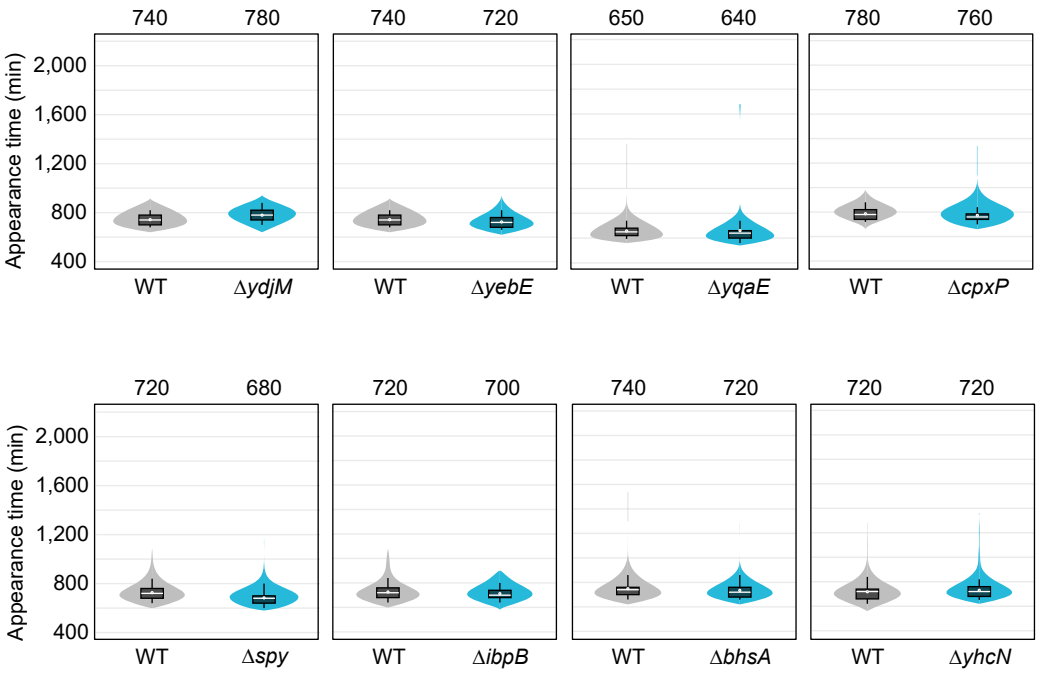

Figure S5. ScanLag analysis of selected deletion mutants.

Wild type (WT) MG1655 and deletion mutants, harboring the empty pBAD plasmid, were treated with L-ara (0.2%) during exponential phase (OD_{600} ~0.25) for 1 hour. ScanLag was applied to determine the colony appearance time after L-ara treatment. For each deletion mutant, colony appearance times are illustrated as violin box plots and compared to a corresponding wild type. Colonies from at least three biological replicates were combined (WT: n≥91; Δ*ydjM*: n=332; Δ*yebE*: n=265; Δ*yqaE*: n=75; Δ*cpxP*: n=84; Δ*spy*: n=263; Δ*ibpB*: n=197; Δ*bhsA*: n=180; Δ*yhcN*: n=293). The white dot indicates the mean. The respective median appearance time (white bar) is shown on top of each plot.

Figure S6

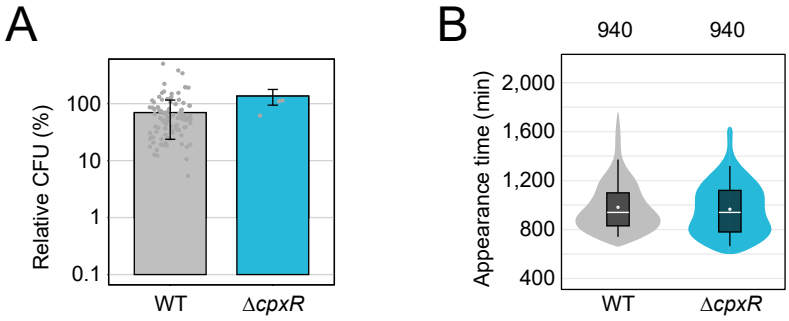

Figure S6. Analysis of the *cpxR* deletion mutant.

Wild type (WT) MG1655 and the Δ*cpxR* mutant, harboring plasmid p0SD-*tisB*, were treated with L-ara (0.2%) during exponential phase (OD_{600} ~0.4) for 1 hour. **(A)** Pre- and post-treatment samples were used to determine relative CFU (%). Bars represent the mean of at least three biological replicates and error bars indicate the standard deviation. Dots show individual data points. **(B)** ScanLag was applied to determine the colony appearance time after L-ara treatment. Colony appearance times are illustrated as violin box plots (WT: n=235; Δ*cpxR*: n=185). The white dot indicates the mean. The respective median appearance time (white bar) is shown on top of each plot.

Figure S7

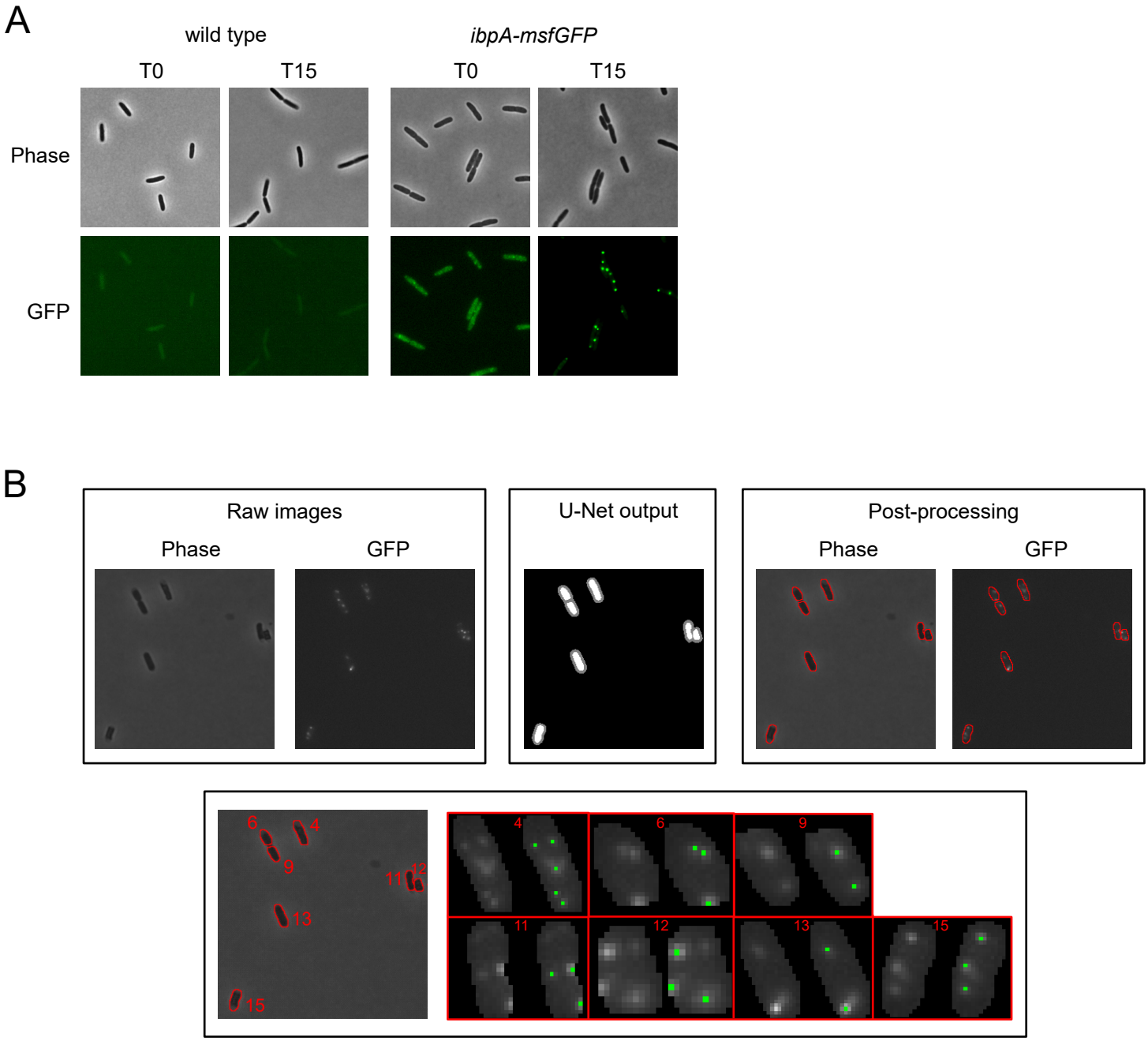

Figure S7. Validation of the *ibpA-msfGFP* reporter and U-Net analysis of msGFP foci.

(A) Wild type MG1655 and reporter strain *ibpA-msfGFP* were grown to exponential phase (T0; OD_{600} ~0.4) and shifted to 47°C for 15 minutes (T15). Phase contrast images are displayed together with corresponding fluorescence images (GFP). **(B)** Exemplary representation of msfGFP foci counting using U-Net. Upper panel: Raw images from phase contrast and fluorescence images (GFP) are applied to post-processing using the U-Net model output for cell segmentation. Lower panel: According to cell shapes, GFP images of single cells are extracted and msfGFP foci are determined.

Figure S8

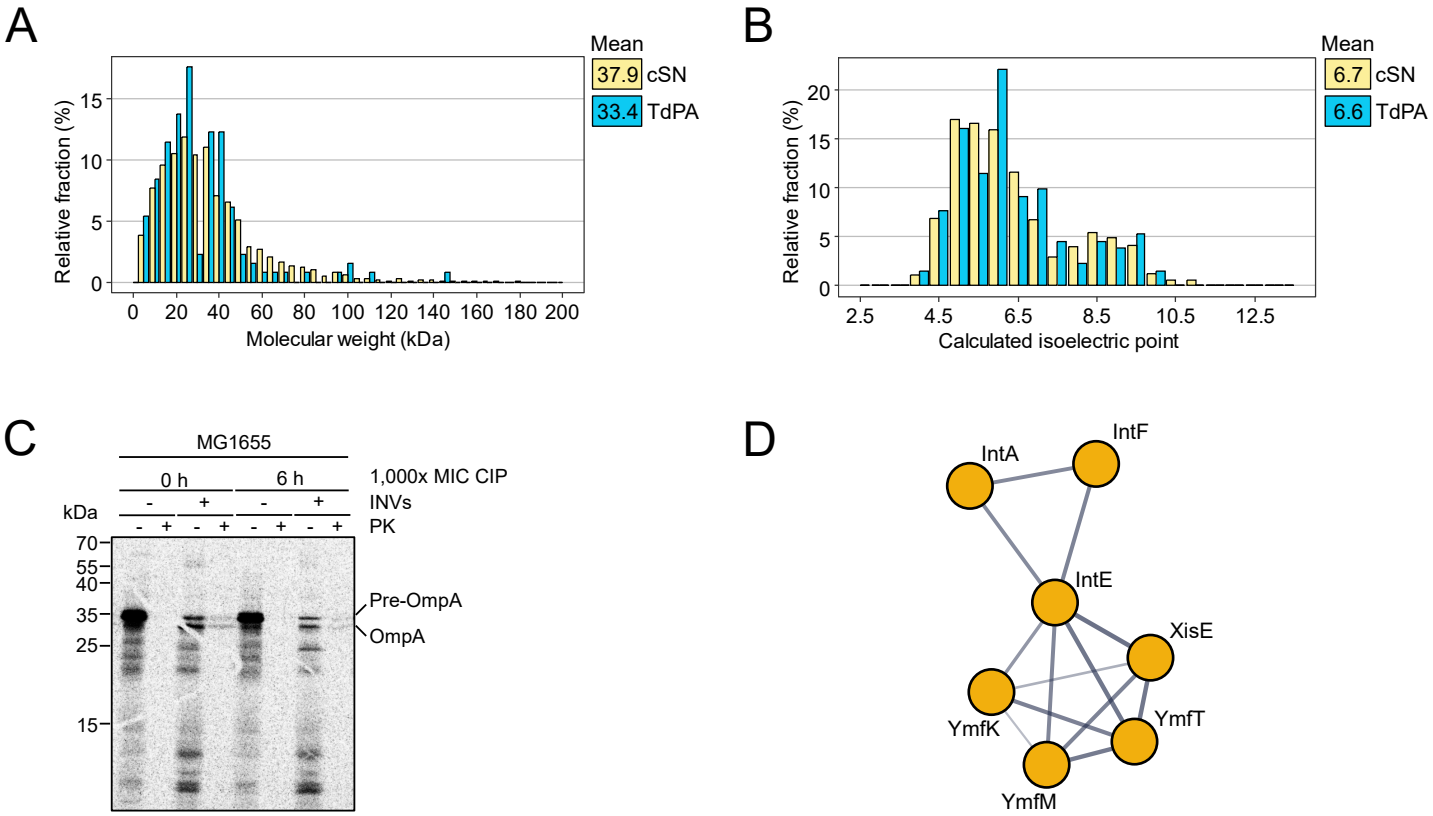

Figure S8. Analysis of protein aggregates and inner membrane vesicles.

(A) Distribution plot of the molecular weight (kDa). The relative fractions are shown for the combined supernatant (cSN) and TisB-dependent protein aggregates (TdPA). Means are displayed in the legend. **(B)** Distribution plot of the calculated isoelectric point. The relative fractions are shown for the combined supernatant (cSN) and TisB-dependent protein aggregates (TdPA).Means are displayed in the legend. **(C)** Cell-free OmpA synthesis was performed in a coupled transcription/translation system using T7 RNA polymerase and CTF extract with purified ribosomes. Reactions were prepared on ice and translation was carried out in the presence of radioactive ^{35}S-methionine/^{35}S-cysteine labelling mix (Perkin Elmer Wiesbaden, Germany). Radioactively labelled OmpA was used in in-vitro translocation reaction with two different inner membrane vesicles (INVs). In one case *E. coli* K-12 wild type MG1655 cells were harvested for membrane preparation at an OD_{600} of 1.2-1.6 (0 h), while in the other case *E. coli* K-12 wild type MG1655 cells were treated with 1,000x MIC of ciprofloxacin (CIP) for six hours (6 h), starting at an OD_{600} of 0,4. In order to asses the translocation of OmpA across the inner membrane, after synthesis it was incubated with INVs (0,1 µg protein) for 25 minutes at 37°C and treated with Proteinase K (PK) (0.2 mg/ml PK for 30 minutes at 25℃). INVs were not added to the control reactions in order to show complete digestion of OmpA with PK in the absence of INVs. All samples were precipitated with 5% TCA for at least 30 minutes, separated on SDS-PAGE and analyzed by autoradiography. Indicated are pre-OmpA and mature OmpA, which occurs after signal sequence cleavage. (D) Protein-protein association network of prophage proteins in TisB-dependent protein aggregates (TdPA). The network was revealed by a multi-protein search using the STRING database (https://string-db.org/), indicating the enrichment of the corresponding proteins within the category ‘viral process and bacteriophage tail fiber assembly’. The thickness of connecting lines indicates the confidence of the respective interaction.

Figure S9

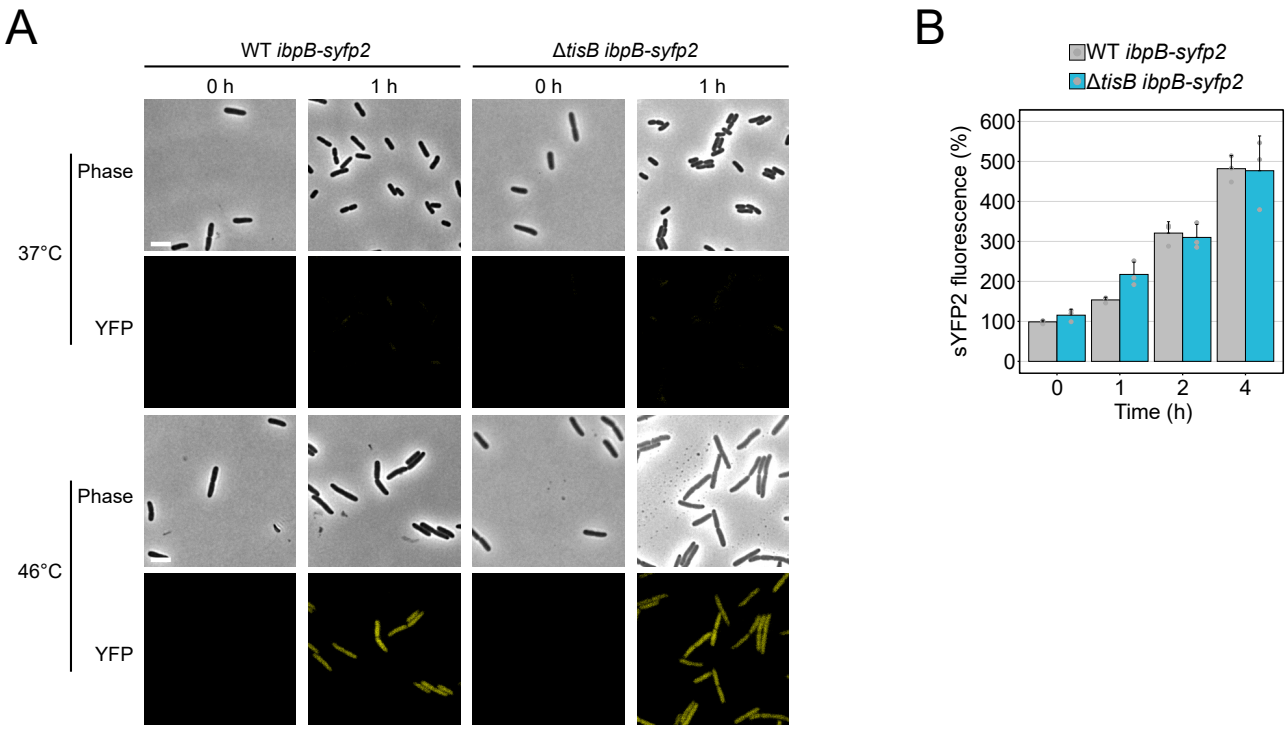

Figure S9. Induction of the heat shock response.

(A) Wild type (WT) *ibpB-syfp2* and Δ*tisB ibpB-syfp2* were grown to an OD_{600} of ~0.4 at 30°C and subsequently shifted to 37°C and 46°C. Samples were collected before (0 h) and after (1 h) the temperature shift and analyzed by microscopy. Phase contrast images are displayed together with corresponding fluorescence image (YFP). White bars represent a length scale of 2 µm. **(B)** Wild type (WT) *ibpB-syfp2* and Δ*tisB ibpB-syfp2* were grown to an OD_{600} of ~0.4 at 30°C and subsequently shifted to 37°C and 46°C. Samples were collected before (0 h) and after (1 h, 2 h, 4 h) the temperature shift. Fluorescence was measured using a plate reader, and the relative sYFP2 fluorescence was calculated in comparison to the fluorescence at 37°C. Bars represent the mean of three biological replicates and error bars indicate the standard deviation. Dots show individual data points.

3

SCIENTIFIC REPORTS

Relevance of charged and polar amino acids for functionality of membrane toxin TisB

Florian H. Leinberger & Bork A. Berghoff

scientific reports

Check for updates

OPEN

Relevance of charged and polar amino acids for functionality of membrane toxin TisB

Florian H. Leinberger[1] & Bork A. Berghoff[1,2]✉

Bacterial dormancy is marked by reduced cellular activity and the suspension of growth. It represents a valuable strategy to survive stressful conditions, as exemplified by the long-term tolerance towards antibiotics that is attributable to a fraction of dormant cells, so-called persisters. Here, we investigate the membrane toxin TisB (29 amino acids) from the chromosomal toxin-antitoxin system *tisB/istR-1* in *Escherichia coli*. TisB depolarizes the inner membrane in response to DNA damage, which eventually promotes a stress-tolerant state of dormancy within a small fraction of the population. Using a plasmid-based system for moderate *tisB* expression and single amino acid substitutions, we dissect the importance of charged and polar amino acids. We observe that the central amino acids lysine 12 and glutamine 19 are of major importance for TisB functionality, which is further validated for lysine 12 in the native context upon treatment with the DNA-damaging antibiotic ciprofloxacin. Finally, we apply a library-based approach to test additional TisB variants in higher throughput, revealing that at least one positive charge at the C-terminus (either lysine 26 or 29) is mandatory for TisB-mediated dormancy. Our study provides insights into the molecular basis for TisB functionality and extends our understanding of bacterial membrane toxins.

Keywords Type I toxin-antitoxin systems, Pore formation, Membrane depolarization, ATP depletion, Antibiotic persistence

Toxin-antitoxin (TA) systems are widely distributed among prokaryotes. They are classified into different types according to the nature of the antitoxin (protein or RNA) and the mode of toxin inhibition. Under non-stress conditions, activity or synthesis of the toxin is prevented by the antitoxin. However, certain events may release inhibition of the toxin, which promotes toxicity by interference with essential cellular functions, resulting in growth inhibition or even cell death[1,2]. TA systems are regularly found on mobile genetic elements (MGEs), such as plasmids and prophages, and contribute to the stable inheritance of these MGEs in expanding populations[1,3]. TA systems are also present in chromosomes, sometimes in fairly high numbers[4]. Even though the biological functions of many chromosomal TA systems are less well understood, it has been observed that they contribute to the defense against bacteriophages or support survival in stressful environments[5,6].

Type I TA systems are ubiquitous and defined by an RNA antitoxin that translationally represses the toxin messenger RNA (mRNA) by antisense-mediated binding. Under certain stress conditions the toxin mRNA either out-titrates the RNA antitoxin or the RNA antitoxin is depleted. Either way, toxin translation is enabled and toxicity occurs[7]. Type I toxins are usually small hydrophobic proteins with sizes below 50 amino acids (AAs), containing a central transmembrane helix (TMH) as well as short N- and C-terminal extensions. Upon targeting of the inner membrane, they disturb membrane functioning or even modulate cell morphology[7,8]. One well-characterized type I toxin is HokB from the *hokB/sokB* TA system in *Escherichia coli*. HokB has a total size of 49 AAs and a TMH consisting of 23 AAs (positions 7–29). The C-terminal extension is localized in the periplasm and contains a cysteine residue (C46) that is essential for dimerization and pore formation *via* intermolecular disulfide bridges[9]. While intermediate HokB pores are probably narrow and cause breakdown of the proton motive force (PMF) by allowing protons to traverse the inner membrane, mature pores have an effective radius of ~0.6 nm and promote ATP efflux[10], and potentially the movement of several other small molecules and ions. The resulting energy deprivation is expected to induce antibiotic tolerance *via* formation of dormant cells (i.e., persisters)[10,11].

Another well-characterized type I toxin is TisB from the *tisB/istR-1* TA system in *E. coli*. The *tisB* gene is under LexA control and strongly transcribed under DNA damage (SOS) conditions[12,13]. The RNA antitoxin

[1]Institute for Microbiology and Molecular Biology, Justus Liebig University Giessen, 35392 Giessen, Germany. [2]Present address: Institute of Molecular Biology and Biotechnology of Prokaryotes, University of Ulm, 89069 Ulm, Germany. ✉email: bork.berghoff@uni-ulm.de

IstR-1 and structural features within the *tisB* mRNA represent a threshold for TisB production, contributing to phenotypic heterogeneity due to uneven TisB levels among individual cells[14]. TisB has a total size of 29 AAs and a TMH consisting of 20 AAs (positions 6–25). Unlike HokB, the TisB toxin does not contain cysteine residues that might promote dimerization *via* intermolecular disulfide bridges. However, TisB also forms pores and causes PMF dissipation, which is accompanied by ATP depletion and further downstream effects, such as reactive oxygen species (ROS) formation, protein aggregation and cytosolic condensation[15–17]. The concomitant dormancy favors the establishment of a small fraction of antibiotic-tolerant persister cells[14,18].

TisB contains three positively charged lysines (K12, K26 and K29) and two negatively charged aspartates (D5 and D22), resulting in a net charge of + 1. Different models were suggested to explain the molecular basis for TisB functionality. The 'anion-selective pore' model is based on in vitro experiments with planar lipid membranes. The model predicts that TisB forms pores with a relatively small diameter of ~ 0,15 nm and that the net charge of + 1 favors anionic selectivity, likely causing collapse of the PMF because hydroxyl anions migrate from the cytoplasm to the periplasm[19]. The 'charge-zipper' model is based on molecular dynamics simulations and predicts that TisB forms an antiparallel dimer-of-dimers that is stabilized by a multitude of salt bridges and hydrogen bonds, involving the two positively charged AAs K12 and K26, the two negatively charged AAs D5 and D22, and the polar AA glutamine Q19[20,21]. The resulting TisB pore is predicted to discharge the PMF *via* direct passage of protons from the periplasm to the cytoplasm. Even though the two models are not necessarily mutually exclusive, they have not been substantiated by analyses in living *E. coli* cells. Here, we apply a plasmid-based system for moderate *tisB* expression and amino acid substitutions to reveal the importance of charged and polar amino acids for TisB functionality. The results are discussed with regard to the two prevailing models.

Results

Lysine 12 and glutamine 19 are essential for TisB-mediated cellular effects

Toxin TisB is not widely distributed among bacteria and only found within the family of *Enterobacteriaceae* within the class of Gammaproteobacteria[22]. A multiple alignment revealed that the five charged AAs (D5, K12, D22, K26 and K29) and the polar glutamine (Q19) are well conserved among species that are closely related to the *E. coli* wild-type strain MG1655, including *Salmonella enterica*, *Shigella flexneri*, *Citrobacter freundii*, *Citrobacter koseri*, and *Klebsiella pneumoniae* (Fig. 1a). The polar asparagine (N2) was not conserved in the investigated TisB homologs and, therefore, not further considered for investigation. As visualized by a helical wheel projection, the charged AAs and Q19 constitute a hydrophilic face, which is opposed to the hydrophobic face formed by the majority of AAs with a hydrophobic side chain (Fig. 1b). Hence, TisB can be considered as an amphipathic protein. It is intuitive to assume that the hydrophilic faces of several TisB monomers are directed towards each other to form a water-filled pore, whereas the hydrophobic faces are aligned with the lipid bilayer of the inner membrane. Hence, the charged and polar AAs may significantly contribute to TisB functionality, as also suggested by the 'anion-selective pore' and 'charge-zipper' models[19–21]. To test the significance of individual AAs, we made use of a recently established plasmid-based *tisB* expression system using a Shine-Dalgarno-free upstream region (denoted p0SD-*tisB*), which allows moderate production of TisB by the addition of L-arabinose (L-ara) without causing cell death of *E. coli* MG1655[16]. Even though the expression system does not produce lethal TisB levels, we cannot exclude that it may lead to unwanted side effects due to saturation of the membrane and potential (off-) targets. However, the system is suitable to bypass regulation by the antitoxin IstR-1 and is expected to be sensitive to even subtle changes in TisB activity. The charged and polar AAs were individually substituted with the hydrophobic AA leucine (L) by mutagenesis PCR of the plasmid. Leucine was chosen because it has a molecular weight of ~ 131 Dalton, which is comparable to the substituted amino acids. All TisB variants had a higher grand average of hydropathy (GRAVY) value than native TisB (Supplementary Fig. S1) and were hence expected to localize to the membrane. To confirm membrane localization of the TisB variants, we first constructed the corresponding mutations on plasmid p0SD-*3xFLAG-tisB* for western blot detection of 3xFLAG-TisB in cytoplasmic and membrane fractions. All 3xFLAG-TisB variants were exclusively detected in the membrane fraction, as supported by detection of control proteins YchF (cytoplasmic) and YidC (inner membrane; Fig. 1c). Hence, the AA substitutions had no effect on integration of TisB into the membrane. We noticed that the 3xFLAG-TisB variants differed slightly in their gel migration (Fig. 1c), which was however not reproducible and varied between individual western blot replicates (Supplementary Fig. S2). We also confirmed that *tisB* expression levels were comparable between the different constructs and that no major mRNA degradation occurred (Supplementary Fig. S3). Since the 3xFLAG-tag attenuates TisB functionality (data not shown), we used the p0SD-*tisB* plasmid for all subsequent physiological experiments.

It is known that cell growth is inhibited upon induction of *tisB* expression from plasmids[15,16,23]. Growth curve analysis demonstrated that wild-type TisB stopped cell growth within 30 min after its induction during exponential phase (Fig. 1d). While the K29L variant still caused full growth inhibition, the D5L, D22L and K26L variants were functionally attenuated, as displayed by an incomplete growth inhibition. In contrast, growth inhibition did not occur with the K12L and Q19L variants; growth was comparable to the empty vector control (Fig. 1d). In order to determine whether growth inhibition was accompanied by ATP depletion, intracellular ATP levels were quantified. A one-hour induction of wild-type TisB with L-ara led to a ~ 30-fold decrease of intracellular ATP levels, whereas the empty vector control was unaffected by the L-ara treatment (Fig. 1e). ATP measurements of strains producing TisB variants largely conformed to the growth inhibition data, with D5L being the only exception. While the D22L and K26L variants showed intermediate ATP depletion of ~ 5-fold, the D5L and K29L variants caused ATP depletion comparable to wild-type TisB. In contrast, the K12L and Q19L variants only caused minor ATP depletion of less than 2-fold (Fig. 1e). From these experiments we conclude that K12 and Q19 are mandatory for full growth inhibition, which is concomitant with substantial ATP depletion.

It has been shown that ATP depletion is a major driving force for protein aggregation in bacteria, which in turn impacts the duration of the dormant state[24,25], and we have recently observed that TisB is able to cause

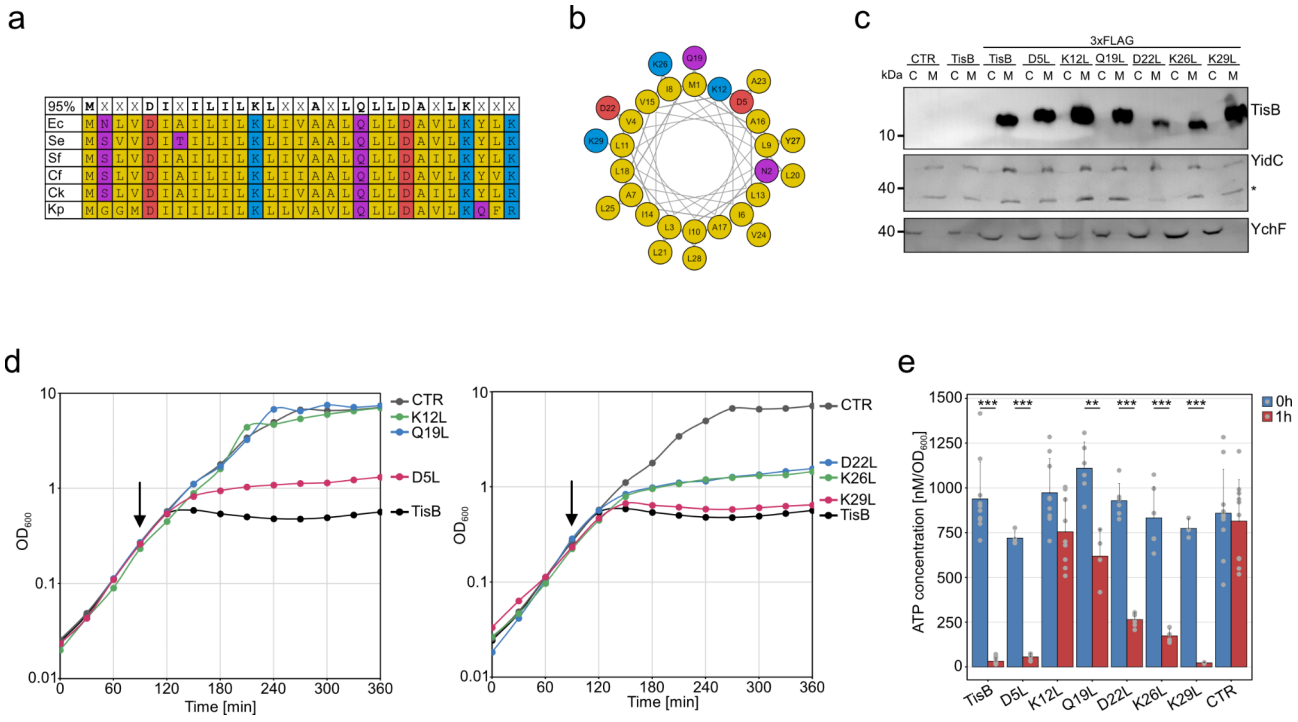

Fig. 1. Importance of single amino acids for TisB functionality. (**a**) Conservation analysis of TisB. Conservation levels of TisB were determined *via* BLAST. Amino acids with 95% conservation are in bold. *E. coli* K-12 (Ec), *Salmonella enterica* serovar Typhimurium (Se), *Shigella flexneri* (Sf), *Citrobacter freundii* (Cf), *Citrobacter koseri* (Ck), and *Klebsiella pneumoniae* (Kp). Amino acids color code: nonpolar (yellow), polar (purple), acidic (red), and basic (blue). (**b**) Helical wheel projection of TisB. Same color code as in (a). (**c**) Western blot analysis of TisB localization. Wild type MG1655, harboring p0SD-*3xFLAG-tisB* (3xFLAG-TisB) and variants with different amino acid substitutions, were treated with L-ara (0.2%) during exponential phase for one hour. p0SD-*tisB* (TisB) and an empty pBAD plasmid (CTR) were used as controls. Cytoplasmic (C) and membrane (M) fractions were isolated from total protein samples using ultracentrifugation, followed by Tricine-SDS-PAGE and western blot detection. An anti-3xFLAG antibody was used for detection of 3xFLAG-TisB. Anti-YidC (membrane) and anti-YchF (cytoplasm) antibodies were used as fractionation controls. For unedited western blot images, see Supplementary Fig. S2. (**d**) Growth inhibition by TisB. Wild type MG1655, harboring p0SD-*tisB* (TisB) and variants with different amino acid substitutions, were treated with L-ara (0.2%) during exponential phase (arrow). An empty pBAD plasmid (CTR) was used as control. Data points of OD_{600} measurements represent the mean of at least three biological replicates (TisB: $n=9$; CTR: $n=9$; D5L: $n=3$; K12L: $n=3$; Q19L: $n=3$; D22L: $n=6$; K26L: $n=3$; K29L: $n=3$). (**e**) TisB-dependent ATP depletion. Wild type MG1655, harboring p0SD-*tisB* (TisB) and variants with different amino acid substitutions, were treated with L-ara (0.2%) during exponential phase for one hour. An empty pBAD plasmid (CTR) was used as control. Pre- and post-treatment samples were analyzed using a luciferase-based assay to measure cellular ATP levels (nM per OD_{600}). Bars represent the mean of at least three biological replicates (TisB: $n=7$; CTR: $n=9$; D5L: $n=4$; K12L: $n=9$; Q19L: $n=4$; D22L: $n=6$; K26L: $n=4$; K29L: $n=3$). Error bars indicate the standard deviation. ANOVA with post-hoc Tukey HSD test was performed (*** $p<0.001$; ** $p<0.01$).

protein aggregation in *E. coli* MG1655[16]. To further validate functionality of the TisB variants, we tested their ability to cause protein aggregation by applying an established reporter strain that produces a monomeric superfolder GFP (msfGFP) fused to the small heat shock protein IbpA[26]. If protein aggregates occur, the IbpA-msfGFP fluorescence changes from a dispersed pattern to the occurrence of distinct cytoplasmic foci. Expression of wild-type *tisB* and its mutant alleles was induced by L-ara for one hour and the formation of IbpA-msfGFP foci was monitored by fluorescence microscopy. Before induction, *E. coli* cells displayed a dispersed fluorescence pattern (Fig. 2). In contrast, induction of wild-type TisB and most TisB variants led to foci formation, which was indicative of protein aggregation. However, foci were absent in the case of K12L and Q19L variants (Fig. 2). These results agree with the growth analysis data and ATP measurements, and further underscore the importance of K12 and Q19 for full TisB functionality.

TisB-mediated protection against antibiotics is abrogated in lysine 12 and glutamine 19 mutants

TisB-mediated persistence is a well-established phenomenon, and it has been shown that *tisB* expression increases the number of persister cells after treatment with different antibiotics, such as the gyrase inhibitor ciprofloxacin, the cell wall synthesis inhibitor ampicillin, and the protein synthesis inhibitor streptomycin[18].

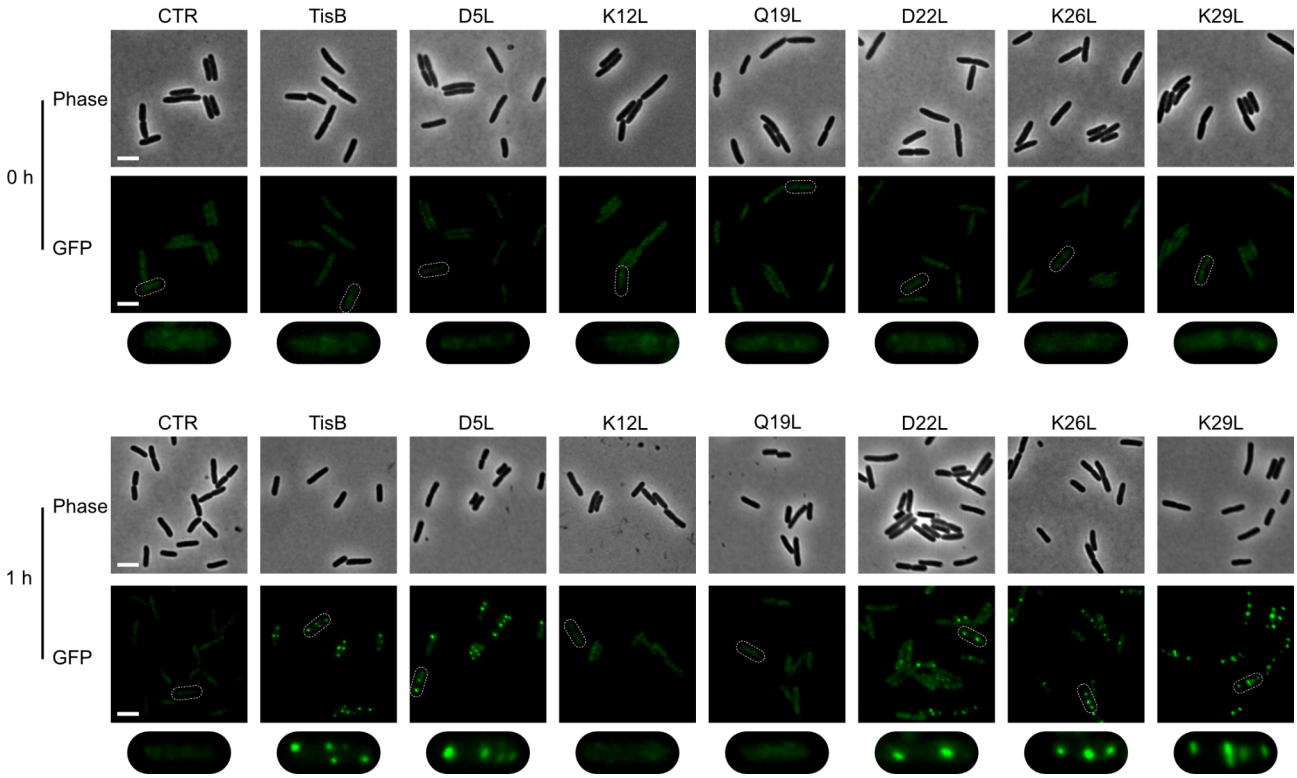

Fig. 2. TisB-dependent protein aggregation. Reporter strain MG1655 *ibpA-msfGFP*, harboring p0SD-*tisB* (TisB) and variants with different amino acid substitutions, were treated with L-ara (0.2%) during exponential phase for one hour. An empty pBAD plasmid (CTR) was used as control. Pre- and post-treatment samples were analyzed by microscopy. Phase contrast (phase) images are displayed together with corresponding fluorescence images (GFP). White bars represent a length scale of 2 µm. The area surrounding a single cell observed in the GFP image (white dashed line) is magnified and shown below the original images for closer inspection.

Transcription of the native *tisB* gene is strongly induced as part of the SOS response upon treatment with UV light or DNA-damaging drugs, such as ciprofloxacin (CIP)[12–14]. Here, we tested whether transcription of *tisB* is inducible by the ROS hydrogen peroxide (H_2O_2) or the protein synthesis inhibitor kanamycin (KAN) in *E. coli* MG1655. H_2O_2 was chosen because it is known to induce the SOS response[27] but has a different mode of action as compared to CIP. KAN was chosen because it is not able to induce the SOS response at sub-inhibitory concentrations in *E. coli*[28], and we were curious whether a high-dose KAN treatment would lead to induction of *tisB*. Indeed, both H_2O_2 and KAN increased the steady-state levels of *tisB* mRNA after one hour of treatment. However, while H_2O_2 caused a strong induction that was almost comparable to the CIP treatment, KAN only caused a very slight increase in *tisB* mRNA levels (Fig. 3a). We subsequently tested whether heterologous *tisB* expression from p0SD-*tisB* was able to provide protection against the three different agents. Cultures were first treated with L-ara for 30 min to induce *tisB*, and subsequently treated with one of the agents for 240 min (CIP and KAN) or 120 min (H_2O_2). Induction of *tisB* itself led to a slight decrease in colony forming units (CFU), indicating growth stasis and moderate toxicity (Fig. 3b). However, after treatment with the two antibiotics CIP and KAN, an enhanced survival was observed in comparison to the empty vector control (Fig. 3b and Supplementary Fig. S4). Interestingly, TisB did not protect against H_2O_2. On the contrary, while the empty vector control was almost unaffected by H_2O_2, survival of the *tisB* expression strain showed a 20-fold reduction (Fig. 3b and Supplementary Fig. S4). We conclude that TisB protects against bactericidal antibiotics by promoting a state of cellular inactivity[29], but that the combination of TisB toxicity and H_2O_2 represents a lethal situation, from which it is difficult to recover[15].

Since wild-type TisB provided almost full protection against CIP (Fig. 3b), we applied this antibiotic to elucidate functionality of the TisB variants. In agreement with the previous experiments, the D5L and K29L variants were fully functional, whereas the K12L and Q19L variants were non-functional. The D22L and K26L variants showed intermediate protection against CIP (Fig. 3c). The results mainly mirrored the ATP measurements (Fig. 1e), suggesting that ATP depletion is one of the main drivers of TisB-mediated inactivity and antibiotic tolerance[30,31].

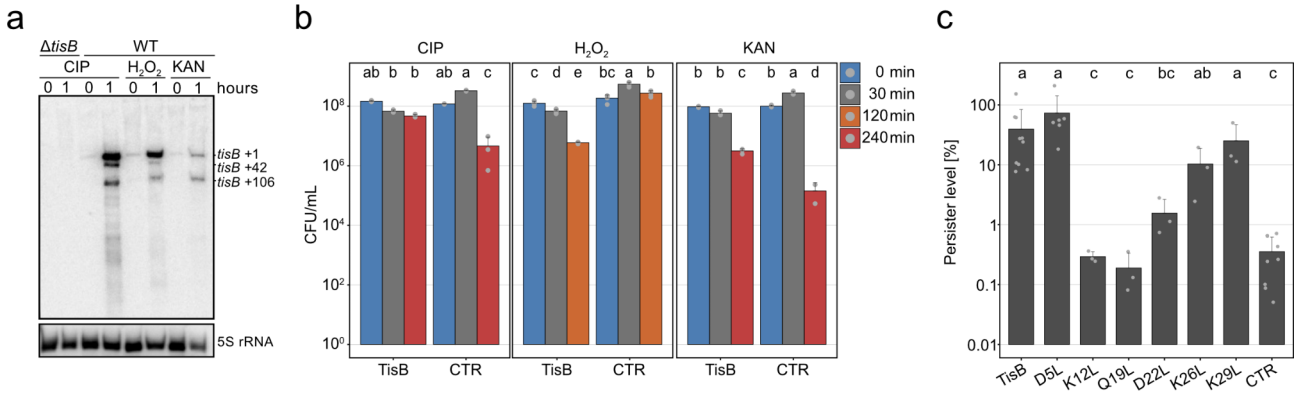

Fig. 3. TisB-induced stress tolerance. (**a**) Northern blot analysis of *tisB* induction. Wild type MG1655 (WT) and a *tisB* deletion strain were treated with either 10 µg/mL CIP, 10 mM H_2O_2, or 200 µg/mL KAN during exponential phase for one hour. Total RNA was separated using urea-polyacrylamide gels and blotted onto nylon membranes. A radioactive probe was applied for specific *tisB* mRNA detection. Numbers refer to *tisB* primary (+1) and processed mRNAs (+42 and +106). 5S rRNA was probed as loading control. For unedited northern blot images, see Supplementary Fig. S3. (**b**) Stress tolerance after TisB induction. Wild type MG1655, harboring either TisB-*tisB* (TisB) or an empty pBAD plasmid (CTR), were treated with L-ara (0.2%) during exponential phase for 30 min to induce *tisB* expression. Cells were subsequently treated with either 10 µg/mL CIP for four hours, 10 mM H_2O_2 for two hours, or 200 µg/mL KAN for four hours. Cells before (0 min), after L-ara (30 min), and after treatment with stress agents (120–240 min) were plated on LB agar plates to determine colony counts (CFU/mL). Bars represent the mean of at least two biological replicates (CIP: TisB: $n=3$; CTR: $n=3$ | H_2O_2: TisB: $n=3$; CTR: $n=3$ | KAN: TisB: $n=3$; CTR: $n=2$). Error bars indicate the standard deviation. ANOVA with post-hoc Tukey HSD test was performed independently for each treatment, and a compact letter display was applied to present significant groups. (**c**) Persistence induced by TisB. Wild type MG1655, harboring TisB-*tisB* (TisB) and variants with different amino acid substitutions, were treated with L-ara (0.2%) during exponential phase for 30 min to induce *tisB* expression. An empty pBAD plasmid (CTR) was used as control. Cells were subsequently treated with 10 µg/mL CIP for four hours. Cells before L-ara and after CIP were plated on LB agar plates to determine relative persister levels. Bars represent the mean of at least three biological replicates (TisB: $n=10$; CTR: $n=9$; D5L: $n=6$; K12L: $n=3$; Q19L: $n=3$; D22L: $n=3$; K26L: $n=3$; K29L: $n=3$). Error bars represent the standard deviation. ANOVA with post-hoc Tukey HSD test was performed, and a compact letter display was applied to present significant groups.

Lysine 12 is essential for TisB functionality and persister formation in the native context

To transfer our observations to the native *tisB* context, we constructed two different *tisB* mutant alleles in the *E. coli* MG1655 chromosome by recombineering techniques: the aspartate at position 5 was replaced with an asparagine (D5N), and the lysine at position 12 was replaced with a leucine (K12L). Based on the previous results, we expected the D5N allele to be fully functional and the K12L allele to be non-functional. Both mutant alleles were compared to wild type MG1655 and a *tisB* deletion strain. To induce *tisB* expression from the chromosomal locus, cultures were subjected to a high-dose CIP treatment (10 µg/mL) for six hours. This condition is known to reveal TisB-dependent effects[16] and was used here to observe physiological consequences of the chromosomal manipulations.

First, we quantified the ATP levels. In the CIP-treated wild type and D5N strain, ATP levels dropped by 2 to 3-fold, whereas ATP levels even slightly increased in the *tisB* deletion and K12L strain (Fig. 4a). These observations indicate a CIP-induced ATP decline that is based on TisB activity. Next, we determined the persister frequency (Fig. 4b) and the duration of dormancy (Fig. 4c), as measured by the colony appearance time after CIP treatment[32,33]. In both measurements, the D5N strain was comparable to the wild type with a persister frequency of ~0.1% and a colony appearance time of ~1,250 min. The K12L strain, on the other hand, had a significantly reduced persister frequency of ~0.01%, which was comparable to the *tisB* deletion strain (Fig. 4b). Likewise, the colony appearance time was reduced to ~850 min (Fig. 4c), demonstrating that functional TisB is needed to increase both the persister frequency and the duration of dormancy. In conclusion, the chromosomal manipulations confirmed our expectations and further strengthened the essentiality of K12.

A library approach reveals further determinants of TisB functionality

So far, we were able to demonstrate that replacing some of the charged or polar AAs with the hydrophobic AA leucine led to reduced (D22L and K26L) or abolished TisB functionality (K12L and Q19L). To further reveal the importance of charged AA residues and their positions within the TisB peptide chain, we constructed a small library of expression plasmids containing 12 mutated *tisB* sequences. The wild-type *tisB* sequence was included as a positive control. The single-stranded library (oligo pool) was converted into a double-stranded DNA library and subsequently cloned into plasmid pSL0002 for arabinose-inducible *tisB* expression from the P_{BAD} promoter (Fig. 5a)[34]. The resulting plasmid library was transformed into *E. coli* MG1655, and individual colonies were

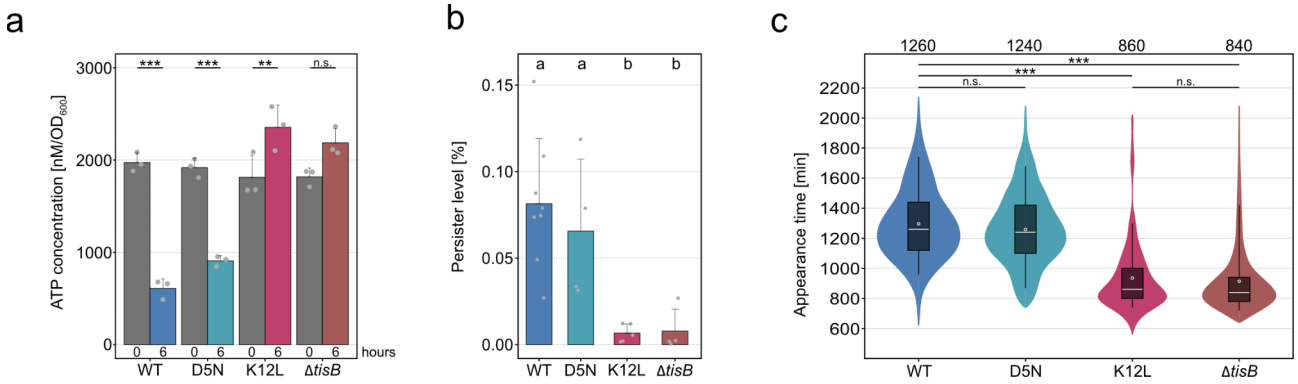

Fig. 4. Lysine 12 is essential for TisB-dependent antibiotic persistence. Wild type MG1655 (WT), a *tisB* deletion strain, and two chromosomal amino acid substitutions (D5N and K12L) were treated with CIP (10 µg/mL) during exponential phase for six hours. (**a**) TisB-dependent ATP depletion. Pre- and post-treatment samples were analyzed using a luciferase-based assay to measure cellular ATP levels (nM per OD_{600}). Bars represent the mean of three biological replicates. Error bars indicate the standard deviation. ANOVA with post-hoc Tukey HSD test was performed (*** $p < 0.001$; ** $p < 0.01$; n.s.: not significant). (**b**) Persister cell survival. Cells before and after treatment were plated on LB agar plates to determine relative persister levels. Bars represent the mean of at least four biological replicates (WT: $n = 8$; D5N: $n = 4$; K12L: $n = 5$; Δ*tisB*: $n = 4$). Error bars represent the standard deviation. ANOVA with post-hoc Tukey HSD test was performed, and a compact letter display was applied to present significant groups. (**c**) Persister cell recovery. The ScanLag method was applied to determine the colony appearance time after CIP treatment. Colony appearance times are illustrated as violin box plots. Colonies from at least two biological replicates were combined (WT: $n = 741$; D5N: $n = 930$; K12L: $n = 165$; Δ*tisB*: $n = 375$). The white dot indicates the mean. The respective median appearance time (white bar) is shown on top of each plot. Strains were compared using a pairwise Wilcoxon rank sum test (*** $p < 0.0001$; n.s.: not significant).

transferred into a 96-well plate together with empty vector and p0SD-*tisB* controls. The experimental layout was expected to result in a > 6-fold coverage of the library, and sequencing of the plate revealed that each variant was represented by at least two individual clones. After overnight cultivation in regular LB medium, cells were transferred into a new 96-well plate containing LB medium with the inducer L-ara. Growth of individual clones was monitored in a plate reader to assess functionality of the TisB variants (Fig. 5a).

Only the Q19D variant was able to fully inhibit growth, demonstrating that Q19 can be functionally replaced by a negatively charged aspartate. In contrast, replacing Q19 with a positively charged lysine (Q19K) led to a non-functional TisB variant (Fig. 5b). Neither Q19D nor Q19K were able to compensate for the loss of functionality of the K12L substitution. Furthermore, we were not able to obtain functionality when replacing K12 with either an aspartate (K12D) or arginine (K12R), demonstrating that TisB has a strict requirement for a lysine at position 12 (Fig. 5b). In contrast to the D22L substitution, which still showed intermediate functionality (cf. Fig. 1d), a D22K variant was non-functional and was also not able to compensate the K12D substitution (Fig. 5b). Finally, replacing the positively charged residues at the C-terminus by negatively charged aspartates either attenuated (K26D and K29D single substitutions) or completely abolished functionality (K26D K29D double substitution), indicating the importance of positive charges at the C-terminus. In line with this, a K26L K29L double substitution was non-functional as well (Fig. 5b). According to the 'anion-selective pore' model, a net charge of + 1 favors anion selectivity and, hence, TisB functionality[19]. However, we were not able to correlate the net charge of the tested TisB variants with their functionality (Supplementary Fig. S5).

Discussion

Most type I toxins are membrane proteins with a small size and high hydrophobicity, features that have complicated their direct investigation in living cells. To bypass this limitation, and to learn more about the mode of action, type I toxins have been studied in model lipid bilayers (in vitro) or by molecular dynamics simulations (in silico)[10,19–21,35]. These analyses have pushed forward models of how these toxins organize themselves in the inner membrane to fulfill their functions. In this study, we aimed at substantiating the prevailing in vitro and in silico models for TisB by physiological experiments with *E. coli*.

Both in vitro and in silico models predict that charged and polar AAs are important for TisB functionality. By replacing individual AAs with leucine, we demonstrate that K12 and Q19 are most important for a variety of TisB-dependent phenotypes, including growth inhibition, ATP depletion, protein aggregation, and antibiotic tolerance[16,18,23]. Interestingly, moderate *tisB* expression almost fully protects against the DNA-damaging antibiotic CIP, whereas *tisB* expression is a disadvantage when cells are challenged with oxidative stress by H_2O_2. We have shown before that TisB itself provokes generation of ROS, such as superoxide, and that a failure in ROS detoxification may delay or even prevent recovery[15]. We conclude that TisB-dependent dormancy is an efficient means to avoid CIP-induced DNA damage[18,36], but that the combined effect of endogenous ROS production and H_2O_2 administration cannot be efficiently tolerated by TisB-producing cells. Alternatively, TisB might compromise the ability to efficiently detoxify H_2O_2, but this needs further investigation.

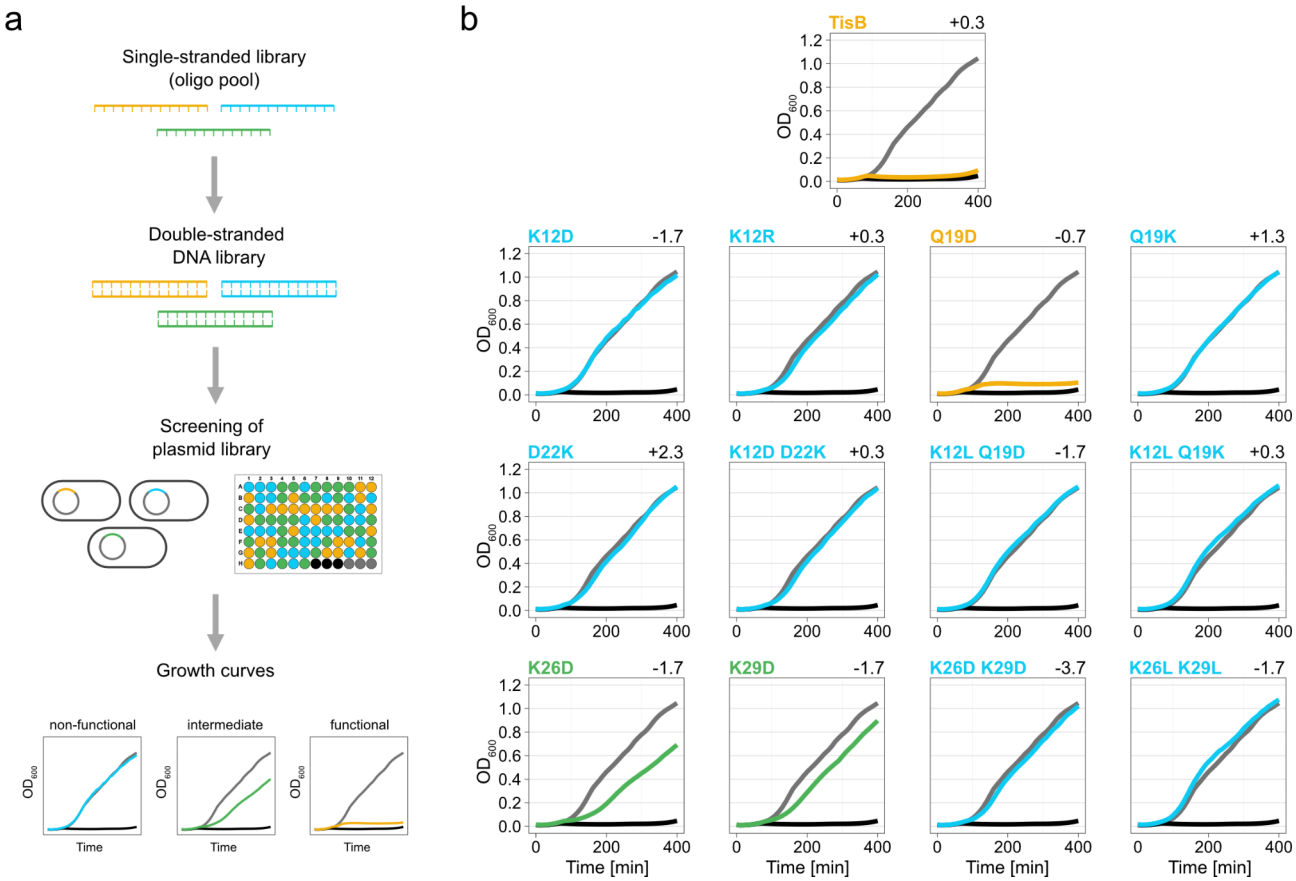

Fig. 5. Screening of a *tisB* expression library. (**a**) Schematic representation of generation and screening of the *tisB* expression library. A single-stranded DNA library, representing various *tisB* variants, was converted into a double-stranded DNA library *via* PCR and cloned into expression plasmids. Plasmids were transformed into wild type MG1655 and screened with respect to growth inhibition in the presence of L-ara (0.2%) in a 96-well format. TisB variants were categorized as non-functional (blue), intermediate (green), and functional (yellow). (**b**) Screening of the *tisB* expression library. After growth analysis, results for each TisB variant were combined to generate mean growth curves (native TisB: $n=7$; K12D: $n=2$; K12R: $n=5$; Q19D: $n=6$; Q19K: $n=7$; D22K: $n=4$; K12D D22K: $n=2$; K12L Q19D: $n=7$; K12L Q19K: $n=5$; K26D: $n=4$; K29D: $n=3$; K26D K29D: $n=4$; K26L K29L: $n=2$). Three biological replicates of p0SD-*tisB* (black) and an empty pBAD plasmid (grey) were included as controls. The individual net charge of each TisB variant (as calculated with the Prot pi Protein Tool) is represented on the top right of each plot.

But how can we accommodate our physiological data with the current TisB models? Gurnev and colleagues applied synthetic TisB for conductance measurements in planar membranes consisting of the model lipid diphytanoyl-phosphatidylcholine[19]. These experiments indicated that TisB forms narrow pores, which maintain cooperativity in honeycomb-like clusters. Based on their experiments with K26A and D5A variants, it was further suggested that a positive net charge promotes anionic selectivity of the TisB pore. According to this in vitro model, hydroxyl anions traverse the inner membrane and discharge the PMF by neutralizing protons in the periplasm. However, our experiments do not support anionic selectivity, since the net charge shows no correlation with TisB functionality in living *E. coli* cells. We conclude that selectivity in the complex environment of a natural membrane may be different than in model membranes. Using pH-sensitive fluorescent proteins it has been demonstrated in *E. coli* that the DNA-damaging antibiotics nalidixic acid and ofloxacin cause loss of pH homeostasis and acidification of the cytoplasm[17,37]. In case of ofloxacin, cytoplasmic acidification could be linked to TisB[17], and we therefore suggest that TisB acts as a protonophore, which enables discharge of the proton gradient and cytoplasmic acidification. Whether the TisB pore has a rather broad specificity and allows the opposing transition of protons and hydroxyl anions remains an unexplored possibility.

Another intriguing question concerns the oligomeric state of TisB within the inner membrane. In silico analyses by molecular dynamics simulations predict that the basic unit of TisB oligomers is an antiparallel dimer that is stabilized *via* a ladder of salt bridges, a so called 'charge-zipper'[22]. Subsequent refinements of the simulations suggested that TisB assembles into a tetramer that is best described as an antiparallel dimer-of-dimers[21]. Based on proximity estimations, the model makes the prediction that the basic dimer is mainly stabilized by two K12-D22 salt bridges and one Q19-Q19 hydrogen bond. In support of the 'charge-zipper' model, we observed here that both K12D and D22K single substitutions abolished TisB functionality, likely because the mandatory salt bridges

were not formed. However, TisB still showed intermediate functionality when D22 was replaced with a leucine. Furthermore, we expected that a D22K substitution should be able to compensate for the functionality loss of a K12D substitution due to establishment of alternative D12-K22 salt bridges. However, the K12D D22K double substitution was not functional, which contradicts the 'charge-zipper' model. The Q19 residues were assumed to coordinate both the basic dimer and the dimer-of-dimers through a variety of Q19-Q19 and K12-Q19 hydrogen bonds[21]. Interestingly, we observed that a Q19D substitution was still fully functional, suggesting that K12-D19 salt bridges may compensate for the loss of Q19-mediated hydrogen bonds. In summary, our data supports an essential role of the positively charged K12 residue, since it could not be functionally replaced by any of the tested AAs, not even by the positively charged arginine. We further suggest that K12-Q19 interactions may be more important for TisB oligomerization than K12-D22 interactions but cannot exclude alternative explanations for the observed effects. We conclude that further analyses of native TisB are needed to reveal the oligomeric state of TisB and the particular influence of the charged and polar amino acids.

Replacement of K26 or K29 with a negatively charged aspartate impaired TisB functionality. Similarly, in the case of the type I toxin ZorO (29 AAs) in *E. coli* O157:H7 EDL933, replacement of the C-terminal lysine K29 with a negatively charged glutamate prevented growth inhibition and ATP depletion by ZorO[38]. We further show that TisB has a requirement for at least one positively charged AA (either K26 or K29) at its C-terminus, since substitution of both lysines completely abolished functionality. Similar observations were made for the type I toxin AapA1 in *Helicobacter pylori* (30 AAs). In *H. pylori*, the two C-terminal lysines, K29 and K30, could not be truncated without losing toxicity[35]. Similarly, in *Staphylococcus aureus*, the toxic peptide $SprG1_{31}$ (31 AAs) needs two C-terminal lysines, K30 and K31, for full toxicity. Interestingly, the two lysines could not be swapped to the N-terminus to retain toxicity[39]. These observations raise the question of how the C-terminal positive charges, which are not integral to the TMH, contribute to toxicity. One possibility is that the positively charged C-terminus is important to establish an initial attachment of the toxins to the negatively charged inner membrane, which is followed by hydrophobic interactions and membrane integration[40,41]. The positively charged residues may also provide orientation of the toxins within the membrane due to electrostatic repulsion by protons in the periplasm, which is the foundation of the so-called 'positive-inside rule'[42]. In case of TisB, the positive charges may accommodate the C-terminus in the cytoplasm, while the N-terminus extends into the periplasm, a so-called N_{out}-C_{in} orientation[43]. However, a strict N_{out}-C_{in} orientation is not consistent with an antiparallel TisB orientation predicted by the 'charge-zipper' model. It also raises the questions whether TisB affects its own orientation as soon as the electrostatic repulsion is alleviated by discharge of the PMF and neutralization of the periplasm. Hypothetically, TisB adopts different PMF-sensitive configurations within the inner membrane, similar to what has been described for phage holins[44].

Finally, the importance of charged AA residues may differ between different type I toxins. In case of the Fst toxin (33 AAs) in *Enterococcus faecalis*, the charged residues at the N-terminus (K2 and D3) seem to be more important for toxicity than the highly charged C-terminus[45], albeit progressive truncation of the C-terminus reduced toxicity[46]. The IbsC toxin in *E. coli* is comparably short (19 AAs) and only has one charged residue at its N-terminus (R3), which is dispensable for toxicity[47]. It, therefore, remains challenging to define common rules for type I toxin functionality based on charged AAs. We suggest that high-throughput screens of synthetic toxin libraries, including chimeras of natural toxins and engineered toxins, may help to further dissect the importance of certain amino acids and their positioning within the peptide chain.

Methods

Growth conditions

E. coli strains (Supplementary Table S1) were grown in Lysogeny Broth (LB) under conditions of 37 °C and a rotational speed of 180 rpm. When temperature-sensitive plasmids were used, the cultivation temperature was adjusted to 30 °C while maintaining the same rotational speed. Antibiotics were added to pre-cultures as required, with concentrations of 50 µg/mL for kanamycin, 15 µg/mL for chloramphenicol, 200 µg/mL for ampicillin, and 6 µg/mL for tetracycline. Pre-cultures were obtained from single colonies, grown overnight, and subsequently diluted at a ratio of 1:100 into fresh LB medium to start experimental cultures. The growth curves were monitored in 30-min intervals at 600 nm using a Fisher Scientific cell density meter (model 40).

Construction of plasmids

Plasmids p0SD-*tisB* and p0SD-3xFLAG-*tisB*[16] were used as templates for site-directed mutagenesis PCR to generate amino acid substitutions. Primers are listed in Supplementary Table S3. After PCR, the template DNA was digested using DpnI (Thermo Fisher Scientific). The PCR product was transformed into chemically competent MG1655 cells, and clones were selected on LB agar plates containing ampicillin (200 µg/mL). All plasmids were verified by Sanger sequencing (Microsynth SeqLab) and are listed in Supplementary Table S2.

Chromosomal manipulations

Lambda red recombineering was applied to generate gene deletions and point mutations in the MG1655 chromosome[48]. For expression of λ red genes, the temperature-sensitive plasmid pSIM5 was used[49]. Gene deletions were constructed by insertion of resistance cassettes *via* homologous recombination according to standard protocols[48]. Point mutations were introduced *via* a scarless, two-step λ red protocol using *sacB* as counter-selection marker[14]. The resulting strains (Supplementary Table S1) were verified by diagnostic PCR and Sanger sequencing (Microsynth SeqLab). Primers for λ red recombineering are listed in Supplementary Table S3.

Determination of colony counts and persister levels

Exponential-phase cultures (OD_{600} ~ 0.4) were treated with L-ara (0.2%) for 60 min to induce *tisB* expression. In case cultures were subsequently treated with CIP (10 µg/mL), H_2O_2 (10 mM), or KAN (200 µg/mL), the L-ara

treatment was reduced to 30 min. If cultures were treated with CIP (10 µg/mL) alone, the treatment duration was adjusted to six hours. Samples were collected before and after treatments, washed and serially diluted with 20 mM $MgSO_4$, and then plated on LB agar plates. The colonies were counted after approximately 20 h (pre-treatment samples) or 40 h (post-treatment samples). The colony counts were used to calculate the colony forming units per milliliter (CFU/mL). The survival upon CIP treatment (i.e., persister level) was determined by calculating the ratio of treated and untreated samples. *P*-values were calculated using an ANOVA followed by a post-hoc Tukey's HSD test, implemented in R statistical language (https://www.r-project.org/).

Analysis of colony growth

The ScanLag method was used to analyze colony growth[32]. LB agar plates from CIP experiments were covered with black felt, positioned on scanners, and incubated at a temperature of 37 °C. Time series of images were captured using Epson Perfection V39 scanners under the control of the *ScanningManager* application[50]. TIFF files were generated every 20 min over a total duration of 40 h. Image processing was performed using MatLab (MathWorks), using functions *PreparePictures*, *setMaskApp*, *TimeLapse*, and *ScanLagApp*. After image processing, the appearance and growth times were extracted. The time of appearance is characterized by a colony size of 10 pixels, while the growth time is defined as the duration required for a colony size to increase from 80 to 160 pixels. The data was used to construct violin box plots *via* Power BI Desktop (Microsoft). *P*-values were calculated using a pairwise Wilcoxon rank sum test in R statistical language (https://www.r-project.org/).

ATP measurements

Exponential-phase cultures (OD_{600} ~ 0.4) were treated with L-ara (0.2%) for one hour or with CIP (10 µg/µL) for six hours. Pre- and post-treatment samples (1 mL) were extracted. Cell pellets were harvested *via* centrifugation (13,000 rpm, 3 min), and the supernatants were discarded. The cells were rinsed with 1 mL of NaCl (0.9%) and resuspended in 1 mL of LB medium. A mixture was prepared by combining 100 µL of the samples with 100 µL of BacTiter-Glo reagent (Promega). Mixtures were incubated for 5 min in the dark. The luminescence was quantified using an Infinite M Nano + microplate reader (Tecan). The values obtained were converted to nM, using the slope formula of an ATP calibration curve, and normalized to the OD_{600}. *P*-values were calculated using an ANOVA followed by a post-hoc Tukey's HSD test, implemented in R statistical language (https://www.r-project.org/).

Fluorescence microscopy

Exponential-phase cultures (OD_{600} ~ 0.4) were treated with L-ara (0.2%) for 60 min. Samples were collected both prior to and post-treatment. Samples were then placed on 1% agarose pads in 1x phosphate-buffered saline (PBS). The agarose pads were positioned on a microscopy slide, and the cells were covered with a cover slip. Imaging was performed using a Leica DMI6000 B inverted microscope, equipped with an HCX PL APO 100x/1.4 differential interference contrast (DIC) objective. The images were captured using a pco.edge sCMOS camera and processed with VisiView software (version 4.3.0, Visitron Systems GmbH). For fluorescence images (GFP), a custom filter set was used (T495lpxr, EX470/40m; EM525/50, Chroma Technology). The exposure time was set to 50 ms, with a binning factor of 2 and an offset of 0.0. The captured images were saved in the TIFF format and subsequently processed using the open-source software ImageJ (version 1.53k).

Northern blot analysis

Exponential-phase cultures (OD_{600} ~ 0.4) were treated with CIP (10 µg/mL), H_2O_2 (10 mM), or KAN (200 µg/mL) for one hour. Total RNA of pre- and post-treatment samples was isolated using the acid-phenol method as described[13]. Northern blot analysis was performed with 5 µg of total RNA. The RNA was separated using a 10% polyacrylamide gel, containing 1x TBE and 7 M urea. Separation was done at 300 V for an approximate duration of three hours. The separated RNA was transferred onto a Roti Nylon plus membrane (Roth) *via* semi-dry electroblotting at 250 mA for three hours, followed by UV-crosslinking. The membrane was pre-hybridized using Church buffer [0.5 M phosphate buffer (pH 7.2), 1% (w/v) bovine serum albumin, 1 mM EDTA, 7% (w/v) SDS] at a temperature of 42 °C for one hour. Hybridization with radioactively labelled probes was performed overnight at the same temperature. Specific probes were generated by end-labeling of oligodeoxyribonucleotides (Supplementary Table S3) using T4 Polynucleotide Kinase (New England Biolabs) and [γ-^{32}P]-ATP (Hartmann Analytic). After hybridization, membranes were washed (5x SSC, 0.01% SDS) and exposed to phosphorimaging screens (Bio-Rad). Screens were analyzed using a Molecular Imager FX and the Quantity One 1-D Analysis Software (Bio-Rad).

Sample generation for western blot analysis

For detection of 3xFLAG-TisB, exponential-phase cultures (OD_{600} ~ 0.4) were treated with L-ara (0.2%) for one hour. Pre- and post-treatment samples (40 mL) were collected, pelleted at 10,000 rpm and 4 °C for 10 min, washed with 2 mL NaCl (0,9%), and centrifuged at 13,000 rpm and 4 °C for 3 min. Cells were washed with cold phosphate buffer (50 mM), centrifuged as before, and subsequently resuspended in 4 mL cold phosphate buffer (50 mM). Cells were lysed by sonication (3 × 30 s, 7 cycles, 70%) using a Bandelin Sonopuls and the ultrasonic immersion probe MS 73. Lysates were centrifuged at 600 rpm for 10 min to remove cell debris. Cytoplasmic and membrane fractions were separated using ultracentrifugation of the supernatants at 105,000 x *g* for 45 min at 4 °C. Supernatants were transferred to new tubes, while the pellets were dissolved in 3 mL 50 mM phosphate buffer containing 0.2% sodium lauroyl sarcosinate. Samples were incubated up to 2 h at room temperature to solubilize membrane proteins. Protein concentrations were determined using the Bradford assay. Proteins were precipitated overnight using four times the sample volume of cold acetone. Samples were centrifuged at 13,000 rpm and 4 °C for 10 min and washed two times with 500 µL cold acetone. Afterwards, acetone was

removed by allowing evaporation at room temperature for 15 min. Proteins were adjusted to a concentration of 5 µg/µL in phosphate buffer (50 mM). Finally, SDS sample buffer (12% SDS, 6% β-mercaptoethanol, 30% glycerol, 0.05% Coomassie blue, 150 mM Tris/HCl at pH 7.0) was added for a final concentration of 2.5 µg/µL.

Western blot analysis

Protein separation was performed using Tricine-SDS-PAGE with a 16% separation polyacrylamide gel and 6% collection polyacrylamide gel. Prior loading, samples with SDS buffer were incubated at 37 °C for 15 min (boiling of samples was avoided because it may cause aggregation of membrane proteins). An initial voltage of 100 V was applied until samples entered the separation gel, after which electrophoresis was conducted at 300 V for approximately three hours. Proteins were transferred onto a PVDF membrane *via* semi-dry electroblotting overnight at 0.4 mA/cm^2. Membranes were subsequently stained with Ponceau S solution and documented. Membranes were blocked with 5% milk powder in 1x PBST (PBS + 0.1% Tween20) for one hour. For detection of 3xFLAG-TisB, membranes were incubated with an HRP-conjugated monoclonal IgG α-FLAG antibody (Sigma-Aldrich) in 1x PBST with 3% BSA at room temperature for 90 min, followed by visualization using the Lumi-Light Western Blotting Substrate (Roche). For detection of YidC and YchF, membranes were incubated with a rabbit α-YidC and a rabbit α-YchF antibody, respectively, in 1x PBST with 3% BSA at room temperature for 90 min. Subsequently, membranes were incubated with an alkaline phosphatase-conjugated goat α-rabbit antibody in 1x PBST with 3% BSA at room temperature for 90 min. For visualization, CDP-Star (Roche) and AP-buffer (0.1 M Tris/HCl, 0.1 M NaCl, pH 9.5) were used. All signals were documented using a chemiluminescence imager (PeqLab) with the FusionCapt Advance software (Vilber Lourmat). For sequential detection of proteins, membranes were stripped using stripping buffer (0.1 M glycine, 0,37% HCl) at room temperature for one hour. After stripping, membranes were blocked once again with 5% milk powder in 1x PBST for 90 min.

Construction and analysis of a *tisB* expression library

The *tisB* library was ordered as an oligo pool from IDT (Integrated DNA Technologies). All *tisB* sequences contained the alternative 5' untranslated region (UTR) from plasmid p0SD-*tisB* for moderate *tisB* expression[16]. In addition, each sequence was extended by universal 5' and 3' adapter sequences containing BbsI recognition and primer binding sites (Supplementary Table S4). The single-stranded oligo pool was converted into a double-stranded DNA library by PCR using primers targeted towards the adapter sequences (Supplementary Table S3). The DNA library was subsequently cloned into plasmid pSL0002 using Golden Gate cloning as described elsewhere[34]. The resulting plasmid library was transformed into electrocompetent *E. coli* MG1655 cells. Ninety individual colonies were transferred into a transparent 96-well plate containing 150 µL LB medium per well. Strains containing either an empty vector or p0SD-*tisB* were loaded in triplicates and used as controls. The plate was incubated overnight at 37 °C and 180 rpm, and subsequently used for Sanger sequencing (Microsynth SeqLab). In addition, the overnight plate was used to inoculate two new 96-well plates; the first containing LB medium (growth control plate) and the second containing LB medium with L-ara (0.2%) for induction of *tisB* expression. Growth was monitored at 600 nm in an Infinite M Nano + microplate reader (Tecan) adjusted to 37 °C and orbital shaking (amplitude 3.5 mm). Data was evaluated using the *growthcurver* package in R Studio.

Data availability

Datasets are available from the corresponding author upon reasonable request.

Received: 12 July 2024; Accepted: 23 September 2024
Published online: 03 October 2024

References

1. Jurėnas, D., Fraikin, N., Goormaghtigh, F. & Van Melderen, L. Biology and evolution of bacterial toxin-antitoxin systems. *Nat. Rev. Microbiol.* **20**, 335–350 (2022).
2. Harms, A., Brodersen, D. E., Mitarai, N. & Gerdes, K. Toxins, targets, and triggers: an overview of Toxin-Antitoxin Biology. *Mol. Cell.* **70**, 768–784 (2018).
3. Hayes, F. & Toxins-Antitoxins Plasmid maintenance, programmed cell death, and cell cycle arrest. *Science*. **301**, 1496–1499 (2003).
4. Gerdes, K., Christensen, S. K. & Løbner-Olesen, A. Prokaryotic toxin–antitoxin stress response loci. *Nat. Rev. Microbiol.* **3**, 371–382 (2005).
5. Leroux, M. & Laub, M. T. Toxin-antitoxin systems as Phage Defense Elements. *Annu. Rev. Microbiol.* **76**, 21–43 (2022).
6. Ronneau, S. & Helaine, S. Clarifying the link between toxin–antitoxin modules and bacterial persistence. *J. Mol. Biol.* **431**, 3462–3471 (2019).
7. Shore, S. F. H., Leinberger, F. H., Fozo, E. M. & Berghoff, B. A. Type I toxin-antitoxin systems in bacteria: from regulation to biological functions. *EcoSal Plus* eesp00252022 (2024).
8. Nonin-Lecomte, S., Fermon, L., Felden, B. & Pinel-Marie, M. L. Bacterial type I toxins: folding and membrane interactions. *Toxins (Basel)*. **13**, 490 (2021).
9. Wilmaerts, D. et al. HokB monomerization and membrane repolarization control Persister Awakening. *Mol. Cell.* **75**, 1031–1042e4 (2019).
10. Wilmaerts, D. et al. The persistence-inducing toxin HokB forms dynamic pores that cause ATP leakage. *mBio*. **9**, e00744–e00718 (2018).
11. Verstraeten, N. et al. Obg and membrane depolarization are part of a microbial bet-hedging strategy that leads to antibiotic tolerance. *Mol. Cell.* **59**, 9–21 (2015).
12. Vogel, J., Argaman, L., Wagner, E. G. H. & Altuvia, S. The small RNA IstR inhibits synthesis of an SOS-induced toxic peptide. *Curr. Biol.* **14**, 2271–2276 (2004).
13. Berghoff, B. A., Karlsson, T., Källman, T., Wagner, E. G. H. & Grabherr, M. G. RNA-sequence data normalization through in silico prediction of reference genes: the bacterial response to DNA damage as case study. *BioData Min.* **10**, 30 (2017).
14. Berghoff, B. A., Hoekzema, M., Aulbach, L. & Wagner, E. G. H. two regulatory RNA elements affect TisB-dependent depolarization and persister formation. *Mol. Microbiol.* **103**, 1020–1033 (2017).

15. Edelmann, D. & Berghoff, B. A. Type I toxin-dependent generation of superoxide affects the persister life cycle of *Escherichia coli*. *Sci. Rep.* **9**, 14256 (2019).
16. Leinberger, F. H. et al. Protein aggregation is a consequence of the dormancy-inducing membrane toxin TisB in *Escherichia coli*. *bioRxiv* 2024.02.22.581605 https://doi.org/10.1101/2024.02.22.581605 (2024).
17. Cayron, J., Oms, T., Schlechtweg, T., Zedek, S. & Van Melderen, L. TisB protein is the single molecular determinant underlying multiple downstream effects of ofloxacin in *Escherichia coli*. *Sci. Adv.* **10**, eadk1577 (2024).
18. Dörr, T., Vulic, M. & Lewis, K. Ciprofloxacin causes persister formation by inducing the TisB toxin in *Escherichia coli*. *PLoS Biol.* **8**, e1000317 (2010).
19. Gurnev, P. A., Ortenberg, R., Dörr, T., Lewis, K. & Bezrukov, S. M. Persister-promoting bacterial toxin TisB produces anion-selective pores in planar lipid bilayers. *FEBS Lett.* **586**, 2529–2534 (2012).
20. Schneider, V. et al. Tetrameric charge-zipper assembly of the TisB peptide in membranes—computer simulation and experiment. *J. Phys. Chem. B*. **123**, 1770–1779 (2019).
21. Steinbrecher, T. et al. Peptide-lipid interactions of the stress-response peptide TisB that induces bacterial persistence. *Biophys. J.* **103**, 1460–1469 (2012).
22. Coray, D. S., Wheeler, N. E., Heinemann, J. A. & Gardner, P. P. Why so narrow: distribution of anti-sense regulated, type I toxin-antitoxin systems compared with type II and type III systems. *RNA Biol.* **14**, 275–280 (2017).
23. Unoson, C. & Wagner, E. G. H. A small SOS-induced toxin is targeted against the inner membrane in *Escherichia coli*. *Mol. Microbiol.* **70**, 258–270 (2008).
24. Pu, Y. et al. ATP-dependent dynamic protein aggregation regulates bacterial dormancy depth critical for antibiotic tolerance. *Mol. Cell.* **73**, 143–156e4 (2019).
25. Dewachter, L. et al. The dynamic transition of persistence toward the viable but nonculturable state during stationary phase is driven by protein aggregation. *mBio* **12**, e0070321 (2021).
26. Govers, S. K., Mortier, J., Adam, A. & Aertsen, A. Protein aggregates encode epigenetic memory of stressful encounters in individual *Escherichia coli* cells. *PLoS Biol.* **16**, e2003853 (2018).
27. Goerlich, O., Quillardet, P. & Hofnung, M. Induction of the SOS response by hydrogen peroxide in various *Escherichia coli* mutants with altered protection against oxidative DNA damage. *J. Bacteriol.* **171**, 6141 (1989).
28. Baharoglu, Z. & Mazel, D. *Vibrio cholerae* Triggers SOS and Mutagenesresponsesponsewidearange Ranantibioticsiotics: a Route towards Multiresistance. *Antimicrob. Agents Chemother.* **55**, 2438–2441 (2011).
29. Lewis, K. Persister cells. *Annu. Rev. Microbiol.* **64**, 357–372 (2010).
30. Shan, Y. et al. ATP-Dependent persister formation in *Escherichia coli*. *mBio*. **8**, e02267–e02216 (2017).
31. Conlon, B. P. et al. Persister formation in *Staphylococcus aureus* is associated with ATP depletion. *Nat. Microbiol.* **1**, 16051 (2016).
32. Levin-Reisman, I. et al. Automated imaging with ScanLag reveals previously undetectable bacterial growth phenotypes. *Nat. Methods*. **7**, 737–739 (2010).
33. Spanka, D. T., Konzer, A., Edelmann, D. & Berghoff, B. A. High-throughput proteomics identifies proteins with importance to postantibiotic recovery in depolarized persister cells. *Front. Microbiol.* **10**, 378 (2019).
34. Köbel, T. S. et al. An easy-to-use plasmid toolset for efficient generation and benchmarking of synthetic small RNAs in bacteria. *ACS Synth. Biol.* **11**, 2989–3003 (2022).
35. Korkut, D. N. et al. Structural insights into the AapA1 toxin of *Helicobacter pylori*. *Biochim. Biophys. Acta Gen. Subj.* **1864**, 129423 (2020).
36. Edelmann, D. et al. Elevated expression of Toxin TisB protects persister cells against ciprofloxacin but enhances susceptibility to mitomycin C. *Microorganisms*. **9**, 943 (2021).
37. Booth, J. A. et al. Antibiotic-induced DNA damage results in a controlled loss of pH homeostasis and genome instability. *Sci. Rep.* **10**, (2020).
38. Bogati, B., Shore, S. F. H., Nipper, T. D., Stoiculescu, O. & Fozo, E. M. Charged amino acids contribute to ZorO toxicity. *Toxins (Basel)*. **15**, 32 (2022).
39. Fermon, L. et al. Mechanism of action of *sprG1*-encoded type I toxins in *Staphylococcus aureus*: from membrane alterations to mesosome-like structures formation and bacterial lysis. *Front. Microbiol.* **14**, 1275849 (2023).
40. Scheglmann, D., Werner, K., Eiselt, G. & Klinger, R. Role of paired basic residues of protein C-termini in phospholipid binding. *Protein Eng.* **15**, 521–527 (2002).
41. Cao, Z., Zhao, L., Yan, T. & Liu, L. Effects of C-terminal lys-arg Residue of AapA1 protein on toxicity and structural mechanism. *Toxins (Basel)* **15**, (2023).
42. Andersson, H. & von Heijne, G. Membrane protein topology: effects of delta mu H+on the translocation of charged residues explain the 'positive inside' rule. *EMBO J.* **13**, 2267–2272 (1994).
43. Fontaine, F., Fuchs, R. T. & Storz, G. Membrane localization of small proteins in *Escherichia coli*. *J. Biol. Chem.* **286**, 32464–32474 (2011).
44. Young, R. Phage lysis: do we have the hole story yet? *Curr. Opin. Microbiol.* **16**, 790–797 (2013).
45. Weaver, K. E. et al. Identification and characterization of a family of toxin-antitoxin systems related to the *Enterococcus faecalis* plasmid pAD1 par addiction module. *Microbiol. (Reading)*. **155**, 2930–2940 (2009).
46. Holmes, A., Sadlon, J. & Weaver, K. Charged residues flanking the transmembrane domain of two related toxin-antitoxin system toxins affect host response. *Toxins (Basel)* **13**, (2021).
47. Mok, W. W. K., Patel, N. H. & Li, Y. Decoding toxicity: deducing the sequence requirements of IbsC, a type I toxin in *Escherichia coli*. *J. Biol. Chem.* **285**, 41627–41636 (2010).
48. Datsenko, K. A. & Wanner, B. L. One-step inactivation of chromosomal genes in *Escherichia coli* K-12 using PCR products. *Proc. Natl. Acad. Sci. USA*. **97**, 6640–6645 (2000).
49. Datta, S., Costantino, N. & Court, D. L. A set of recombineering plasmids for gram-negative bacteria. *Gene*. **379**, 109–115 (2006).
50. Levin-Reisman, I., Fridman, O., Balaban, N. Q. & ScanLag High-throughput quantification of colony growth and lag time. *J. Vis. Exp.* **e51456** https://doi.org/10.3791/51456 (2014).

Acknowledgements

We would like to thank Nicole Scheerer for excellent technical assistance; Nasrine Bekhedda, Bahar Asian, Christoph Binsfeld, Annabel Metje, and Marlon Esenkan for experimental support; Hans-Georg Koch (University of Freiburg) for providing YidC and YchF antibodies. This research was funded by the German Research Council (DFG) in the framework of the SPP 2002 (BE 5210/3-1 and BE 5210/3-2 to B.A.B.).

Author contributions

F.H.L. performed the experiments. F.H.L. and B.A.B. designed the study, analyzed the data, and wrote the manuscript.

Funding
Open Access funding enabled and organized by Projekt DEAL.

Declarations

Competing interests
The authors declare no competing interests.

Additional information
Supplementary Information The online version contains supplementary material available at https://doi.org/10.1038/s41598-024-73879-7.

Correspondence and requests for materials should be addressed to B.A.B.

Reprints and permissions information is available at www.nature.com/reprints.

Publisher's note Springer Nature remains neutral with regard to jurisdictional claims in published maps and institutional affiliations.

3.1

Supplement

Relevance of charged and polar amino acids for functionality of membrane toxin TisB

Supplementary Figures

Relevance of charged and polar amino acids

for functionality of membrane toxin TisB

Florian H. Leinberger and Bork A. Berghoff

This file contains:

Figures S1 to S5

Figure S1

Name	Sequence	GRAVY	Net Charge
TisB	MNLVDIAILILKLIVAALQLLDAVLKYLK	1.62	+0.3
D5L	MNLVLIAILILKLIVAALQLLDAVLKYLK	1.87	+1.3
K12L	MNLVDIAILILLLIVAALQLLDAVLKYLK	1.88	-0.7
Q19L	MNLVDIAILILKLIVAALLLLDAVLKYLK	1.87	+0.3
D22L	MNLVDIAILILKLIVAALQLLLAVLKYLK	1.87	+1.3
K26L	MNLVDIAILILKLIVAALQLLDAVLLYLK	1.88	-0.7
K29L	MNLVDIAILILKLIVAALQLLDAVLKYLL	1.88	-0.7
K12D	MNLVDIAILILDLIVAALQLLDAVLKYLK	1.63	-1.7
K12R	MNLVDIAILILRLIVAALQLLDAVLKYLK	1.60	+0.3
Q19D	MNLVDIAILILKLIVAALDLLDAVLKYLK	1.62	-0.7
Q19K	MNLVDIAILILKLIVAALKLLDAVLKYLK	1.60	+1.3
D22K	MNLVDIAILILKLIVAALQLLKAVLKYLK	1.60	+2.3
K12D D22K	MNLVDIAILILDLIVAALQLLKAVLKYLK	1.62	+0.3
K12L Q19D	MNLVDIAILILLLIVAALDLLDAVLKYLK	1.88	-1.7
K12L Q19K	MNLVDIAILILLLIVAALKLLDAVLKYLK	1.87	+0.3
K26D	MNLVDIAILILKLIVAALQLLDAVLDYLK	1.63	-1.7
K29D	MNLVDIAILILKLIVAALQLLDAVLKYLD	1.63	-1.7
K26D K29D	MNLVDIAILILKLIVAALQLLDAVLDYLD	1.64	-3.7
K26L K29L	MNLVDIAILILKLIVAALQLLDAVLLYLL	2.15	-1.7

Figure S1. Sequences of TisB variants.

Sequences of the tested TisB variants are shown. Nonpolar amino acids (yellow), polar amino acids (purple), acidic amino acids (red), and basic amino acids (blue). The grand average of hydropathy (GRAVY) value was calculated with the GRAVY CALCULATOR (https://www.gravy-calculator.de/). The net charge was calculated with the Prot pi Protein Tool (https://www.protpi.ch/Calculator/ProteinTool).

Figure S2

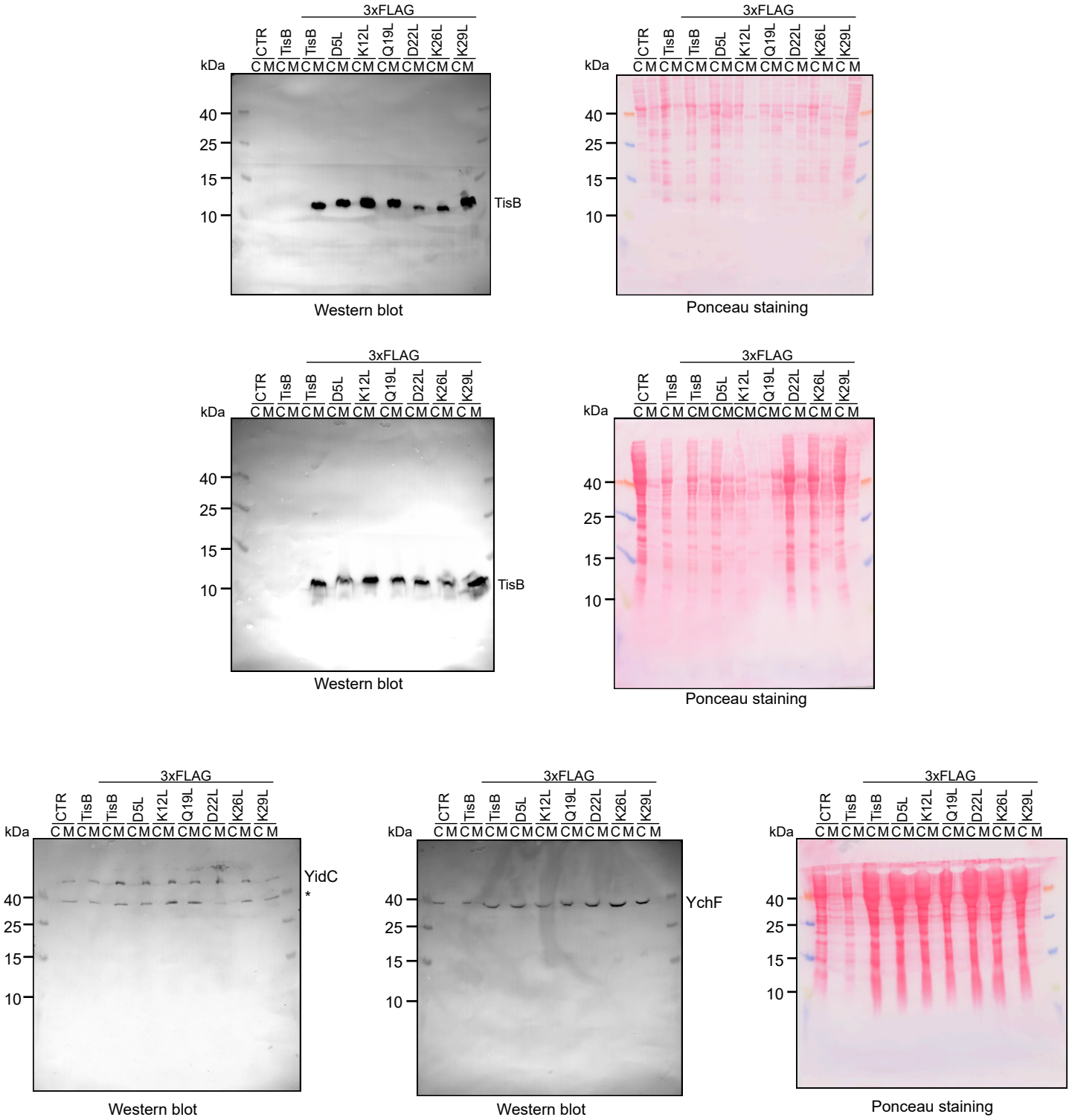

Figure S2. Raw images of western blots.

Unedited western blot and Ponceau staining images shown in Figure 1. Wild type MG1655, harboring p0SD-*3xFLAG-tisB* (3xFLAG-TisB) with different amino acid substitutions, was treated with L-ara (0.2%) during exponential phase. p0SD-*tisB* (TisB) and an empty pBAD plasmid (CTR) were used as controls. Cytoplasmic (C) and membrane (M) fractions were isolated from total protein samples using ultracentrifugation, followed by Tricine-SDS-PAGE. Proteins were blotted onto PVDF membranes. Anti-YidC (membrane) and anti-YchF (cytoplasm) antibodies were used for detection of control proteins. An anti-3xFLAG antibody was used for detection of 3xFLAG-TisB.

Figure S3

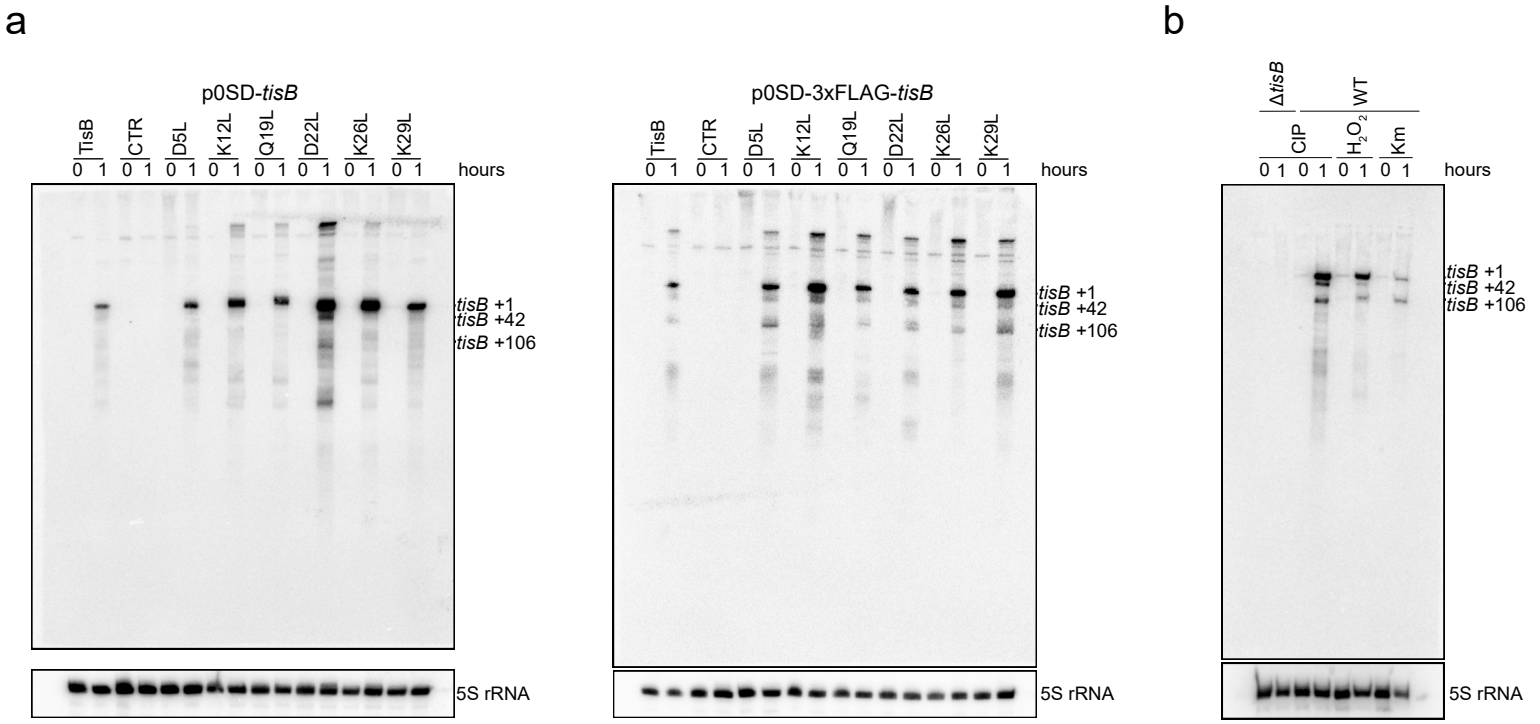

Figure S3. Raw images of northern blots.

(a) Expression analysis of *tisB*. Wild type MG1655, harboring either p0SD-*tisB* or p0SD-*3xFLAG-tisB* with different amino acid substitutions, was treated with L-ara (0.2%) during exponential phase for one hour. An empty pBAD plasmid (CTR) was used as control. Total RNA was separated on urea-polyacrylamide gels and blotted onto nylon membranes. Radioactive probes were applied for detection of *tisB* mRNA and 5S rRNA.

(b) Unedited northern blot images shown in Figure 3a. Wild type MG1655 (WT) and a *tisB* deletion strain were treated with either 10 µg/mL CIP, 10 mM H_2O_2, or 200 µg/mL KAN during exponential phase (OD_{600} ~0.4) for one hour. Total RNA was separated on urea-polyacrylamide gels and blotted onto nylon membranes. Radioactive probes were applied for detection of *tisB* mRNA and 5S rRNA.

Figure S4

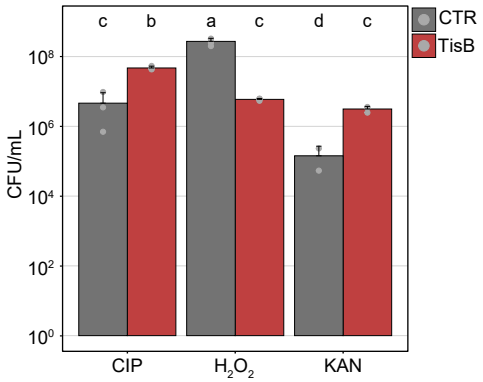

Figure S4. TisB-induced stress tolerance.

Stress tolerance after TisB induction. Wild type MG1655, harboring either p0SD-*tisB* (TisB) or an empty pBAD plasmid (CTR), was treated with L-ara (0.2%) during exponential phase for 30 minutes to induce *tisB* expression. Cells were subsequently treated with either 10 µg/ml CIP for four hours, 10 mM H_2O_2 for two hours, or 200 µg/mL KAN for four hours. After treatment with stress agents, cells were plated on LB agar plates to determine colony counts (CFU/ml). Bars represent the mean of at least two biological replicates (CIP: TisB: n=3; CTR: n=3 | H_2O_2: TisB: n=3; CTR: n=3 | KAN: TisB: n=3; CTR: n=2). Error bars indicate the standard deviation. ANOVA with post-hoc Tukey HSD test was performed, and a compact letter display was applied to present significant groups.

Figure S5

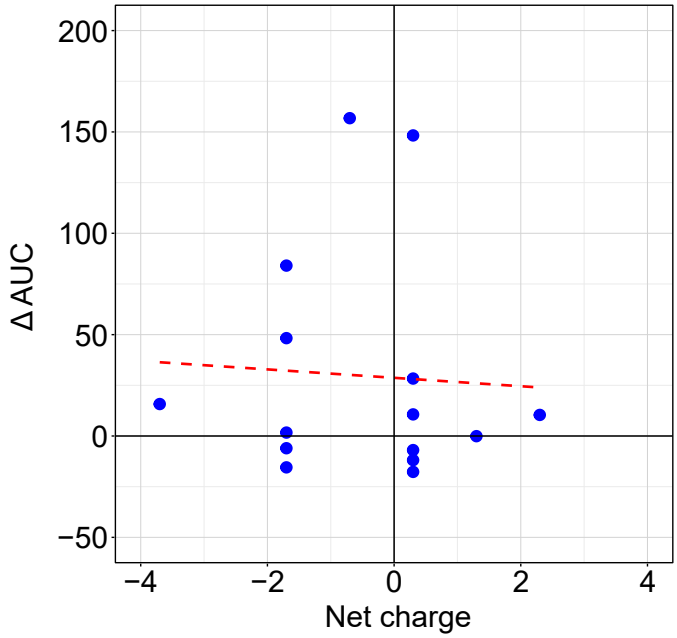

Figure S5. Correlation between net charge and growth inhibition.

Growth curves from Figures 5b were used to determine the area under the curve (AUC) for each TisB variant using the *growthcurver* package in R Studio. An empty pBAD plasmid was used as control to determine ΔAUC values, which were plotted against the net charge of the corresponding TisB variant. The Pearson correlation coefficient (r = -0.056, p = 0.843) was calculated using R statistical language (https://www.r-project.org/).

VI. Acknowledgments

This dissertation would not have been possible without the guidance, support, and encouragement of many individuals. I am deeply grateful to everyone who has contributed to my academic journey, whether through mentorship, collaboration, or personal support. In the following, I would like to express my heartfelt gratitude to those who have played a significant role in the completion of this work.

First of all, I would like to thank my supervisor, **Bork Berghoff**. His tireless support, provision of the necessary resources and insightful answers to all my questions have contributed significantly to the success of this work. His constant support and encouragement of my professional and personal development are invaluable. I am extremely grateful.

I am grateful to **Kai Thormann**, who agreed to serve as a second reviewer and provided valuable suggestions along the way. I appreciate his expertise and the time he invested. I would also like to thank **Till Schäberle** and **Oliver Rossbach**, who agreed to serve as examiners for my disputation.

I would also like to thank my collaborators, such as **Markus Oberpaul**, who spontaneously helped me with my flow cytometer experiments and saved me so much valuable time and effort. I would like to thank **Ana Natriashvili** and **Hans-Georg Koch** for their help with the membrane transport experiments and the opportunity to work in their lab for a week. Their support provided me with valuable insights and progress. I would also like to thank **Maximilian Ulbrich** for his incredibly fast help with the quantitative analysis of the protein aggregate foci. His expertise contributed greatly to the success of my analysis. I would like to thank **Liam Cassidy** and **Andreas Tholey** for their assistance in performing and interpreting the proteomic analyses.

I wish to acknowledge **Daniel Edelmann**, **Nicole Schmid** and **Sebastian Schmidt**, who laid the foundation for my experiments with their preliminary work on the moderate expression system or the initial chaperone experiments.

Special thanks go to my colleague **Robina**, who not only always brought a good mood into the lab, but also actively helped out when time was short. She enriched the work very much with her positive nature and provided the lab with her sometimes special kind of music.

Many thanks to **Sophie** and **Theresa**, who always kept me up to date on what was going on in the lab and supported me when time was short. Not to forget the rest of the institute for making me almost forget about the stressful days and for the many game nights

I am grateful to **Jan** and **Lena**, who made an important contribution to the quality of this work as proofreaders. In addition to Jan and Lena, I would also like to thank **Stefanie** and **Franzi**, all of them have been by my side since the beginning of my studies and who I have always been able to rely on when I needed help.

Special thanks go to my brother **Steffen**, who not only proofread the manuscript, but also helped me with technical questions and constructions like the counting pen or the introduction to new software like LaTex. His creative and practical support has enriched this work.

Last, but with the greatest gratitude, I dedicate this work to my parents, **Herbert** and **Elisabeth**.

From the beginning, they have supported me in all my endeavors, be it by encouraging my curiosity, giving me the opportunity to complete an exchange year, or providing me with the valuable experience of a private school for business informatics. They have not only given me an education, but also taught me the value of hard work and perseverance. Your support, patience and love have made me what I am today. I am eternally grateful to you.

VII. Declaration

I declare that I have completed this dissertation single-handedly without the unauthorized help of a second party and only with the assistance acknowledged therein. I have appropriately acknowledged and cited all text passages that are derived verbatim from or are based on the content of published work of others, and all information relating to verbal communications. I consent to the use of an anti-plagiarism software to check my thesis. I have abided by the principles of good scientific conduct laid down in the charter of the Justus Liebig University Giessen „Satzung der Justus-Liebig-Universität Gießen zur Sicherung guter wissenschaftlicher Praxis“ in carrying out the investigations described in the dissertation.

Information on tools based on artificial intelligence (AI) such as ChatGPT or SchulKI from OpenAI or Gemini from Google to create my dissertation:

☐ ~~I did not use an AI tool to create this text.~~

☒ I used an AI tool in the following areas (multiple answers possible):

- ☐ ~~Finding ideas, stimulating my creativity~~
- ☒ Understanding concepts, researching facts and definitions
- ☒ Optimizing a text I wrote
- ☐ ~~Creating entire text passages according to my specifications~~

I used the following AI tools to improve various aspects of my text, leveraging their benefits to enhance its quality:

- Scite.ai was employed to identify the most suitable references from my personal literature collection.
- Adobe Acrobat Reader AI-Assistant was used to confirm the references provided by Scite.ai. Subsequently, a second control was conducted manually.
- DeepL was used to optimize the original text.

Place, Date: _____ Signature: _____

Florian Leinberger